

Background investigation and new practical analysing method for lateral railway bridge dynamics

study of lateral dynamics of railway bridges and development of practical analysing method.

Sijian Deng

A thesis presented for the degree of
Master of Science



Faculty of Civil Engineering and Geo-science Iv-Infra
Delft University of Technology Iv-Groep
The Netherlands
November 22, 2014

Abstract

Dynamics of railway bridges is a complicated problem that normally needs numerical simulation to conduct researches. However, this thesis takes advantage of the numerical results provided in D181 reports and based on these results, further conclusions are made by using them in analytical model.

Recently long span railway bridges being designed in the Netherlands are being rejected by a particular EN1991-2 criterion that requires bridges to possess a first lateral natural frequency higher than 1.2Hz. Due to the fact that generally bridge's first lateral natural frequency decreases as the span increases, it can be seen that 1.2Hz criterion is rejecting almost all bridge with a span longer than 150m.

This report succeeds in pursuing the original documents of 1.2Hz criterion and the knowledge in the documents initiates further researches on the lateral dynamics of railway bridges. Besides 1.2Hz criterion itself, following topics are researched with the information provided by D181 report series:

1. Train-bridge lateral resonance mechanisms, including axle repeat pattern resonance and kinematic movement resonance,
2. Lateral force on tracks caused by the operation of railway vehicle and key parameters influencing the force,
3. Lateral wavelength of trains running in the Netherlands, including axle repeat pattern wavelength and kinematic movement wavelength

Taking advantage of the items above, a practical method for checking the lateral railway bridge dynamics is developed to quantify the lateral dynamic resonance response of railway under horizontal dynamic vehicle load. This method aims to serve for engineering purposes and provide an alternative way of verifying railway bridge lateral dynamics other than 1.2Hz criterion. The practical method is developed by an analytical approach, based on the VAMPIRE simulation results in D181 DT329.

An illustration of the usage of the practical method is conducted on the basis of a real bridge project. The method is also implemented in Matlab scripts to automate the checking procedure.

Keywords:— Eurocode, D181, railway bridge dynamics, lateral dynamics, rail dynamics, analytical solution, 1.2Hz criterion, train wavelength, nosing force, lateral force on track

Acknowledgements

Hereby I would like to express my deepest appreciation to all those who helped me in completing this thesis and my engineering studies.

First of all, I would like to thank to Matthijs van Almen, my daily supervisor at Iv-Infra, for his patient guidance during the entire thesis process. His guidance is like the light that helps me finding the right path in the darkness. Nevertheless, his way of thinking also enlightened me. I would never have completed the thesis without his help.

I also want to express my appreciation to Prof. Frans Bijaard, Dr. Roland Abspoel, Dr. Michaël Steenbergen, Prof. Rolf Dollevoet, the members of the thesis committee from Delft University of Technology. Their professional knowledge and general interest in the topic were valuable assets to my work.

Special thanks to Michel Koop, who provided me with the opportunity to carry out this research at Iv-Infra, to Charalampos Bouras, who was always eager to provide help whenever I needed, and to all the colleagues at the steel department of Iv-Infra, who provided me a friendly atmosphere.

I really appreciate the help of Ron van der Zwan and the access to ERRI D181 research resources he provided. I also appreciate Paul Vos, Jean-Jacques Reber sharing their background information of D181 committee. Same appreciation goes to Alan Minnis from DeltaRail for providing the information of D181 DT329 researches.

Thanks to the contributors of both StackOverflow who generously sharing the knowledge and L^AT_EX for maintaining such an incredible package.

I am deeply grateful to my parents, Guolin Deng and Jiafen Wang, who always believed in me and were supporting my studies in The Netherlands.

Last but not least, I am thankful to all my friends in Delft, who gave me many unforgettable memories during my studies.

Sijian Deng
Delft, November 22, 2014

Contents

1	INTRODUCTION	8
1.1	Summary of topic	8
1.2	Motivation of the thesis	8
1.3	Objectives and research question	9
1.4	Main steps	9
1.5	Outline of the report	10
2	Basic concepts of railway bridge dynamics	11
2.1	Basic railway dynamic effects	11
2.1.1	Sources induce transverse dynamic reactions	11
2.1.2	Lateral movement of a wheelset on straight track	11
2.1.2.1	Theory according to Klingel	11
2.1.2.2	Hunting movement	13
2.1.3	Single and two-point contact between wheel and rail	13
2.2	Wheel-Rail Interface	14
2.2.1	Wheelset and track dimensions	14
2.2.2	Conicity and Equivalent Conicity of Wheels	15
2.2.3	Worn wheel profiles	15
2.3	Lateral Track Irregularities	16
2.4	Dynamic theories	16
2.4.1	Natural frequencies and shapes of bridge	17
2.4.2	Basic resonance concept	18
2.5	Analysing methods for lateral dynamics of railway bridges	19
2.5.1	Modal analysis	20
2.5.2	Analysis by modal superposition	20
2.5.3	Numerical methods	20
2.5.3.1	VAMPIRE	21
3	Literature Review of regulations regarding lateral railway bridge dynamics in 1991-2	22
3.1	Factors influencing dynamic behaviour	22
3.2	Requirements for railway bridge verification	23
3.3	Horizontal transverse dynamic effects	23
3.3.1	Nosing force	23
3.3.2	Verification of the Limit States	24
3.3.3	Serviceability limit states - traffic safety	24
3.3.3.1	Transverse deformations and vibrations	24
3.4	Conclusion	25

4 Investigation of report series created by D181 Committee Group	26
4.1 Introduction	26
4.1.1 Structure of report series	26
4.1.2 Items of interests in report series	26
4.2 Investigation of DT329	27
4.2.1 Methodology of Parametric Research DT329	27
4.2.2 Modelling	27
4.2.2.1 Model of bridge	27
4.2.2.2 Bridge parameters	28
4.2.2.3 Vehicle parameters	28
4.2.2.4 Track	29
4.2.2.5 Contact data	29
4.2.2.6 Data produced	29
4.2.3 Investigation of resonance phenomenon studied in DT329	30
4.2.3.1 Resonance caused by axle repeat pattern	30
4.2.3.2 Resonance caused by kinematic movement of trains	30
4.2.3.3 Apparent shift in resonance frequency	31
4.3 Investigation of RP6	32
4.3.1 Debate on proposed 1.2Hz criterion	32
4.3.2 Lateral forces on railway bridges	33
4.3.2.1 Basic characteristics of lateral force on railway bridges	33
4.3.2.2 Refining of lateral force model	35
4.3.2.3 Application of lateral force model	37
4.4 Evaluating nosing force proposed by EN1991-2	38
4.5 Conclusion of D181 report series	39
5 Lateral wavelength research on Dutch railway vehicles	40
5.1 Effects investigated in wavelength study	40
5.2 Equivalent conicity used in this study	40
5.3 Study on wavelength of lateral kinematic movement	41
5.3.1 Comparison between Klinge movement and train kinematic movement studied in D181 DT329	41
5.4 Assess of wavelength bandwidth based on realistic data of Dutch Rail/Vehicle	42
5.5 Lateral wavelength of axle repeat pattern of Dutch Railway Vehicles	43
5.6 Conclusion of wavelength study	44
6 Essentials of analytical approach to be adopted in practical checking method	45
6.1 Introduction	45
6.2 Overview	45
6.3 The model, its assumptions and field of application	45
6.4 Solution deduction	46
6.5 Damping	48
6.6 Verification of the explicit solution	49
7 New practical method for checking lateral resonance response of railway bridges based on VAMPIRE simulation results	51
7.1 Introduction	51
7.2 Overview of this chapter	51
7.3 Development of refined load model	52
7.3.1 Overview of VAMPIRE numerical simulation method and analytical method	52
7.3.2 Finding equivalent lateral force amplitude for specific cases	53

7.3.3	Key parameter for equivalent force amplitude and hypothesis expression for refined load model	54
7.4	Verification of the method	56
8	Finalizing the method for practical usage using real bridge parameters	59
8.1	Conclusion	60
9	Recommendations on improvement on Eurocode	62
9.1	Recommendations of this thesis	62
9.2	Other lateral railway bridge dynamics related criteria extracted from other codes	62
9.2.1	Requirements for traffic safety(horizontal)	62
9.2.2	Requirements for traffic safety on derailment: Railway vehicle derailment mechanism and safety criteria	63
9.2.3	Flange climb derailment	63
9.2.4	Derailment caused by guage widening and rail rollover	63
9.2.5	Derailment caused by track panel shift	65
9.2.6	Derailment caused by vehicle lateral instability	65
9.2.7	Requirements for traffic serviceability(horizontal)	66
10	Conclusion	67
11	Recommandations on future reserachses	68
Appendices		69
A	Plots and diagrams used in D181 DT 329	70
B	Speeds which do not require dynamic compatibility checks	86
C	MU-Groups and MU-Classes	89
C.1	Definition	89
C.1.1	Train parameters of MU-Class CB_1	89
C.1.2	Train parameters of MU-Class CB_2	89
C.1.3	Train parameters of MU-Class AB_1	89
C.1.4	Train parameters of MU-Class AB_2	90
C.1.5	Train parameters of MU-Class AB_3	90
C.1.6	Train parameters of MU-Class AB_4	90
C.1.7	Train parameters of MU-Class SA_1	90
C.1.8	Train parameters of MU-Class SA_2	90
D	Regression commands for R console	93
E	Matlab scripts	94
E.1	fog.m	94
E.2	Speedenvelop.m	96
F	Train vehicles	98
F.1	Locomotives	98
F.1.1	4-axle locomotives	98
F.1.2	6-axle locomotives	98
F.2	Trains in Netherlands	98

List of Figures

1.1	Logic relationship of chapters	10
2.1	Wheelset biconus in general position. Extracted from Esveld ¹⁴ , Figure 2.2	12
2.2	Klingel movement. Extracted from Esveld ¹⁴ , Figure 2.3	12
2.3	Undisturbed lateral movement of a wheelset. Extracted from Esveld ¹⁴ , Figure 2.4 .	13
2.4	Influence of flanging on lateral wheelset movement. Extracted from Esveld ¹⁴ , Figure 2.5	13
2.5	Increase in amplitude and frequency with speed and the development of instability. Extracted from Esveld ¹⁴ , Figure 2.6	14
2.6	Single and double contact of wheel-rail interface	14
2.7	Wheelset and track dimensions for straight normal gauge track. Extracted from Esveld ¹⁴ , p.17	15
2.8	$y - \Delta r$ curves. Difference between conical and worn wheel profiles. Extracted from Esveld ¹⁴ , 2.4	16
2.9	Lateral deviation definition. Lateral deviations y_p for each rail with 1: running surface, 2: reference line and 3: centre line of running table	17
2.10	Mass beam model of span L	18
2.11	Amplitude-frequency characteristic. Extracted from Metrikine ¹⁹ , 2.2.2	19
2.12	A sample project being conducted in VAMPIRE	21
4.1	Overview of modelling setups for different studies conducted in DT329	27
4.2	Bridge parameter combination	28
4.3	Workflow of kinematic resonance research	31
4.4	Sketch of Possible Explanation for Apparent Shift in Resonant Frequency. Extract from D181Committee ¹¹ , Appendix 2	32
4.5	Figure B1 extracted from D181Committee ¹¹	34
4.6	Figure B2 extracted from D181Committee ¹¹	34
4.7	Figure B7 extracted from D181Committee ¹¹	35
4.8	Total peak lateral track forces over all track qualities(worn profile scenario neglected)	38
5.1	Example of a 2-axle freight wagon	42
5.2	Example of a 4-axle freight wagon	42
6.1	Schematic representation of a generic beam crossed by a harmonic load	45
6.2	Reference plot extracted from Abu-Hilal and Mohsen ³ . Condition: $\alpha = 0.25$, $\zeta = 0.05$, $\beta = 1$. Y axis for dynamic amplification factor.	49
6.3	Time history of dynamic amplification factor in mid-span of the beam. Parameters: $EJ = 2.43e10 Nm^2$, $L = 54m$, $\mu = 6000 kg/m$, $c = 29.26 m/s$	50
7.1	Workflow of the creation of analytical method	52

7.2	Figure C1 extracted from D181Committee ¹¹	54
7.3	Figure C3 extracted from D181Committee ¹¹	54
7.4	Figure C9 extracted from D181Committee ¹¹	55
7.5	Figure C12 extracted from D181Committee ¹¹	56
7.6	Figure C13 extracted from D181Committee ¹¹	57
7.7	Figure C14 extracted from D181Committee ¹¹ . An minor error is observed in y-axis label. Upper boundary of y-axis should be 0.116	57
7.8	Comparison between VAMPIRE peak simulation result and analytical peak result	58
8.1	Peak deflection at mid-span with regard to changing train speed. Parameters: $EJ = 6.56e12Nm^2$, $L = 255m$, $\mu = 20478kg/m$, $c_{min} = 1m/s$, $c_{max} = 30m/s$	60
9.1	Forces at flange contact location. Extracted from Iwnicki ¹⁷ , Figure8.4	64
9.2	Gauge widening derailment. Extracted from Iwnicki ¹⁷ , Figure8.18	64
9.3	Lateral track panel shift. Extracted from Iwnicki ¹⁷ , Figure8.27	65
9.4	Wheelset oscillates around the track centre. Extracted from Iwnicki ¹⁷ , Figure8.28	66
A.1	BR CLASS 56 LOCOMOTIVE. Extract from D181Committee ¹¹ , Appendix 2	71
A.2	BR CLASS 56 LOCOMOTIVE. Extract from D181Committee ¹¹ , Appendix 2	72
A.3	UIC FREIGHT WAGON (LADEN). Extract from D181Committee ¹¹ , Appendix 2	73
A.4	UIC FREIGHT WAGON (LADEN). Extract from D181Committee ¹¹ , Appendix 2	74
A.5	FS ETR500 LOCOMOTIVE. Extract from D181Committee ¹¹ , Appendix 2	75
A.6	FS ETR500 LOCOMOTIVE. Extract from D181Committee ¹¹ , Appendix 2	76
A.7	FS ETR500 COACH. Extract from D181Committee ¹¹ , Appendix 2	77
A.8	FS ETR500 COACH. Extract from D181Committee ¹¹ , Appendix 2	78
A.9	FS E444 LOCOMOTIVE. Extract from D181Committee ¹¹ , Appendix 2	79
A.10	FS E444 LOCOMOTIVE. Extract from D181Committee ¹¹ , Appendix 2	80
A.11	UIC COACH. Extract from D181Committee ¹¹ , Appendix 2	81
A.12	UIC COACH. Extract from D181Committee ¹¹ , Appendix 2	82
A.13	Horizontal track irregularities for freight trains. Extract from D181Committee ¹⁰ , Figure 2.1	83
A.14	Horizontal track irregularities for standard passenger trains. Extract from D181Committee ¹⁰ , Figure 2.1	84
A.15	Horizontal track irregularities for high speed passenger train. Extract from D181Committee ¹⁰ , Figure 2.1	85
B.1	Speed limit (in km/h) in relationship Line Category/Locomotive Class and vehicle type. Extract from CEN ⁸ , Appendix F	86
B.2	LATERAL WHEEL AND AXLE FORCES FOR BRIDGES. Extract from D181Committee ¹⁰ , Fig 3.1	87
B.3	Example run file. Extracted from D181Committee ¹¹ .	88
C.1	Train parameters related to MU-Groups. Extracted from CEN ⁸ , Annex C	90

List of Tables

2.1	Alignment - AL - Standard deviation. Extracted from CEN ⁴ , Table B.6	17
3.1	Maximum horizontal rotation and maximum change of radius of curvature	25
4.1	Peak Lateral Track Force Over All Track Qualities. Extracted From D181Committee ¹¹ , Tab. B1	36
5.1	Approximate lateral kinematic wavelength calculated by improved Klingel formula .	42
5.2	Wavelength of kinematic movement generated by realistic value	43
5.3	Wavelength of axle repeat pattern(m)	44
7.1	Comparison between input parameters of DT329 VAMPIRE simulations and analytical model	53
7.2	Parameter setups and equivalent force amplitude for C1,C3,C9	55
7.3	Comparison of results of simulation output and analytical output using refined load model	58
A.1	Axle repeat patterns and typical frequencies. Extracted from D181Committee ¹¹ , Appendix C	70
A.2	Kinematic wavelength ranges per vehicle, with BR P1 profiles. Extracted from D181Committee ¹¹ , Appendix C	70
C.1	Relationship MU-groups - MU-classes	89
C.2	Explanation of train parameters. Extracted from CEN ⁸ , Annex C	90
C.3	Train parameters for conformity with MU-Class CB_1	91
C.4	Train parameters for conformity with MU-Class CB_2	91
C.5	Train parameters for conformity with MU-Class AB_1	91
C.6	Train parameters for conformity with MU-Class AB_2	91
C.7	Train parameters for conformity with MU-Class AB_3	91
C.8	Train parameters for conformity with MU-Class AB_4	91
C.9	Train parameters for conformity with MU-Class SA_1	92
C.10	Train parameters for conformity with MU-Class SA_2	92

Chapter 1

INTRODUCTION

1.1 Summary of topic

Lateral railway bridge dynamics is an engineering topic that related to both bridge structure and operating railway vehicles. There is little knowledge about lateral dynamics of railway bridges among structural engineers, but it is only until recently this topic catches focus. The reason is that an Eurocode criterion regarding the topic is frequently rejecting new long span railway bridge designs.

Although there's no records of bridge/vehicle failure due to lateral railway vehicle dynamic loading, it is found during the research process of this thesis that ERRI(former UIC) had already done investigation on this topic before 1994 and presented the results in D181 report series. This information of D181 is hardly known to both researchers and engineers after Eurocode EN1991-2's publication in 1994. However, several criterion proposed by D181 committee were adopted in EN1991-2.

Throughout D181 report series and EN1991-2, it can been seen that almost no attention is put on lateral dynamics of long span railway bridges. This thesis aims to review both documents and conduct further researches on the topic and propose a simpler 'engineering' verification method of lateral dynamics of railway bridges.

1.2 Motivation of the thesis

The lateral dynamic behaviour of steel railway bridges are minimally discussed in Eurocodes and designers lack knowledge of background of the criteria proposed in the code. For example, there is one criterion in Eurocode requiring railway bridges should have a lateral natural frequency higher than 1.2Hz. However, this criterion is becoming more and more unsuitable for modern bridge designs because longer span provides lower natural frequencies. For bridges having span longer than 100m, it is almost guaranteed that the first lateral natural frequency of the bridge is lower than 1.2Hz, and unable to meet the requirement of EN1991-2.

Since for most bridge designs, changing the bridge parameters to meet the 1.2Hz criterion isn't a viable option because it's expensive to add stiffness to the bridge, the projects need a solution to solve the problem. To gain more knowledge on the topic, a research on the background of 1.2Hz criterion is initiated by Iv-Infra, presented in this report. The discovery in the background research stimulates further researches including domestic lateral wavelength of trains in the Netherlands, lateral force on tracks, simpler engineering verification method, etc.

1.3 Objectives and research question

The report has following objectives.

- Provide insight into lateral dynamics of railway bridges. Since the general knowledge about the
- Find the source of 1.2Hz criterion. Interpret its original intention by reviewing the original documents. Give a conclusion on the correctness of 1.2Hz criterion based on the interpretation.
- Find alternative strategy for validating the lateral dynamics of railway bridges
- Develop a practical method based on newly found strategy

The research question can be summarized as:

Conclude the correctness of current existing criterion on lateral railway bridge dynamics and develop new practical method for checking lateral dynamics of railway bridges based on an alternative checking strategy.

1.4 Main steps

In order to carry out the objectives and research questions, the thesis will be conducted in following steps:

1. Literature research on the knowledge regarding lateral railway bridge dynamics. This section aims to provide insight to readers so emphasis is placed on fundamental information. Since general dynamics of the bridges are widely discussed and the only thing that differs is that railway bridges are subjected to railway vehicle loads, literature research also focuses on conveying basic knowledge of dynamics of railway vehicles.
2. Find the original reports that proposed the 1.2Hz criterion and assess the content of these reports. Further investigate the research process and conclusions of these reports to yield more useful information for following researches.
3. Using the knowledge in the original reports, study the dynamics properties of trains running in the Netherlands.
4. Develop a practical method for simple calculating the time-history of the dynamic response of the bridge under train vehicle load on the basis of numerical simulation results provided by D181 committee in their report series.
5. Apply above developed practical method on a real project to finalize the method for engineering usage and as well as illustrates the usage of the method.

1.5 Outline of the report

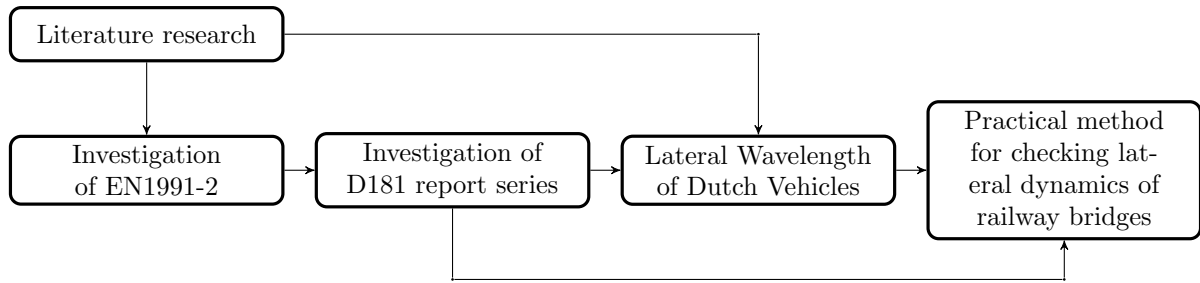


Figure 1.1: Logic relationship of chapters

The logic relationship of selected chapters is illustrated in Figure 1.1

The report is created in following structure:

1. Literature study on basic concepts of railway bridge dynamics.
2. Deep investigation of EN1991-2 supporting research report series
3. Wavelength study
4. Introduction to the analytical method
5. Development of the new practical checking method by adopting the analytical model and outputs of VAMPIRE simulations
6. Suggestions for Eurocode
7. Conclusions

Chapter 2

Basic concepts of railway bridge dynamics

In this chapter basic concepts of railway bridge dynamics will be described in order to provide preliminary relevant knowledge for following chapters. The knowledge will be introduced in the order of railway dynamics related only to bridge dynamics related.

2.1 Basic railway dynamic effects

2.1.1 Sources induce transverse dynamic reactions

According to da Silva Dias¹³, Fryba¹⁵ and CEN⁵, following sources are identified:

- Sinusoidal motion of conical wheels along cylindrical rail heads. See Section.2.1.2.1
- Horizontal track irregularities. See Section.2.3
- Centrifugal forces on curved tracks. This source is not discussed because only straight tracks are discussed in this thesis.
- Train switches. This source is not discussed because of the same reason as above item.

2.1.2 Lateral movement of a wheelset on straight track

Following knowledge in all subsections of this section is extracted from Esveld¹⁴.

2.1.2.1 Theory according to Klingel

If a wheelset with conical tire profiles is laterally displaced from central position, this displacement is counteracted due to different rolling radii of the wheels. This results in a periodical movement of the wheelset which was described by Klingel in 1883 and is therefore often referred to as the Klingel movement. When analysing the case, the wheelset is modelled as a biconus travelling on an ideally straight track as shown in Figure.2.1.

The Klingel movement is therefore purely a kinematic movement in which forces play no part in the derivation. As a result, Figure.2.2 visualizes the Klingel movement. The lateral displacement y is a harmonic, undamped function of the distance co-ordinate x as long as the amplitude moves within the flangeway clearance f_{wc} . This is illustrated in Figure.2.3.

Introducing the speed, the time domain frequency of the Klingel movement is:

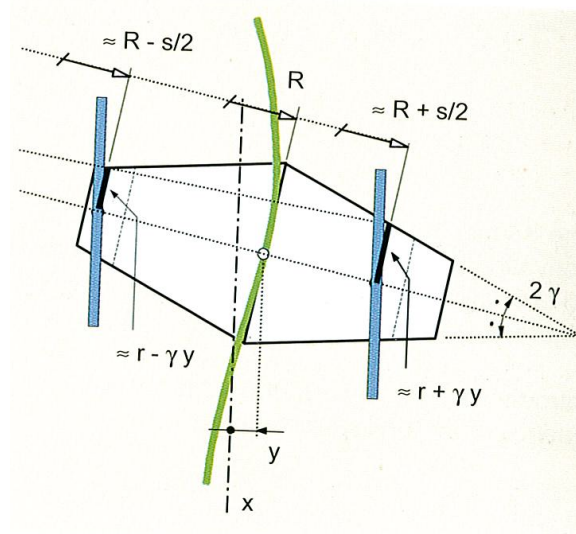


Figure 2.1: Wheelset biconus in general position. Extracted from Esveld¹⁴, Figure 2.2

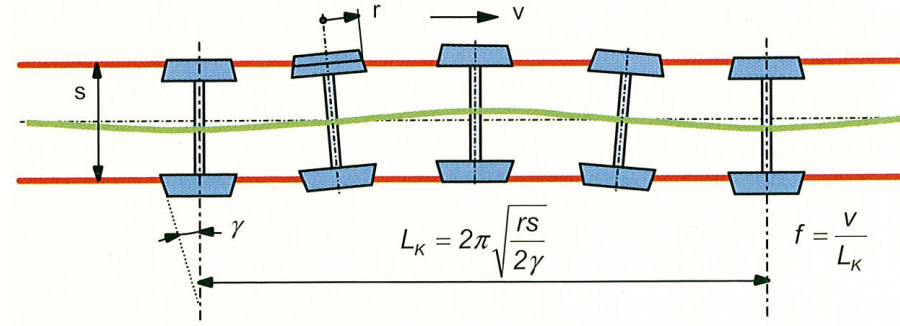


Figure 2.2: Klingel movement. Extracted from Esveld¹⁴, Figure 2.3

$$f = \frac{V}{L_k}$$

and hence the maximum lateral acceleration can be calculated as:

$$\ddot{y}_{max} = 4\pi^2 y_0 \frac{v^2}{L_k^2}$$

If the frequency f coincides with one of the natural frequencies of the rolling stock, the vehicle ride becomes unstable. The lateral acceleration, which is a measure of the forces, shows the adverse effect of high speed and/or small wavelength. A conicity, for example, of 1:40 in comparison with 1:20 therefore gives a greater wavelength and a lower lateral acceleration at the same speed. The progressively increasing conicity in the case of worn profiles due to increasing lateral axle movement, therefore, has an adverse effect in this respect.

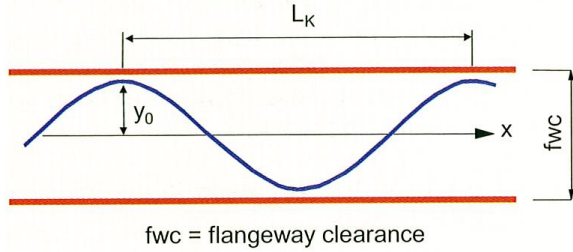


Figure 2.3: Undisturbed lateral movement of a wheelset. Extracted from Esveld¹⁴, Figure 2.4

2.1.2.2 Hunting movement

It should be noted that the Klingel theory is simple and instructive but does not include the effect of coupled axes, mass forces, and adhesion forces. In reality, the amplitude y_0 of the Klingel movement is dependent on alignment, dynamic vehicle behaviour, and the speed of the rolling stock.

Generally speaking, y_0 due to slip will increase with speed until it is equal to half the flangeway clearance. Flanging then occurs as a result of which the axle will rebound.

This means that the lateral movement takes on a completely different behaviour which is known as hunting. As shown in the drawing in Figure 2.4 the movement changes from a harmonic to a zig-zag shape. The wavelength becomes shorter and the frequency increases quickly until it is in the critical range for the rolling stock and resonance occurs.

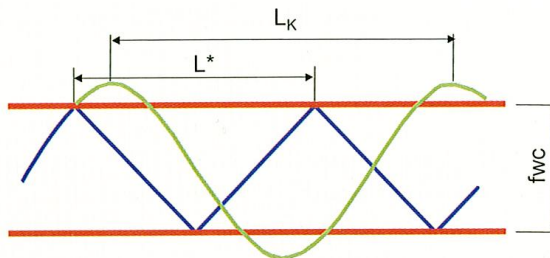


Figure 2.4: Influence of flanging on lateral wheelset movement. Extracted from Esveld¹⁴, Figure 2.5

This phenomenon is shown in Figure 2.5. The bogie design, as far as conicity and flangeway clearance are concerned, must be such that stable running is always guaranteed for the speed range in which the vehicle is to be used.

2.1.3 Single and two-point contact between wheel and rail

In the case of single-point contact, according to Figure 2.6a, wheel load and lateral force act on the same point. This situation occurs when using worn wheel profiles. In the case of two-point contact, shown in Figure 2.6b, the application points do not coincide.

Flanging occurs in the situation of double contact.

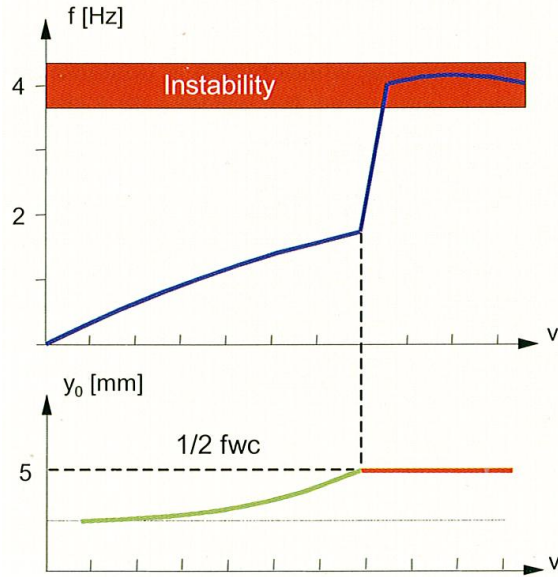


Figure 2.5: Increase in amplitude and frequency with speed and the development of instability. Extracted from Esveld¹⁴, Figure 2.6

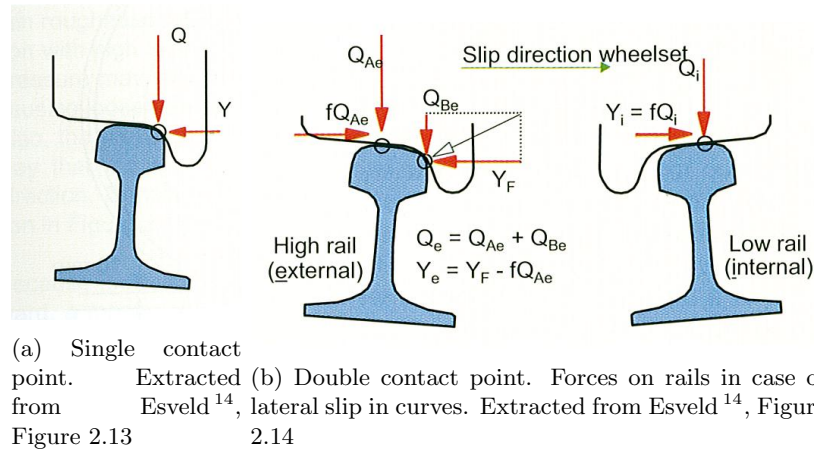


Figure 2.6: Single and double contact of wheel-rail interface

2.2 Wheel-Rail Interface

Following knowledge in all subsections of this section is extracted from Esveld¹⁴.

2.2.1 Wheelset and track dimensions

Generally the track gauge is used as a distance measured between the two rails, more specifically the distance between the inside of the railheads measured 14mm below the surface of the rail. By choosing 14 mm the measurement is less influenced by lipping or lateral wear on the rail head and by the radius $r = 13$ mm of the rail head face. On normal track the gauge is 1435^{+10}_{-3} mm with a maximum gradient of 1:3000. For

new track, however, NS apply the following standards:

1. Mean gauge per 200 m: 1435^{+10}_{-1} mm
2. Standard deviation within a 200 m section less than 1 mm

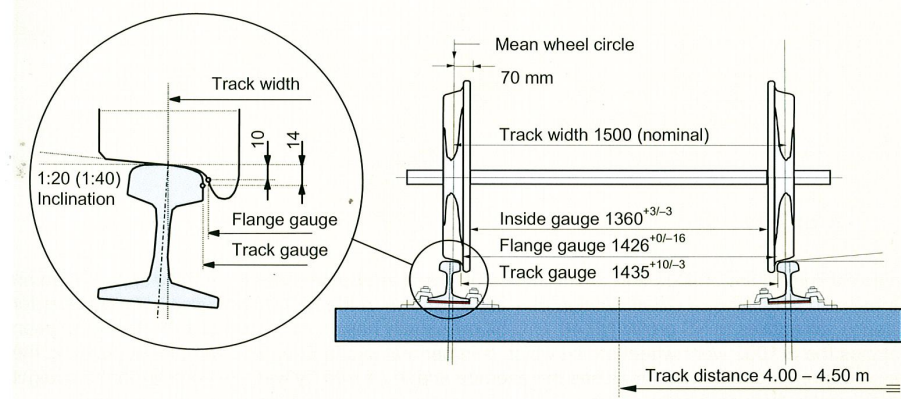


Figure 2.7: Wheelset and track dimensions for straight normal gauge track. Extracted from Esveld ¹⁴, p.17

2.2.2 Conicity and Equivalent Conicity of Wheels

Originally conical tire profiles with an inclination of 1:20 were used. Since a centrally applied load on the railhead is desired, a rail inclination of 1:20, as shown in Figure 2.1, was also selected; this for instance still applies to NS profile NP 46. UIC 54 rail usually has an inclination of 1:40. This inclination matches the S 1002 worn wheel profile which is in general use in Europe. During manufacturing the tires are given a profile which matches the average shape cause by wear. In contrast to the straight conical profile this has a hollow form.

It is clear that regarding a worn profile the conicity depends on the actual shape of the rail head and tire, including any wear, track gauge, and rail inclination. Likewise, elastic deformation of the wheelset and rail fastenings plays a role.

Generally, the effective or equivalent conicity is defined as:

$$\gamma_e = \frac{\Delta r}{2y} = \frac{r_1 - r_2}{2y}$$

Here $r_1 - r_2$ is the instantaneous difference in rolling radius of the wheel treads; generally speaking this is a non-linear function of the lateral displacement y of the wheelset with respect to the central position. The difference between conical and worn profiles is given in Figure 2.8. To enable numerical comparisons γ_e is determined at a certain lateral displacement $y = \bar{y}$.

2.2.3 Worn wheel profiles

A perfectly conical wheel profile is unstable as far as its shape is concerned, but will take on a shape that is stable as the effect of wear.

Practical research has shown that over a period of time wheel profiles stabilise with wear at an equivalent conicity of 0.2 to 0.3. With regards to running stability, the equivalent

conicity must remain below 0.4 and to ensure the centering effect it must be greater than 0.1.

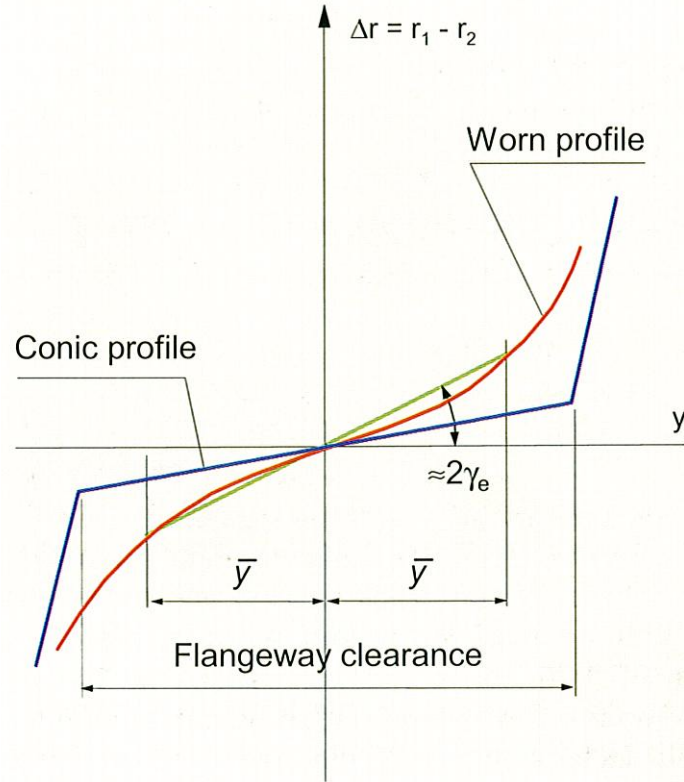


Figure 2.8: $y - \Delta r$ curves. Difference between conical and worn wheel profiles. Extracted from Esveld¹⁴, 2.4

With a conical profile the conicity is constant and above equation becomes:

$$\gamma_e = \frac{\Delta r}{2y} = \frac{(r + \gamma y) - (r - \gamma y)}{2y} = \gamma$$

2.3 Lateral Track Irregularities

This section describes allowable lateral track irregularities defined in EN13848-5CEN⁴.

Lateral alignment irregularities was defined in EN13838-1. It states:"Deviation y_p in y-direction of consecutive positions of point P... on any rail, expressed as an excursion from the mean horizontal position (reference line) covering the wavelength ranges stipulated below and calculated from successive measurements ...". See Figure 2.9.

For lateral deviations, the following wavelengths shall be considered: $D1 = 3 - 25m$, $D2 = 25 - 70m$ and $D3 = 70 - 200m$.

Table 2.1 defines the allowable standard deviation for lateral track irregularities. Lateral track irregularity has great influence on vehicle's lateral dynamic behaviour.

2.4 Dynamic theories

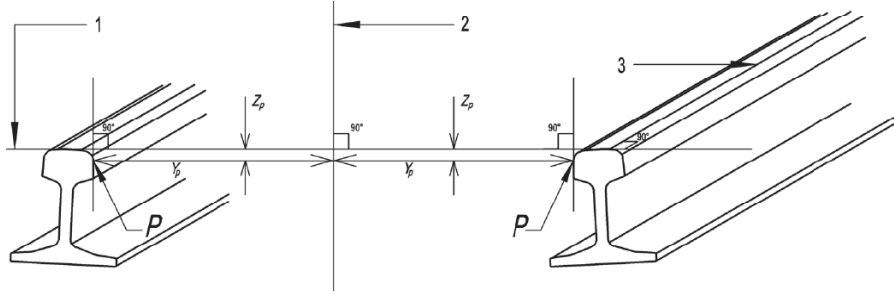


Figure 2.9: Lateral deviation definition. Lateral deviations y_p for each rail with 1: running surface, 2: reference line and 3: centre line of running table

Table 2.1: Alignment - AL - Standard deviation. Extracted from CEN⁴, Table B.6

Speed(km/h)	Standard deviation(mm)
$V \leq 90$	1.5 to 1.8
$80 < V \leq 120$	1.2 to 1.5
$120 < V \leq 160$	1.0 to 1.3
$160 < V \leq 230$	0.8 to 1.1
$230 < V \leq 300$	0.7 to 1.0

2.4.1 Natural frequencies and shapes of bridge

Undamped Euler-Bernoulli beam theory is adopted to obtain natural wave shapes and frequencies of a bridge structure. This theory is the simplest bridge dynamic model which assumes that the bridge behaves as a vibrating uniform beam.

The bridge is simply supported at both ends, and the stiffness is specified as a deflection at the mid span per unit span length arising from a static point load of 100kN at mid span.

The equation of vibration of a uniform beam is:

$$\frac{\partial^2 y}{\partial t^2} + a^2 \frac{\partial^4 y}{\partial x^4} = 0$$

where:

y = deflection of beam

x = coordinates along longitudinal axis

t = time

$a^2 = EI/m$

EI = flexural rigidity

and, m = mass per unit length

The general solution is:

$$y(x, t) = (A \cos pt + B \sin pt)(C \cos kx + D \sin kx + F \cosh kx + G \sinh kx)$$

which consists of independent time and distance parts. The distance dependent part of the solution gives the family of mode shapes which the beam will exhibit. Thus, generally, a beam has mode shapes which satisfy:

$$y(x) = C \cos kx + D \sin kx + F \cosh kx + G \sinh kx$$

For a beam which is simply supported at either end the general solution simplifies, giving a family of normalized amplitude mode shapes as follows:

$$y_r = \sin \frac{r\pi x}{L}$$

for $r = 1, 2, 3, \dots, n$ and $L = \text{spanlength}$

with corresponding angular frequencies, ω_r , of:

$$\omega_r = \frac{r^2\pi^2}{L^2} \sqrt{\frac{EI}{m}}$$

thus natural frequencies f_r of beam, are:

$$f_r = \frac{r^2\pi}{2L^2} \sqrt{\frac{EI}{m}}$$

2.4.2 Basic resonance concept

The most simplest resonance scenario happens at a one degree-of-freedom mass-spring system loaded by a force whose frequency coincides with the natural frequency of mass-spring system.

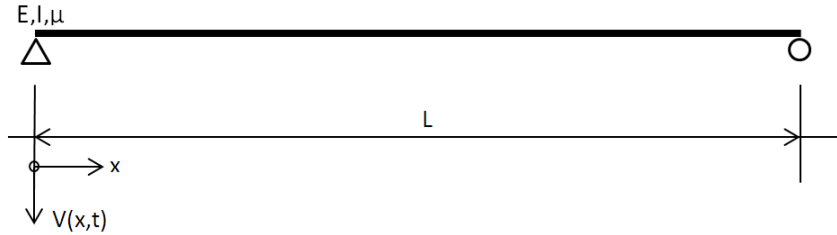


Figure 2.10: Mass beam model of span L

Assume there is a simple one degree-of-freedom mass-spring system and an external force is acting on it. The force is given as $F(t) = F_0 \cos(\omega t)$. In this case the equation of motion takes the form

$$m\ddot{x} + kx = F_0 \cos(\omega t) \quad (2.1)$$

The general solution can be written as

$$x(t) = A \cos(\omega_n t) + B \sin(\omega_n t) + \frac{F_0}{k} \frac{1}{1 - \omega^2/\omega_n^2} \cos(\omega t) \quad (2.2)$$

where $\omega_n = 2\pi\sqrt{k/m}$

The unknown constants A and B depend on the initial conditions.

The steady-state solution is given as:

$$x_{\text{steady}} = X \cos(\omega t) = \frac{F_0}{k} \frac{1}{1 - \omega^2/\omega_n^2} \cos(\omega t) \quad (2.3)$$

The amplitude of vibrations of the mass-spring system is given by:

$$|X| = \left| \frac{F_0}{k} \frac{1}{1 - \omega^2/\omega_n^2} \right| \quad (2.4)$$

The amplitude-frequency dependencies is shown in 2.11

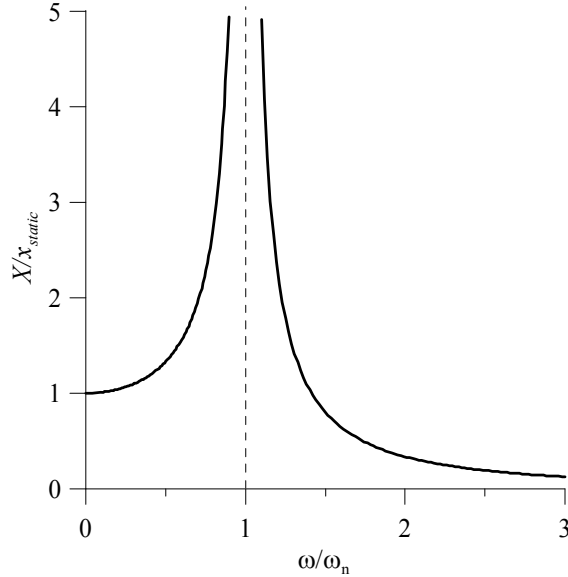


Figure 2.11: Amplitude-frequency characteristic. Extracted from Metrikine¹⁹, 2.2.2

When the frequency of force equals frequency of mass-spring system, the amplitude of vibration is infinitely high. It means system becomes unstable and normally it's a dangerous sign. This phenomenon is called resonance.

Resonance can also happen when a harmonic force is loaded on an Euler-Bernoulli beam. It can be loaded anywhere on the beam to produce resonance.

2.5 Analysing methods for lateral dynamics of railway bridges

Several analysing methods for vertical dynamics of railway bridges were briefed in UIC²³, A6.2. Methods that can be applied also on lateral direction are selected:

Various programs are available and details can be found in ERRI report D 214/RP7 (see Bibliography - page 43); they can be used to calculate the dynamic response under live train loads, of isostatic bridges, series of isostatic decks, continuous bridges using the beam theory, the dynamic response of plates and by taking into account the two longitudinal and transversal modes. They can also run calculations for orthotropic square plates and skew plates.

...

Two types of analyses can be carried out: with or without interaction with the train.

The most problematic cases, for example special structures (bridges with long spans such as bowstring bridges), have to be solved using generic finite element programs.

Various programs such as ANSYS, NASTRAN, ABAQUS, SAP, FASTRUDL and so on, can be used to obtain the modal responses of bridge decks. Modelling can be done with beam models using torsional characteristics if the bridge is not a skew bridge and the structure is not a special case (see above). However, spatial modelling is necessary in such cases.

Dynamic analysis of a structure can be used to resolve a system of differential equations of lesser importance. Two fundamental approaches may be implemented: one method

consists in solving the system of equation by direct integration, whereas the other defines the solution based on the natural modes of vibration of the structure. This is known as modal superposition.

2.5.1 Modal analysis

Knowledge on modal analysis is extracted from UIC²³

Modal analysis is used to calculate the natural modes and frequencies of the model, as well as resulting variables(participation factors, effective modal masses)

For undamped, free vibrations, the equation of movement without a second element is reduced to:

$$[K] - \omega^2 [M][\Phi_i] = 0$$

where Φ represents the circular frequency vector (=pulse) and $[\Phi]$ is the modal crossing matrix consisting of natural orthonorm modal vectors $[\Phi_i]$ in relation to $[M]$ or $[K]$.

In principle, all the modes with natural frequencies lower than the cut-off frequency should be retained; in practice, the modes retained are often those making an important contribution to the response(criterion of the sum of effective modal mass of the structure). When the natural vectors are calculated, the modal matrix is formed $[\Phi]$ after which the ω_i can be deduced.

2.5.2 Analysis by modal superposition

Knowledge on modal superposition is extracted from UIC²³

The fundamental equation of the dynamic approach represents a system of N simultaneous differential equations, where N is the number of degrees of freedom of the structure. If three-dimensional modelling is used, this number N is equal to six times the number of nodes less the number of ddl blocked at the supprt. When the number increases to a value that is very high for large models, the size of the problem needs to be reduced by transformation techniques. Solving the differential equations then becomes faster and is more accurate.

The integration method used is now as follows: for each mode i, the resulting equation gives an evaluation introduced by the Duhamel integral of the Fourier transform. The sum of the solutions gives the full response. The integration approach for mobile loads is a slow process.

Modal superposition is used to accurately quantify the respective contributions of each mode to the total dynamic response and to identify the risks of resonance and dynamic amplification of some types of stresses.

2.5.3 Numerical methods

Knowledge on numerical methods is extracted from UIC²³

When the analysis uses numerical methods to directly integrate the dynamic equation, the loads become the dynamic system in the case of vehicles and their internal behaviour impacts the response from the structure.

- the two systems can be considered separate systems,
- the vehicle can be considered a finite element.

This last method takes track profile defects into account and deduces the force of interaction between the structure and the vehicle as well as the internal forces in the dynamic system that is built.

In this method, the equation of the dynamics is solved, with or without prior transformation, by using the conventional algorithms for numerical resolution of second-degree differential equations. These numerical methods calculates the response to regularly spaced time intervals(in general). The selected time pitch determines the accuracy of the results and has a bearing on the length of computer calculations.

Numerical integration methods are all based on the search for balanced solutions of the dynamic equation at regular time intervals.

2.5.3.1 VAMPIRE

VAMPIRE is a FEM simulation software developed by DeltaRail. It allows the user to build a dynamic model of any rail vehicle and study the response of the vehicle to real measured track geometry or user specified inputs in the form of track displacements and external force inputs. Rail vehicles can be modelled with simulated instrumentation allowing almost any aspect of behaviour to be studied.

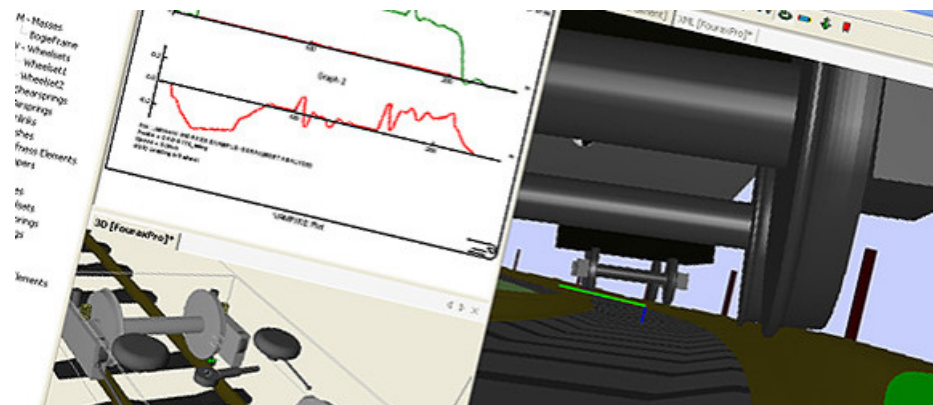


Figure 2.12: A sample project being conducted in VAMPIRE

There are also many similar simulation software on the market which puts emphasis on railway vehicle dynamic behaviour, but VAMPIRE is specially selected for introduction because it was the software used by D181 committee, whose report series originally proposed 1.2Hz criterion by using the assistance of VAMPIRE. Also, the output results provided by D181 reports is an important foundation for the development of new practical method. More detailed description of these VAMPIRE simulation runs will be illustrated in Chapter.4.

Chapter 3

Literature Review of regulations regarding lateral railway bridge dynamics in 1991-2

Eurocode 1990 and Eurocode 1991-2 and their corresponding National Annex are primary codes to be fulfilled through out the whole process of conducting a railway bridge in Netherlands. It is of great importance to study dynamic effect on railway bridges due to increasing usage of public train service.

This literature review aims to filter out criteria and requirements related to lateral railway bridge dynamics in EN1991-2.

3.1 Factors influencing dynamic behaviour

As stated in CEN⁵, 6.4.2 there are 11 factors influencing dynamic behaviour of a railway bridge. The principal factors which influence dynamic behaviour are:

- the speed of traffic across the bridge
- the span L of the element and the influence line length for deflection of the element being considered
- the mass of the structure
- the natural frequencies of the whole structure and relevant elements of the structure and the associated mode shapes (eigenforms) along the line of the track
- the number of axles, axle loads and the spacing of axles
- the damping of the structure
- vertical irregularities in the track
- the unsprung/sprung mass and suspension characteristics of the vehicle
- the presence of regularly spaced supports of the deck slab and/or track (cross girders, sleepers etc.)
- vehicle imperfections (wheel flats, out of round wheels, suspension defects etc.)
- the dynamic characteristics of the track (ballast, sleepers, track components etc.)

Other factors may include:

1. The track number of the bridge and their alignment.
2. Multiple trains running on bridge simultaneously.
3. Track alignment

3.2 Requirements for railway bridge verification

CEN⁶ propose following requirements. Criteria regarding lateral direction are bolded.

1. Checks on bridge deformations shall be performed for traffic safety purposes for the following items:
 - vertical accelerations of the deck
 - vertical deflection of the deck throughout each span
 - unrestrained uplift at the bearings(to avoid premature bearing failure)
 - vertical deflection of the end of the deck beyond bearings(to avoid destabilising the track, limit uplift forces on rail fastening systems and limit additional rail stresses)
 - twist of the deck measured along the centre line of each track on the approaches to a bridge and across a bridge(to minimise the risk of train derailment)
 - rotation of the ends of each deck about a transverse axis or the relative total rotation between adjacent deck ends(to limit additional rail stresses, limit uplift forces on rail fastening systems and limit angular discontinuity at expansion devices and switch blades)
 - longitudinal displacement of the end of the upper surface of the deck due to longitudinal displacement and rotation of the deck end(to limit additional rail stresses and minimise disturbance to track ballast and adjacent track formation)
 - **horizontal transverse deflection(to ensure acceptable horizontal track radii)**
 - **horizontal rotation of a deck about a vertical axis at ends of a deck (to ensure acceptable horizontal track geometry and passenger comfort)**
 - **limits on the first natural frequency of lateral vibration of the span to avoid the occurrence of resonance between the lateral motion of vehicles on their suspension and the bridge**
2. Checks on bridge deformations should be performed for passenger comfort, i.e. vertical deflection of the deck to limit coach body acceleration in accordance with A2.4.4.3CEN⁶
3. The limits given in A2.4.4.2 and A2.4.4.3CEN⁶ take into account the mitigating effects of track maintenance (for example to overcome the effects of the settlement of foundations, creep, etc.)

3.3 Horizontal transverse dynamic effects

There's only one criterion in the Eurocodes mentiones that the bridge's first lateral natural frequency should not be lower than 1.2 Hz.

However, as more and more long-span bridges are built nowadays, this requirement is not valid for more bridges. This is because, in general, the lateral natural frequency of a bridge decreases when span increases. For bridges with span longer than 150m, there's few bridge can have a lateral frequency higher than 1.2Hz, according to senior engineers' designing experience.

So it is vital to discuss horizontal dynamic effects for the sake of longer span bridges. In addition, a study has been carried out on the requirements for horizontal vibration of railway bridges to make the results of dynamic analysis usable.

3.3.1 Nosing force

Nosing force is defined in Eurocode 1991-2. Its original background can be found in D181Committee¹⁰, Proposed criteria. It is defined as a representation of actions, in combine with actions like vertical loads, dynamic effects, centrifugal forces, traction and braking forces, etc.

The evidence of RP6 is the background of nosing force in EN1991-2 is the following repeating literature:

In CEN⁵, 6.5.2:

(1)P The nosing force shall be taken as a concentrated force acting horizontally, at the top of the rails, perpendicular to the centre-line of track. It shall be applied on both

straight track....

In D181Committee¹⁰, 4.1B:

These forces shall be applied at the top of the rails in the most unfavourable position and acting horizontally, perpendicular to the track centreline...

With another statement also helps proofing RP6 is the background of nosing force in EN1991-2 in D181Committee¹⁰, 4:Draft Recommendations:

These can therefore be expressed as follows: (Article **6.5.2** of ENV 1991-3 of 1994)...

ENV 1991-3 was renamed to EN 1991-2 in 2003.

Originally in D181Committee¹⁰, 4:Draft Recommendations, nosing forces was defined as lateral forces from vehicle/bridge interaction as a result of **hunting**.

The characteristic value of the nosing force shall be taken as $Q_{sk} = 100kN$. It shall not be multiplied by the factor Φ (CEN⁵, 6.4.5) or by the factor f in CEN⁵, 6.51.

The characteristic value of the nosing force should be multiplied by the factor α in accordance with CEN⁵, 6.3.2 for values of $\alpha \geq 1$

The nosing force shall always be combined with a vertical traffic load.

A detailed analysis on the background of nosing force will be given in Section 4.3.2

3.3.2 Verification of the Limit States

CEN⁵, 6.4.6.5 proposes following principles to be followed during design:

To ensure traffic safety:

1. The verification of maximum peak deck acceleration shall be regarded as a traffic safety requirement checked at the serviceability limit state for the prevention of track instability
2. The dynamic enhancement of load effects shall be allowed for by multiplying the static loading by the dynamic factor Φ defined in CEN⁵, 6.4.5. If a dynamic analysis is necessary, the results of the dynamic analysis shall be compared with the results of the static analysis enhanced by Φ (and if required multiplied by α in accordance with CEN⁵, 6.3.2) and the most unfavourable load effects shall be used for the bridge design.
3. If a dynamic analysis is necessary, a check shall be carried out according to CEN⁵, 6.4.6.6 to establish whether the additional fatigue loading at high speeds and at resonance is covered by consideration of the stresses due to load effects from $\Phi \times LM71$ (and if required $\Phi \times LoadModelSW/0$ for continuous structures and classified vertical load in accordance with CEN⁵, 6.3.2(3) where required). The most adverse fatigue loading shall be used in the design.

3.3.3 Serviceability limit states - traffic safety

3.3.3.1 Transverse deformations and vibrations

199¹, A2.4.4.2.4 proposed that transverse deformation and vibration of the deck shall be checked for characteristic combinations of Load Model 71 and SW/0 as appropriate multiplied by the dynamic factor ϕ and α (or real train with the relevant dynamic factor if appropriate), wind loads, nosing force, centrifugal forces in accordance with CEN⁵, 6 and the effect of a transverse temperature differential across the bridge.

The transverse deflection δ_h at the top of the deck should be limited to ensure:

1. a horizontal angle of rotation of the end of a deck about a vertical axis not greater than the values given in Table. 3.1 , or
2. the change of radius of the track across a deck is not greater than the values in Table. 3.1 , or
3. at the end of a deck the differential transverse deflection between the deck and adjacent track formation or between adjacent decks does not exceed the specified value

Speed range V(km/h)	Maximum horizontal rotation(radian)	Maximum change of radius of curvature	
		Single deck	Multi-deck bridge
$V \leq 120$	α_1	r_1	r_4
$120 \leq V \leq 200$	α_2	r_2	r_5
$V > 200$	α_3	r_3	r_6

NOTE 1 The change of the radius of curvature may be determined using:

$$r = \frac{L^2}{8\delta_h}$$

NOTE 2 The transverse deformation includes the deformation of the bridge deck and the substructure(including piers, piles and foundations).

NOTE 3 The values for the set of α_i and r_i may be defined in the National Annex. The recommended values are:

$$\begin{aligned}\alpha_1 &= 0.0035; \alpha_2 = 0.0020; \alpha_3 = 0.0015; \\ r_1 &= 1700; r_2 = 6000; r_3 = 14000; \\ r_4 &= 3500; r_5 = 9500; r_6 = 17500\end{aligned}$$

Table 3.1: Maximum horizontal rotation and maximum change of radius of curvature

The first natural frequency of lateral vibration of a span should not be less than f_{h0} . The value for f_{h0} may be defined in the National Annex. The recommended value is: $f_{h0} = 1.2\text{Hz}$

Evidence of D181Committee¹⁰ is the origin of CEN⁵, A.2.4.4.2.4(3) is found in D181Committee¹⁰, p4.2: Lateral Frequencies:

In order to avoid the phenomena of lateral resonance in vehicles, the first natural frequency of lateral vibration of the span f_{lt} such that:

$$f_{lt} \geq 1.2\text{Hz}$$

Until now there's no further instructions in EN1991-2 for bridges which can not pass 1.2Hz criterion. However, for bridges longer than 100 meters, they are almost guaranteed to fail 1.2Hz criterion. In order to solve this problem, a detailed analysis is conducted in Sec.4.3.1

3.4 Conclusion

By reviewing EN1991-2 thoroughly, it is found that there are altogether two regulations regarding lateral dynamics of railway bridges. They are:

1. Nosing force(action)
2. 1.2Hz criterion

Although vertical dynamics of railway bridges is focused a lot, there's only two statements about lateral dynamics of railway bridges. What's more, there's no quantifying criteria even if a dynamic analysis is done.

These two regulations have the same background documents: D181 report series. The analysis of D181 report series will be carried out in following chapter.]modeltrackstructure.pdf

Chapter 4

Investigation of report series created by D181 Committee Group

4.1 Introduction

D181 Committee Group is created by UIC, in order to investigate Lateral Forces on Railway Bridges. Some of the proposed criteria in reports created by this committee group are adopted by Eurocode Committee to created Eurocode 1991-2. The goal of this investigation is to summarize the research done by D181 report series and give further conclusion.

The investigation will be done in following aspects:

1. Investigation of DT329
2. Investigation of RP6
3. Conclusion of D181 report series

4.1.1 Structure of report series

Reports involved in the series are listed below in the order of publishing time:

1. RP 1: Summaries of national standards and literature survey
2. RP 2: Submitted programs and example of application
3. RP 3: Dynamic measurements on the steel bridge over the Brenta river on the MilanVenice line at 234 + 0.963 km
4. RP 4: Dynamic measurements on steel bridges over the Vh river by Sala on the MarcheggSzob line at 117 748 km
5. DT 312: Etude de l'influence de la frquence du filtre sur les valeurs mesures des forces verticales et latrales sur les rails
6. RP 5: Dynamic measurements on the metal arched bridge on PKP
7. DT 313: Analyse des dformations latrales d'un pont souple (cas du PONT de LIXHE) Ligne SNCB de TONGRESMONTZEN par J.J. REBER SBB Bau GD
8. DT 329: Parametric study Part 1: Parametric study Initial phase (September 1994) Part 2: Parametric study Phase 2 (February 1995) Authors: L.T. James and G.A. Scott
9. RP 6: Final Report

In this thesis DT 329 and RP 6 are obtained and studied, but other reports in English version are not available to the researcher.

4.1.2 Items of interests in report series

1. Resonance mechanisms studied. They are discussed in DT329. See Section 4.2.3

2. The proposed 1.2 Hz Criterion and its background. It is discussed in RP6. See Section 4.3.1
3. Lateral forces(Nosing force) on the bridges. See Section 4.3.2

4.2 Investigation of DT329

4.2.1 Methodology of Parametric Research DT329

The DT329 research was conducted in two phases. It is noted that all studies were done using VAMPIRE software. The reliability of simulation has been discussed and confirmed in a previous report of D181 Committee¹².

In the initial phase 11 sets of bridge parameters were selected for the simulation. 52 combinations of bridge parameters and train configurations were examined. The goal of the initial phase is to filter out most influencing parameters for bridge dynamics.

In the secondary phase, the influence of selected parameters were categorized into 3 cases. They include:

1. the influence of multiple span bridges (viaducts)
2. the influence of track quality
3. the influence of stiffness/span/frequency on the resonant behaviour of the bridge

They were studied by using the same simulation method used in initial research phase.

4.2.2 Modelling

A special version of VAMPIRE with bridge module implemented was used to run simulation analysis.

For an overview of modelling setup in both research phases, see Figure 4.1. Following paragraphs will give details of modelling.

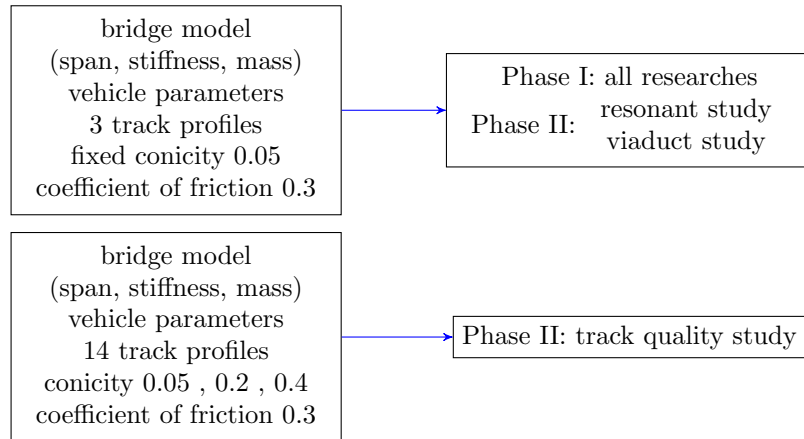


Figure 4.1: Overview of modelling setups for different studies conducted in DT329

4.2.2.1 Model of bridge

The bridge cases were modelled by assuming the bridges to behave as simply supported uniform beams. Transverse beam theory was then used to determine the frequencies and mode shapes of vibration for a given combination of span, mass per unit length and flexural rigidity. The modal information for the bridge was then used in a 'Normal Modes' analysis of the bridge.

For each case, all lateral modes of vibration up to and including 20 Hz were used. In order to prevent this artificially over-simplifying the model, if fewer than five modes were 20 Hz or less, all of the first five were used.

4.2.2.2 Bridge parameters

The spans considered were: 20 m, 33 m, 54 m, 90 m and 120 m. The flexibilities, defined as deflection of mid span over span length due to a static point load of 100 kN at mid span, are: 1/4000, 1/10000, and 1/20000. The mass per unit lengths required are: 2 tonnes/m, 6 tonnes/m, and 10 tonnes/m.

For the initial phase, see Figure 4.2 for a selection of eleven of the possible combinations examined.

Span	Flexibility	Mass/Length	Cases
20	1/10000	6	36-40, 52
33	1/10000	6	41-43
54	1/4000	2	16-20
54	1/4000	10	21-25
54	1/10000	2	1-5
54	1/10000	6	6-10
54	1/10000	10	11-15
54	1/20000	2	26-30
54	1/20000	10	31-35
90	1/10000	6	44-46
120	1/10000	6	47-51

Figure 4.2: Bridge parameter combination

4.2.2.3 Vehicle parameters

Three train types are considered: a typical freight train, a typical standard passenger train, and a typical high speed passenger train. Appendix.A details the parameters used to construct each model. In general, each model consists of a locomotive and a number of identical vehicles appropriate to the train type. The total number of axles in each train is 24. Although effects on the train are only examined on the first vehicle of each type, extra vehicles are added to the train to see what cumulative effects occur to the bridge.

The freight train consists of a British Railways Class 56 locomotive and nine UIC wagons. This has a total length of 131.56 m, which assumes a nominal vehicle coupling distance of 4 m. Runs at 60 km/h and 100 km/h are required.

The standard passenger train consists of an E444 locomotive and five UIC coaches. This has a total length of 143.8 m. It is based on one of two train models used as part of the study of the FS Bridge discussed in report RP 3 of the Committee, differing only by the addition of three extra coaches. This is required to run at 160 km/h and 200 km/h.

The high speed passenger train consists of an ETR500 locomotive and five ETR500 coaches, having a total length of 145.8 m. It is based on the other FS bridge study train model mentioned above, differing from the original by an additional three ETR500 coaches. It is required to run at 300 km/h and 350 km/h.

4.2.2.4 Track

For initial study phase, the track samples used were consistent with each train type. PSD plots of each are shown in Figures A.13 to A.15. Sample TRACKFRT.DAT was used for all analysis runs for the freight train. This is measured data from a typical BR freight line. Sample TRACKPNT.DAT was used for the standard passenger train analysis runs. This is measured data from a part of the BR East Coast main line. Sample TRACKPH.DAT was used for high speed passenger train analysis runs. This is measured data from a typical DB high speed line.

Samples of 500 m were chosen so that there would be 100 m before the bridge and at least 100 m after the bridge for all combinations of span and train length. The initial 100 m is required to check vehicle behaviour on the track irregularity alone, and the portion after the train has left the bridge is required to check that the bridge vibrations decay.

For secondary study phase, the track data used to excite the mathematical models was taken from the British Rail Research library of measured track data. For the viaduct and resonance investigations, the track files used were the same as those used in the first part of the study. For the investigation of the influence of track quality, additional track data was used so as to give the widest possible range of realistic track qualities.

4.2.2.5 Contact data

For each run the same contact data was used, consisting of rails inclined at 1:20, and wheel profiles of conicity of 0.05 (based on standard British Rail 113A rails and PI wheel profiles). The coefficient of friction applied was 0.3.

4.2.2.6 Data produced

For every analysis run the following results were obtained at intervals of 0.01 seconds.

BRIDGE DATA:

Lateral displacement at mid span Lateral acceleration at mid span

VEHICLE LATERAL ACCELERATION DATA:

Loco body at leading pivot

Leading coach/wagon body at leading pivot/axle

Loco leading bogie

Leading coach/wagon leading bogie/axle

TOTAL LATERAL FORCE DATA:

Loco leading bogie

Leading coach/wagon leading bogie/axle

LATERAL FORCES ON INDIVIDUAL WHEELS

Leading coach/wagon, first axle, left and right wheels

Leading coach/wagon, second axle, left and right wheels

Loco, first axle, left and right wheels

Loco, second axle, left and right wheels

In addition, for freight train runs, since the locomotive has two bogies of three axles, the forces on the individual wheels of the third axle were also produced.

Peak values for each of the outputs produced for the required ranges were obtained. For bridge outputs, peak values were taken for the period where any part of the train was on the bridge. For loco and leading coach/wagon outputs, peak values were taken whilst the vehicle in question was in contact with the bridge.

Peak values for each output were then read into a spread sheet where they could be compared more easily to check for emerging trends. The spread sheet has been partially automated to produce graphs of a single output for each train type for a single varying bridge parameter, for given values of the other bridge parameters. Figures 4 to 30 of original D181Committee¹¹ report show typical plots which have been produced in this manner.

4.2.3 Investigation of resonance phenomenon studied in DT329

2 types of resonance were studied in DT329, including:

1. Resonance caused by axle repeat pattern
2. Resonance caused by kinematic movement

The summary of these resonances effects are presented in following paragraphs.

Frequency shift phenomenon is an important characteristics observed from resonance effects lists above. It is explained in Section 4.2.3.3

4.2.3.1 Resonance caused by axle repeat pattern

Axle repeat patterns are wavelength phenomena - regardless of vehicle speed, the repeat length is constant. However, since frequency is speed divided by wavelength, the frequency of the axle repeat patterns vary with train speed. A table of axle repeat pattern lengths, and typical frequencies arising from train speed are given in Figure.A.1

By running train at different speeds shows resonance is possible between train and bridge if the axle passing frequency coincides with the first lateral bridge mode. The effect occurring in bridge lateral displacement over a limited frequency range around the resonance frequency.

However, the speed on theory which should yield resonance effect may be different from the speed that actually triggered resonance.

4.2.3.2 Resonance caused by kinematic movement of trains

Kinematic wavelength also gives rise to frequencies which vary with speed for the same reason. For first lateral bending mode coincidence with kinematic frequency, the kinematic wavelength of each train type had to be established, by running each train at a range of typical operating speeds over a discrete lateral irregularity, and examining the frequency content of the lateral wheel motion. The resulting wavelength ranges are tabulated in Table.A.2. See Figure 4.3 for an overview of workflow of this study.

The most likely possible resonance in the initial studies to be of this type was between the passenger train at 200 km/h (55.556 m/s) on passenger track and BR PI wheel profiles, and a span of 54 m, stiffness 1/10000, mass/length of 6 tonnes/m. This combination was examined by varying the speed between 55.556 - 64.6 m/s over the span, and by varying the stiffness of the span between 117000 and 1112000 running the train at 55.556 m/s. Another combination was examined - the ETR500 train running between 65 - 80 m/s on high speed track and BR PI wheel profiles, for a span of 38 m, stiffness 1110000, and mass/length 10 tonne/m; the span in this case was chosen to coincide with the kinematic wavelength of the coaches.

Coincidence of vehicle kinematic frequency with bridge first lateral bending mode may cause resonance to occur over a broad range of frequencies to a less pronounced effect than coincidence of axle passing frequencies. Evidence of coincidence of kinematic wavelength with length of span has been found in the lateral acceleration of bridges, but was not demonstrated in the lateral bridge displacement in the cases examined. For short kinematic wavelengths, this effect could not be seen, possibly because of lack of time for the bridge to respond.

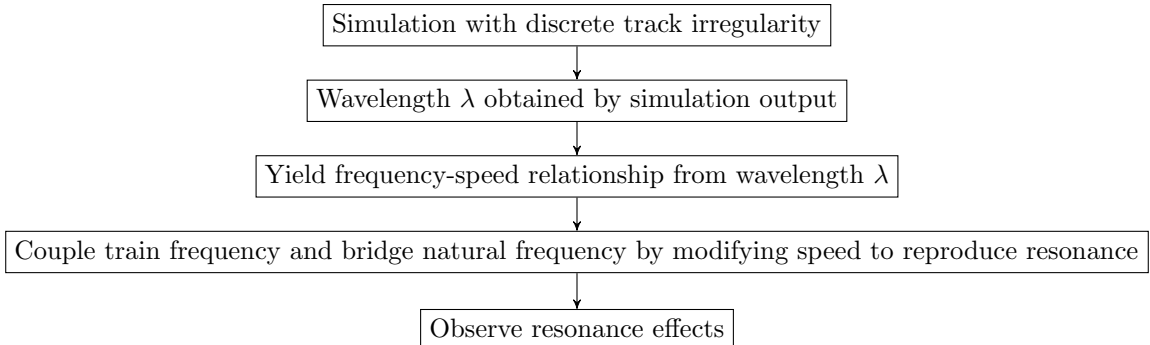


Figure 4.3: Workflow of kinematic resonance research

4.2.3.3 Apparent shift in resonance frequency

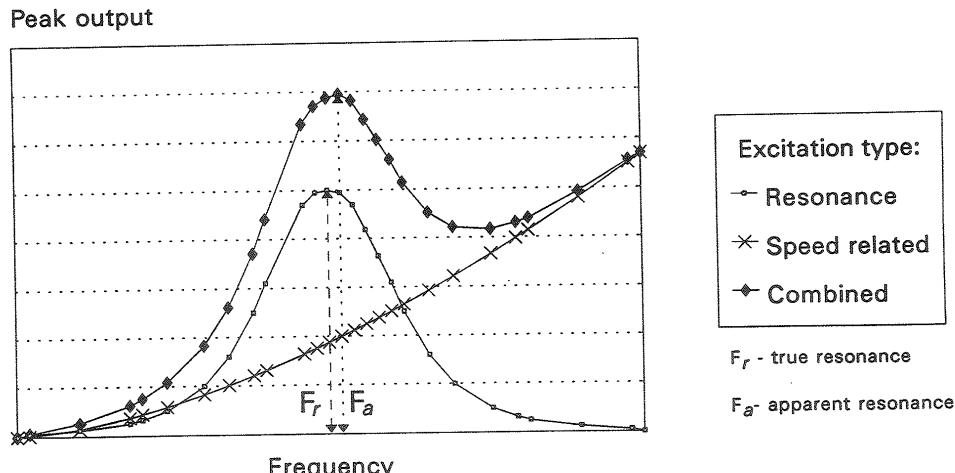
It is frequently observed in the output of both resonance effects that apparent resonance happens at some frequencies higher than frequencies calculated on theory. This is explained in following quote on D181Committee¹¹, Page 13, Secondary Phase. However, the explanation wasn't verified by further studies. They can only be treated as hypothesis.

Although the peak mid span displacement was expected to occur at 28.5 mis, it can be seen that for the runs with just the coaches that the peak occurs at about 32 m/s. This is confirmed to be a resonance-type effect rather than a discrete event in the time histories of the runs, a selection of which are shown in Figure C6(Original report), of which an extract of 100-285m follows as Figure C7(Original report). This speed is mid way between axle passing frequency coinciding with first bending mode of the bridge, and kinematic frequency coinciding with the first bending mode. So, the apparent shift in resonant frequency may be due to a combination of these effects (see discussion of kinematic frequency resonance results). However, an alternative explanation may be that as track forces generally increase with speed, the deflection of the span would be expected to increase. If this effect continued through a resonant band, the peak displacement would appear greater at a speed slightly above that calculated for resonance, as sketched in Figure 4.4.

In the sketch of possible explanation of apparent shift in resonant frequency(Figure 4.4), the combined effect is the superposition of both resonance effect and speed-related effect. Speed-related effect simply increase when speed increase regardless of resonance. Speed is linear to frequency. Thus speed-related effect also simply increase when frequency increases. Resonance effect has an impact where frequency of train and bridge coincides. Speed-related effects is the cause for the frequency shift of combined peak output.

Both explanations indicate that apparent resonance frequency can hardly be predicted. Apparent frequency may even shift into domain lower than theory frequency.

Sketch of Possible Explanation of Apparent Shift in Resonant Frequency



ERRI D181 PARAMETER STUDY
DJ/82879/D001
British Rail Research

Figure C8

Figure 4.4: Sketch of Possible Explanation for Apparent Shift in Resonant Frequency. Extract from D181Committee¹¹, Appendix 2

4.3 Investigation of RP6

4.3.1 Debate on proposed 1.2Hz criterion

The value of frequency limit, 1.2Hz is explained in D181Committee¹⁰, p3.2: Criterion 2:

To avoid the occurrence of resonance in the lateral motion of the vehicles due to the lateral motion of the bridge, a limit value lower than the first natural frequency f_{1t} of the lateral vibration of the span studied should be fixed. The natural frequency for lateral movements is between 0.5 and 0.7 Hz for coaches and between 0.7 and 1 Hz for locomotives. We therefore propose a safety margin $F_{lt} \geq 1.2\text{Hz}$

The original author of report RP6, mr.Graham Scott, was contacted to reveal the background of 'natural frequency for lateral movements'. Mr.Scott is still in charge of the development of software VAMPIRE and he's still active in the field. Unfortunately he was unable to remember what did 'natural frequency for lateral movements' stand for in previous quotes since it was written nearly 20 years ago. He passed me to his colleague Alan Minnis for further questions. Mr.Minnis stated following:

Looking at the values I think they would refer to typical rigid body modes of a vehicle. These are independent of speed and a typical passenger coach with air suspension will have a lower sway frequency of around 0.6Hz which is within 0.5-0.7Hz. Locomotives tend to have a slightly stiffer suspension hence the slightly higher frequency range.

Mr. Minnis statements, combined with results yielded in supporting parametric report DT329 proves 1.2Hz criterion is aiming to avoid occurrence of resonance. But this isn't a feasible strategy for the following reasons:

1. The resonance between rigid body mode of train and first lateral vibration mode of the bridge has never been discussed in all D181 report series. No research proofed this kind of resonance can be critical in real life scenario.
2. There are lots of evidence can be found in report DT329, showing resonance can happen on a bridge with a first lateral natural frequency even higher than 1.2Hz, which is self-conflicting with 1.2Hz criterion. In fact, the resonance could happen at any frequency on theory. However, the magnitude of resonance effect ranges from less pronounced to more pronounced from case to case.

For example, D181Committee¹¹, Page 14,Phase II shows resonance occurs on 1.71Hz:

The first lateral bending mode of this bridge is at 1. 71 Hz. The kinematic wavelength of the passenger coaches is around 34-38 m, giving a kinematic frequency range of 1.46 - 1.63Hz. Speeds of 58.14 m/s(1.53-1.71 Hz)and 64.6m/s(1.7-1.9Hz)were also done. The mid span lateral displacement for each of the time histories are shown in Figure C12(Orignal report). The slowest speed appears to show the greatest resonance.

4.3.2 Lateral forces on railway bridges

4.3.2.1 Basic characteristics of lateral force on railway bridges

It is concluded in initial phase of the study that presence of the bridge doesn't influence the track forces and track quality is a major factor in determining the lateral forces generated by a particular train on D181Committee¹¹, Page 7, Secondary Phase

From the initial study [1], it was concluded that the track quality on a bridge is a major factor in determining the lateral forces generated by a particular train. The D181 Committee therefore asked BRR to determine the peak track forces generated over a wide range of track qualities.

The length of a bridge is small compared to the overall length of a railway track and so track quality on a single bridge may not be representative of that on other bridges on the same route. However the initial study concluded that, in general, the lateral track forces are not influenced by the presence of the bridge.

The resonance effects mentioned in the previous sections were only observed in deflection and acceleration domain due to the reason that the presence of the bridge doesn't influence the track forces.

Influence on the total lateral force as a result of hunting of single vehicle bodies were examined. Three parameters were involved in this parametric research. They were vehicle speed, track irregularities deviation and wheel conicity.

Vehicle speed plays a key role. When speed is 60 km/h for freight trains, in the response output, there is very limited influence by increasing both track deviation and conicity. Different conicity tends to yield same force output. Same as track deviation. See Figure.4.5.

When speed increases, output of different conicity on same track deviation is more scattered. Similarly, increased deviation yields greater output. They are two basic trends observed in all output data.

However, it is uncertain which conicity will yield greater output compared to other 2 conicity setups. Surprisingly, in some cases, best maintained wheel profile (effective conicity 0.05) generates greater output than poorly maintained wheels (effective conicity 0.4). See Figure.4.6. The most

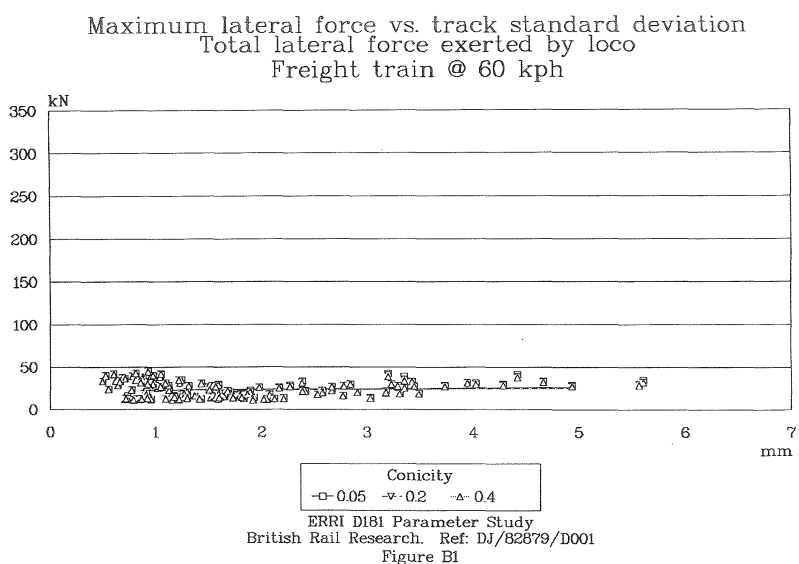


Figure 4.5: Figure B1 extracted from D181Committee¹¹

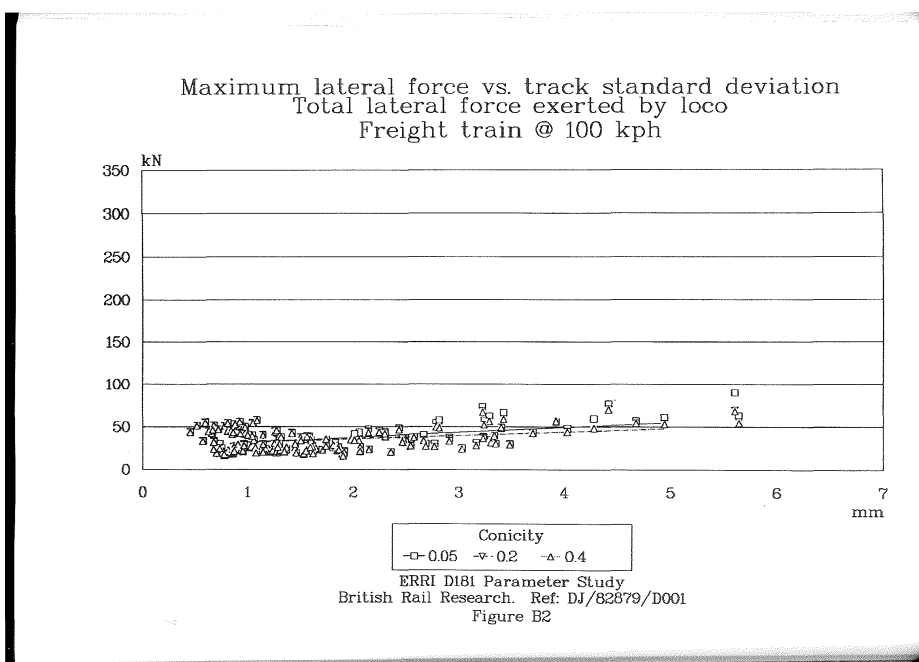


Figure 4.6: Figure B2 extracted from D181Committee¹¹

obvious case of this kind is freight train running at 100 km/h on track with 5.7mm (approximate) deviation.

Different from conicity, the influence of increasing track deviation is simply predictable. Research report DT329 provided an approximate linear function for relationship between lateral force and

track deviation. These linear functions can be extracted from plots B1-B30 of DT329.

Since peak force output of 120 km/h freight train and 200 km/h passenger train are close(2% difference), it is reasonable to conclude that passenger train tends to yield smaller result than freight train at same speed. This is probably due to passenger trains have more sophisticated suspension system designed to suppress lateral motion of the vehicle. Unfortunately, only one speed of 200km/h configuration was available in DT329. But since freight train yields greater output, it is conservative for designer to adopt force output of freight trains for speeds of 60km/h, 100km/h, 120km/h.

It is worthy to point out a suspicious mistake of DT329 in Table.4.1. Report claimed that output data were filtered by statistical analysis. The peak lateral track force was determined from a statistical analysis of lateral track forces as $M \pm 3\sigma$ where M is the mean lateral force value over the segment and σ is the standard deviation over the segment. It does not give a true maximum lateral force but on which is greater than 99.5% of all force values. It is obvious in Table.4.1 that output data of 160kN for freight train wagon was not filtered by statistical analysis. It is the greatest value among all raw output data of freight train running at 100 km/h. See Figure.4.7. This data of 160kN also illustrates that peak forces will be influenced by discrete features in the track geometry which may not be reflected thoroughly in the standard deviation. This thesis report suggest substitute 160kN with 80kN(value by approximate observation). See Table.[note1]4.1

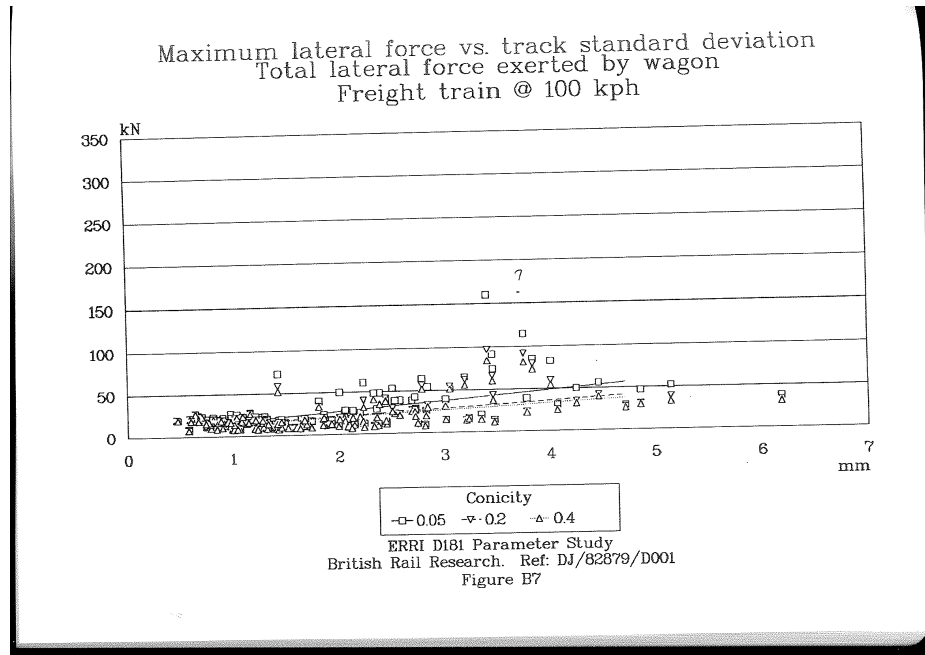


Figure 4.7: Figure B7 extracted from D181Committee¹¹

Speed and track quality are two most sensitive parameters. Control of track quality is more advisable compared to control of wheel conicity due to the reason that influence of track quality deviation is simply approximate linear to force output, whereas influence of wheel conicity has an unpredictable characteristic. Moreover, track quality can be controlled by using a maintenance regime.

4.3.2.2 Refining of lateral force model

Figure.4.8 is created to plot total peak force illustrated in Table.4.1. 5 sets of data available were used to create the plot. 3 of them are data of freight train running at 60km/h, 100km/h and 120km/h. The other 2 sets of data are passenger train running at 200km/h and high speed train running at

Table 4.1: Peak Lateral Track Force Over All Track Qualities. Extracted From D181Committee¹¹, Tab. B1

Peak lateral force(kN)	Locomotive	Total	Coach/Wagon	Total
Freight 60 km/h	50		60	110
Freight 100 km/h	90		160(80) ¹	250(170) ¹
Freight 120 km/h	75		110	185
Passenger 200 km/h	140		50	190
High Speed 350 km/h	125		125	250
Passenger 200 km/h(worn wheels)	190		80	270
High Speed 350 km/h(worn wheels)	330		225	555

Note1: Force value 160kN for wagon of freight train running at 100 km/h is not representative. But it is not filtered by statistical analysis. It is advised to substitute 160kN with 80kN. 80kN is obtained by approximate observation of D181Committee¹¹, Figure B7. As a result, total force is reduced from 250kN to 170kN.

350km/h respectively. Data produced with worn wheels profiles are neglected because they are not representative for normally maintained railway vehicles. Adjacent points were connected by solid lines. Different colour stands for different train types. Red lines and dots stand for freight trains. Blue stands for passenger trains and black stands for high speed trains.

It is indicated that freight trains tends to have the biggest lateral force on track compared to other two kind of trains. And high speed train has lowest lateral force on track. This can be explained by freight trains possessing the most stiff suspension systems, while high speed trains possessing complicated suspension system to suppress lateral motion.

It can also be concluded that the relationship between lateral force and speed is not linear. As a general phenomenon observed, force increment decreases as speed increases. Regressions were made to better illustrate the trend of lateral force increment. Please note these regressions are only sufficient within the speed range plotted.

The first regression made was on freight train because it has the most sets of data. The form of function should satisfy:

1. 0kN lateral force when speed is 0km/h
2. Simply increasing in value but generally decreasing in increment

Finally function form $F = a * v^b$ is selected because its satisfying characteristics. R language was used to perform regression process. The regression result is also in good likelihood with original data. Achieved convergence tolerance was 2.868e-06. The result is presented in Formula.4.1. See Appendix.D for code.

$$F_{lf} = 5.2064 \cdot v^{0.7495} \quad (4.1)$$

Since 1 set of data is available for passenger train, Formula.4.1 is scaled by a constant factor to create regression for passenger trains. Please note that this regression can not be verified because lack of data. However, since freight train has a greater lateral force then passenger train, it is conservative to adopt lateral force of freight train when calculating consequences related to passenger trains. It is still reasonable to adopt this regression since passenger trains are just simply less stiff than freight trains.

Unfortunately, conducting such transient simulations is extremely time and resource consuming. It is impossible for this thesis to carry out more simulations to verify the sufficiency of following scaled regression. More data on passenger train and high speed train is recommended to be produced by future researches.

The scale factor k_{pf} is obtained by comparing force value yielded by Formula.4.1 at 200km/h

and original passenger train force(190kN) data at 200km/h.

$$k_{pf} = \frac{190}{a_{lf} \cdot 200^{b_{lf}}}$$

$$a_{lp} = a_{lf} \cdot k_{pf}$$

merge above two equations, yield

$$a_{lp} = \frac{190}{200^{b_{lf}}} = \frac{190}{200^{0.7495}} \approx 3.58$$

and

$$F_{lp} = a_{lp} \cdot v^{0.7495}$$

thus

$$F_{lp} = 3.58 \cdot v^{0.7495} \quad (4.2)$$

Lateral force for high speed train were obtained in same manner. The scale factor k_{hf} is obtained by comparing force value yielded by Formula.4.1 at 350km/h and original high speed train force(250kN) data at 350km/h.

$$k_{hf} = \frac{250}{a_{lf} \cdot 350^{b_{lf}}}$$

$$a_{lh} = a_{lf} \cdot k_{hf}$$

merge above two equations, yield

$$a_{lh} = \frac{250}{350^{b_{lf}}} = \frac{250}{350^{0.7495}} \approx 3.10$$

and

$$F_{lh} = a_{lh} \cdot v^{0.7495}$$

thus

$$F_{lh} = 3.10 \cdot v^{0.7495} \quad (4.3)$$

4.3.2.3 Application of lateral force model

Formula4.1,4.2 and 4.3 can be used as load forces for different design scenario. However, these loads are normally higher than the load defined in EN1991-2CEN⁵, 6.5.2 Nosing force. EN 1991-2 states that the characteristic value of the nosing force shall be taken as $Q_s k = 100kN$.

It is worthy to note that although in RP6D181Committee¹⁰, Proposed criteria several load model with loading magnitude ranging from 70 kN to 270 kN were originally proposed, EN1991-2 uses a single characteristic value of 100 kN for all design scenarios.

Since no document has explained this modification, this is probably due to the consideration of lower track irregularity deviation during the creation of EN1991-2.

As explained in previous chapter, peak force is generally linear to track standard deviation. Most of the peak lateral force described in DT329 was obtained on track with 7mm standard deviation, while EN13848-5CEN⁴ allows much lower track standard deviation defined in Table 2.1. This means peak lateral force on tracks(if maintained according to Eurocode regulations) is also much smaller than peak force obtained in DT329.

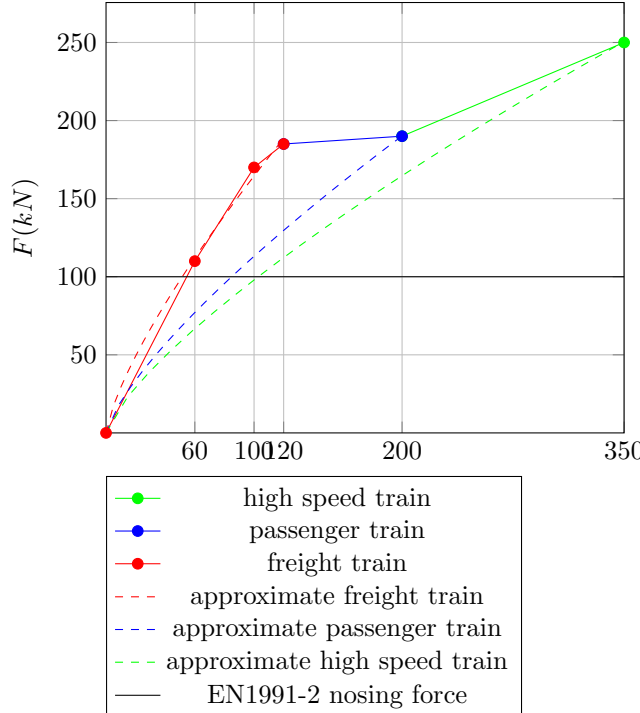


Figure 4.8: Total peak lateral track forces over all track qualities(worn profile scenario neglected)

EN1991-2 states the usage of nosing force. See 3.3.1. Moreover, since loading model is obtained in Figure.4.8, a response solution of the bridge can also be obtained.

This can be done by using the solution in 6 and substitute peak force into the formula as the amplitude of harmonic force F . Development of this method is presented in Chapter.7.

It should be noted that the proposed model in RP6, as well as modified model in EN1991-2, is based on the investigation of first two traction units of the train. It is suspected that when bridge is longer, more traction units can run on the bridge simultaneously, introducing bigger force to the bridge. This can lead to a problem that EN1991-2 is non-conservative in the magnitude of nosing force when applied to longer bridges. However, this suspecting hypothesis is not verified in this chapter.

4.4 Evaluating nosing force proposed by EN1991-2

The evaluation is done by comparing peak result of calculation adopting nosing force and of FEM VAMPIRE simulation on the same bridge.

The bridge in Figure.7.4 is chosen with following parameters:

$$l = 120m$$

$Stiff : 1/10000$ (deflection/span ratio at midspan under 100kN point load at midspan)

$$\mu = 6000kg/m$$

Peak result for VAMPIRE simulation: 17mm

According to section.3.3.1, the characteristic value of the nosing force shall be taken as $Q_{sk} = 100kN$. It shall not be multiplied by the factor Φ or by the factor f . Thus, according to simple support Euler-beam theory, the deflection under 100kN nosing force is:

$$\delta_{nosing} = 120m \cdot 1/10000 = 0.012m = 12mm$$

It can be seen that nosing force doesn't give conservative result compared to VAMPIRE simulations. A resonance effect was reproduced in simulation. Thus the reason for the nonconservative result is although some dynamic actions are taken into account by nosing force, the resonance effect is not included.

4.5 Conclusion of D181 report series

The report series managed to create load models for lateral dynamics railway effects. It is worthy to note that the lateral force on the track wasn't influenced by the presence of the bridge. The major influencing parameter for lateral force is track quality and conicity of the wheel profile.

The resonance phenomenon was successfully reproduced and observed, though its only visible in deflection and acceleration domain. A basic characteristic of resonance, regardless of the type of resonance, is that apparent resonance frequency will shift from resonance frequency calculated on theory. The shift is unpredictable in the sense of both direction and magnitude. The effect related to speed start to creep in when speed is higher, making the effect of resonance less pronounced in higher speed(Figure 4.4).

Please note that every bridge will always have resonance with running train because axle repeat pattern and kinematic movement are both wavelength phenomenon, which means there is always a speed of train yielding a vibration frequency coincides with the first lateral natural frequency of bridge. However, the effect of resonance happening on long-span bridge is usually unpronounced since the speed of the train is low as 2.5m/s to 14m/s when resonance occurs.

Some of the conclusion and proposed criteria in RP6 were adopted in Eurocode 1991-2. One of them is 1.2Hz criterion. It was adopted without amending. The other one is lateral force models. They were adopted in a different name as 'nosing force' in CEN⁵, A6.5.2.

The 1.2Hz criterion was under debate and proofed unreliable in fulfilling its original intention, avoiding occurrence of resonance. There is no research in D181 report series supporting this criterion, nor there exists literature behind the natural frequency of vehicles. This criterion ignored the fact that future bridge designs with long span would certainly have a natural frequency lower than 1.2 Hz. It is advised that Eurocode review this criterion and revise it.

Also, the nosing force proposed doesn't provide conservative result when there is resonance between the vehicle and the bridge.

Chapter 5

Lateral wavelength research on Dutch railway vehicles

As a conclusion in DT329 report, the lateral dynamic effects of railway vehicles are all wavelength phenomenon. The lateral wavelength of trains is a constant characteristics of themselves which doesn't change with outer environment. However, while the wavelength for axle repeat pattern is easy to get, the wavelength for kinematic movement normally requires heavy FEM simulations and post analysis of the response spectrum.

Although it has been concluded in the previous chapter that avoiding resonance frequency is not a correct strategy for dynamics design in general, investigating the wavelength of trains can serve for the practical analysing methods that will be developed in following chapters in an alternative way.

This research aims to investigate both wavelength of trains running in the Netherlands. The axle repeat pattern wavelength is created by collecting all the possible axle layouts. The kinematic movement wavelength is created by developing approximate methods that avoids heavy FEM simulations.

5.1 Effects investigated in wavelength study

Effects investigated in this report will be the same effects investigated in DT 329, which is described in Sec.4.2.3. However, according to the statement in Sec.2.3[Summary of results] in the same report,

Even when the axle repeat frequency matches the first lateral bending mode of each span, there is no evidence that the resonant behaviour of the span and train has any effect on subsequent spans, since the resonant effects do not appear to grow from span to span.

the third investigated resonance effect 'coincidence between the length of the span and the kinematic wavelength of the trailing vehicles' is neglected in this thesis because it is concluded in D181Committee¹¹ that resonance do not grow from span to span.

5.2 Equivalent conicity used in this study

According to Esveld¹⁴, Section.2.6,

Practical research has shown that over a period of time wheel profiles stabilise with wear at an equivalent conicity of 0.2 to 0.3. With regards to running stability, the equivalent conicity must remain below 0.4 and to ensure the centering effect it must be greater than 0.1.

conicity range will be 0.2 to 0.3.

It is suggested by this report that vehicle maintenance sector ensure wheels of train wheels stay in the safe zone of conicity.

5.3 Study on wavelength of lateral kinematic movement

The kinematic movement of the train on the rail is much similar to Klingel movement. This section aims to assess the capability of using Klingel formula to predict the wavelength of the whole train.

Klingel movement is proposed by Klingel which can well predict the moving trend of a single wheelset on a straight railway track. However, the kinematic movement of a certain wheelset assembled into a running train is different from the movement of a single free wheelset. This is due to multiple bodies interact with each other, introducing more complicated mechanism in wheel/rail interaction.

This study focuses on Klingel movement of a bogie. First part of the study will try to discuss the relationship of Klingel frequency of a wheelset and kinematic movement frequency of a whole train. Second part of the study will use realistic data of Dutch railway vehicles to assess the frequency bandwidth of Dutch native trains.

This section will include following parameters to be studied:

- Speed of train, radius of the wheel and conicity of the wheel.
- Gauge distance is fixed to 1435mm according to UIC standard.
- Frequency is linear to speed if other parameters are fixed.

5.3.1 Comparison between Klingel movement and train kinematic movement studied in D181 DT329

In this section the kinematic wave length of trains used in D181 VAMPIRE simulations will be calculated by Klingel's formula and compared with the wavelength value obtained in VAMPIRE simulation.

Klingel's formula: Klingel has done experiments and has given that the wavelength of a single wheelset:

$$\lambda_0 = 2\pi \sqrt{\frac{rG}{2\gamma}}$$

where:

G = Dynamic Gauge

r = Dynamic Wheels Radius

g = Conicity

For 2 wheelsets connected by a bogie:

$$\lambda = \lambda_0 \sqrt{1 + \left(\frac{I}{G}\right)^2}$$

where:

I = Rigid wheel base

By inputting the related train parameters used in VAMPIRE simulations into the Klingel formula, following table is obtained.

By comparing the result from Table.5.1 and kinematic wavelength obtained by D181, extracted as Table.A.2, parametric study results show close prediction for kinematic wavelength of freight train locomotive/coach/wagon. It's because freight train suspension system is simpler and stiffer compared to passenger train's, making the behaviour of train acts more similar to the behaviour of a single wheelset of bigger mass.

Table 5.1: Approximate lateral kinematic wavelength calculated by improved Klingel formula

	Gauge	BWD	Radius	Conicity	Wavelength(λ_0)	Wavelength(λ)
BR CLASS 56 LOCO	1435	4180	290	0.05	12.8175	39.4750
FS E444 LOCO	1435	2600	550	0.05	17.6517	36.5301
FS ETR500 LOCO	1435	3000	550	0.05	17.6517	40.9070
UIC FREIGHT WAGON	1435	0	460	0.05	16.1430	16.1430
FS ETR500 COACH	1435	3000	440	0.05	15.7882	36.5883
UIC COACH	1435	2560	445	0.05	15.8776	32.4718

Wavelength for UIC freight wagon is a special case and it's not meeting the wavelength results in VAMPIRE simulations. This is probably because this car has a different design. It can be seen from in Figure.A.11 that only 2 axles are installed and there's no wagon installed. See Figure.5.1 and Figure.5.2 for their different axle configurations.



Figure 5.1: Example of a 2-axle freight wagon



Figure 5.2: Example of a 4-axle freight wagon

The train parameter used in this part of parametric study is attached in the Appendix.C.

5.4 Assess of wavelength bandwidth based on realistic data of Dutch Rail/Vehicle

The wavelength of passenger coach is highly related to the characteristics of its suspension systems. These data are often difficult to obtain. Since the improved Klingel formula ignored the effect of suspension system, the results in this section is only approximate value for the wavelength of kinematic movement.

Future research is highly recommended to be conducted to study the kinematic wavelength of complete vehicles in the Netherlands, using realistic data of their suspension systems.

Table.5.2 is created by processing Dutch wheel radius and wheelbase data collected from documentra². Thus range of λ is obtained by inputting realistic data in Kingel formula, illustrated in

Table.5.2.

Table 5.2: Wavelength of kinematic movement generated by realistic value

	Gauge	BWD	Radius	Conicity	Wavelength_0()	Wavelength
Freight 2-axle	1435	0	500	0.05	16.8303	16.8303
	1435	0	500	0.2	8.4151	8.4151
	1435	0	500	0.3	6.8709	6.8709
Freight 4-axle	1435	1800	500	0.05	16.8303	26.9988
	1435	1800	500	0.2	8.4151	13.4994
	1435	1800	500	0.3	6.8709	11.0222
Passenger	1435	2500	460	0.05	16.1430	32.4275
	1435	2500	460	0.2	8.0715	16.2137
	1435	2500	460	0.3	6.5904	13.2385
	1435	2750	460	0.05	16.1430	34.8947
	1435	2750	460	0.2	8.0715	17.4473
	1435	2750	460	0.3	6.5904	14.2457
Locomotive	1435	2400	500	0.05	16.8303	32.7960
	1435	2400	500	0.2	8.4151	16.3980
	1435	2400	500	0.3	6.8709	13.3889
	1435	2950	500	0.05	16.8303	38.4751
	1435	2950	500	0.2	8.4151	19.2376
	1435	2950	500	0.3	6.8709	15.7074

For conservative usage, please take the value yielded by 0.3 wheel conicity. However, as proved in previous section, this estimation is in closest estimation of simulation results when concity is 0.05.

5.5 Lateral wavelength of axle repeat pattern of Dutch Railway Vehicles

This section will generate lateral wavelength value of axle repeat pattern of Dutch Railway Vehicles. Although DT329 provided wavelength values for some trains in Table.A.1 but the way of obtaining these values was not mentioned. So an interpretation is needed to understand how to obtain the axle repeat pattern wavelength.

By observing Table.A.1, it can be seen that axle spacing layout is the only raw data needed to generate axle repeat pattern wavelength. The value is regardless of all other parameters. There are several axle space combinations in the table, but only one combination was finally put emphasis on during the analysis phase of axle repeat resonance research. They are

- 'wagon n axle m - wagon n+1 axle m' for freight train,
- 'coach n axle m - coach n+1 axle m' for passenger train,
- 'coach n axle m - coach n+1 axle m' for high speed train.

It's still hard to comprehend above combinations so further interpretation is done by comparing it to train parameters in Appendix.A. It is found

By comparing Fig.C.1 and Table.A.1. It can be seen that 'wagon n axle m - wagon n+1 axle m' means the distance between one axle in the previous car and another axle in next car in the

same location. The same goes for passenger train and high speed train. To better understand this spacing, please see L_Coa in Figure.C.1.

Table 5.3: Wavelength of axle repeat pattern(m)

Type	L_coa min	L_coa max	2*L_coa min	2*L_coa max
CB_1	23.8	25.3	47.6	50.6
CB_2	25.3	27.5	50.6	55
AB_1	14.9	16	29.8	32
AB_2	18.8	19.5	37.6	39
AB_3	17	17.5	34	35
AB_4	18.7	19.2	37.4	38.4
SA_1	9.2	9.8	18.4	19.6
SA_2	12.8	13.5	25.6	27

Lateral wavelength of axle repeat pattern is then obtained by extracting all possible L_Coa values from MU standards in CEN⁸, illustrated in Table.5.3. Detailed information about MU classes can be found in Appendix.C.

After examining the content in analysing section of DT329 resonance study, it is found that double length of L_Coa is not taken into account in analysis phase. This means although D181 committee calculated double length of L_Coa, these values were never used. Thus it is advisable for the usage of lateral axle repeat pattern wavelength, extracting only L_Coa min column and L_Coa max column.

5.6 Conclusion of wavelength study

The lateral resonance effects between running train and railway bridge include two phenomenon: Axle repeat pattern and Kinematic movement. Those two phenomenon are all wavelength phenomenon, which means for every specific train, the wavelength of its axle repeat pattern and kinematic movement remains constant. In other word, the frequency of lateral dynamic effect caused by the operating of trains on bridge is directly related to the speed.

Since the wavelength for the two phenomenon on the same train are not likely to be equal, the possible range of wavelength for both phenomenon were investigated in this chapter. The possible axle repeat pattern wavelength is approximately 10m-30m covering all train types and kinematic wavelength is 13m to 17m covering all train types. It can be seen that axle repeat pattern possess a broader range of wavelength than kinematic movement.

It also can be concluded that for any railway bridge, resonance between the bridge itself and train can happen if the train is running at a corresponding resonance speed according to its wavelength. So avoiding resonance is not a valid strategy to choose, not to mention the apparent frequency shift phenomenon to be discussed in Chapter.4.2.3.

To be noted that these wavelength are also not the exact wavelength in real-life scenario but an estimation, especially for kinematic movement. But it gave away a rough idea about the magnitude of trains' wavelength, and, can be used for practical design purposes. To see the usage of studied wavelength, please see Chapter.7

Chapter 6

Essentials of analytical approach to be adopted in practical checking method

6.1 Introduction

This chapter aims to give a preliminary knowledge of a selected analytical model that simulates the perfect resonance scenario for railway bridge under lateral dynamic load. The knowledge contains the simplified model itself, its assumptions, field of application and explicit solutions.

The output response of the solution to the analytical model is able to provide the maximum bridge response in worst case scenario. Thus it is sufficient to be adopted in practical purposes for verifications of lateral railway bridge dynamics.

6.2 Overview

To give a clear view of this chapter, following overview is created:

1. The model, its assumptions and field of application.
2. Procedure of solution deduction
3. Damping

6.3 The model, its assumptions and field of application

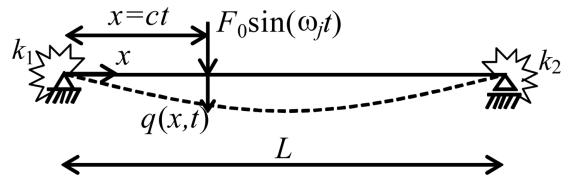


Figure 6.1: Schematic representation of a generic beam crossed by a harmonic load

Presented in Figure 6.1, the model features a simply supported beam which is the simplification of bridge structure and a moving harmonic load introducing resonant dynamic effects caused by the presence of moving train.

The beam is assumed to be uniform in both geometry and material. The stiffness of the beam is the equivalent uniform lateral bending stiffness of the bridge.

The load is moving in the same speed as the train. The magnitude of load amplitude is going to be discussed in the following chapter. The load's self vibration frequency is equal to the first natural lateral bending frequency of the beam.

This model is valid for single span railway bridges that has a sinuous first natural lateral vibration shape.

6.4 Solution deduction

Solution provided by FrybaFrýba¹⁶ is used to analyse the problem. A harmonic moving along a beam is a fundamental dynamics topic and was first solved by S.P.Timoshenko. Fryba further deduced the basic results, and set them forth in the form of useful formulae. This model is used to simulate a perfect resonance scenario which yields conservative results for designing and checking of the dynamics behaviour of the bridge. Deduction procedure is extracted from Frýba¹⁶, Section II.2.1 and presented below.

The solution of the problem of a harmonic concentrated force moving at constant speed c over a simply supported beam with span l is carried out under the same assumptions as that discussed in Chap. 1. The time-variable concentrated force is of the form

$$P(t) = Q \sin \Omega t \quad (6.1)$$

where Q is the amplitude and Ω is the circular frequency of the harmonic force. Vibration of the beam is then described by the equation

$$EJ \frac{\partial^4 v(x, t)}{\partial x^4} + \mu \frac{\partial^2 v(x, t)}{\partial t^2} + 2\mu\omega_b \frac{\partial v(x, t)}{\partial t} = \delta(x - ct)Q \sin \Omega t \quad (6.2)$$

by the boundary conditions (1.2) and by the initial conditions (1.3). The symbols used in 6.2 have the same meaning as those of Chap. 1.

Eq.6.2 together with conditions (1.2) and (1.3) will again be solved by the method of integral transformations. Following the Fourier sine transformation according to (1.9), Eqs.6.2 and (1.2) give

$$\frac{d^2 V(j, t)}{dt^2} + 2\omega_b \frac{dV(j, t)}{dt} + \omega_{(j)}^2 V(j, t) = \frac{Q}{\mu} \sin \Omega t \sin j\omega t \quad (6.3)$$

Solving the above with (1.3) by the Laplace-Carson transformation (1.15) - making use of Eq.(27.24) in doing so and of the notation

$$r_1 = \Omega + j\omega; \quad r_2 = \Omega - j\omega \quad (6.4)$$

we get

$$V^*(j, p) = \frac{Q}{2\mu} \left(\frac{1}{p^2 + r_2^2} - \frac{1}{p^2 + r_1^2} \right) \frac{p^2}{(p + \omega_b)^2 + \omega_{(j)}'^2} \quad (6.5)$$

After inverse transformations of Eq.6.5 according to (27.24) and (1.9) the required result for $t \leq T$ is

$$\begin{aligned}
v(x, t) = & \sum_{j=1}^{\infty} \frac{Q}{\mu l} \left\{ \frac{1}{(\omega_{(j)}^2 - r_2^2) + 4\omega_b^2 r_2^2} [(\omega_j^2 - r_2^2)] (\cos r_2 t - e^{-\omega_b t} \cos \omega_{(j)}' t) \right. \\
& + 2\omega_b r_2 \sin r_2 t - \frac{\omega_b}{\omega_{(j)}'} (\omega_{(j)}^2 + r_2^2) e^{-\omega_b t} \sin \omega_{(j)}' t] \\
& - \frac{1}{(\omega_{(j)}^2 - r_1^2)^2 + 4\omega_b^2 r_1^2} [(\omega_{(j)}^2 - r_1^2) (\cos r_1 t - e^{-\omega_b t} \cos \omega_{(j)}' t) + 2\omega_b r_1 \sin r_1 t \\
& \left. - \frac{\omega_b}{\omega_{(j)}'} (\omega_{(j)}^2 + r_1^2) e^{-\omega_b t} \sin \omega_{(j)}' t] \right\} \sin \frac{j\pi x}{l}
\end{aligned} \tag{6.6}$$

We shall now simplify Eq.6.6 to fit the case most frequently met with in practical applications. Thus, for example, it is entirely satisfactory to use only the first of its terms ($j = 1$); further, as we know from Chap. 1, parameters α and β are usually much smaller than 1 ($\alpha = \omega/\omega_{(1)} \ll 1$, $\beta = \omega_b/\omega_{(1)} \ll 1$). And finally, since in practice a harmonic force is always accompanied by a constant force P , we shall introduce in 6.6 also the deflection v_0 according to (1.21). Following these simplifications Eq.(2.6) takes on the form

$$\begin{aligned}
v(x, t) = & v_0 \frac{Q \omega_{(1)}^2}{p \Omega^2} \frac{1}{(\frac{\omega_{(1)}^2}{\Omega^2} - 1)^2 + 4(\frac{\omega^2}{\Omega^2} + \frac{\omega_b^2}{\Omega^2})} \left\{ \left[\left(\frac{\omega_{(1)}^2}{\Omega^2} - 1 \right)^2 \right. \right. \\
& + 4 \frac{\omega_b^2}{\Omega^2}]^{1/2} \sin(\Omega t + \varphi) \sin \omega t \\
& \left. \left. + 2 \frac{\omega}{\Omega} (\cos \Omega t \cos \omega t - e^{-\omega_b t} \cos \omega_{(1)} t) \right\} \sin \frac{\pi x}{l}
\end{aligned} \tag{6.7}$$

where

$$\tan \varphi = - \frac{2\omega_b/\Omega}{\omega_{(1)}^2/\Omega^2 - 1} \tag{6.8}$$

The beam reaches the state of highest dynamic stressing in the region of resonance, i.e. whenever Ω is close or just equal to $\omega_{(1)}$, i.e.

$$\Omega = \omega_{(1)} \tag{6.9}$$

In such a case Eq.6.7 can further be simplified to

$$v(x, t) = v_0 \frac{Q\omega_{(1)}}{2P} \frac{\cos \omega_{(1)} t}{\omega^2 + \omega_b^2} [\omega (\cos \omega t - e^{-\omega_b t}) - \omega_b \sin \omega t] \sin \frac{\pi x}{l} \tag{6.10}$$

According to (1.21)

$$v_0 = \frac{Pl^3}{48EJ} \approx \frac{2P}{\mu l \omega_{(1)}^2} = \frac{2Pl^3}{\pi^4 E J} \tag{6.11}$$

substitute v_0 into Eq.6.10

$$v(x, t) = \frac{l^3 Q \omega_{(1)}}{\pi^4 E J} \frac{\cos \omega_{(1)} t}{\omega^2 + \omega_b^2} [\omega (\cos \omega t - e^{-\omega_b t}) - \omega_b \sin \omega t] \sin \frac{\pi x}{l} \tag{6.12}$$

And the mid-span response time-history for deflection is :

$$v(l/2, t) = \frac{l^3 Q \omega_{(1)}}{\pi^4 E J} \frac{\cos \omega_{(1)} t}{\omega^2 + \omega_b^2} [\omega(\cos \omega t - e^{-\omega_b t}) - \omega_b \sin \omega t] \quad (6.13)$$

where:

v : deflection of the beam(m)

l : span of the beam(m)

EJ : lateral stiffness of the beam(Nm^2)

Q : amplitude of harmonic load(N)

c : speed of the train(m/s)

ζ : damping ratio

μ : mass per unit length of the beam(kg/m)

ω_1 : first natural circular frequency of the beam

$$\omega_1 = \frac{\pi^2}{l^2} \sqrt{\frac{EJ}{\mu}}$$

$$\omega = \pi c/l$$

$$\omega_b = \frac{1}{2} \zeta \omega_1$$

Above expression is the ready-to-use expression being adopted in practical checking method to be discussed in following chapter.

6.5 Damping

Damping is an important parameter influencing the dynamic behaviour of a structure. 6.2 uses a different form of damping expression ω_b , which can be converted from normal damping coefficient. Equation of motion using damping coefficient:

$$EJ \frac{\partial^4 v(x, t)}{\partial x^4} + \mu \frac{\partial^2 v(x, t)}{\partial t^2} + \chi \frac{\partial v(x, t)}{\partial t} = \delta(x - ct) Q \sin \Omega t \quad (6.14)$$

where χ stands for damping coefficient. By comparing 6.14 and 6.2:

$$\omega_b = \frac{\chi}{2\mu} \quad (6.15)$$

where:

ω_b : circular frequency of damping

χ : damping coefficient

μ : mass per unit length of the bridge

also, in Abu-Hilal and Mohsen³, Page.704 it is mentioned that:

The external and internal damping of the beam are assumed to be proportional to the mass and stiffness of the beam respectively,i.e., $r_a = \gamma_1 \mu ..$, where γ_1 and γ_2 are proportionality constants.

thus:

$$\omega_b = \frac{\gamma_1}{2} \quad (6.16)$$

and it is mentioned in Abu-Hilal and Mohsen³, Eq.8 that:

$$\zeta = \frac{\gamma_1}{\omega_1}$$

so:

$$\gamma_1 = \zeta \omega_1$$

so:

$$\omega_b = \frac{1}{2} \zeta \omega_1 = \frac{1}{2} \frac{\zeta \pi^2}{l^2} \sqrt{\frac{EJ}{\mu}}$$

where ζ is the structure damping ratio stated in EN1991-

Adopting $\zeta = 1\%$ for steel railway bridges. This ζ value is used among all DT329 simulations run files. See Figure.B.3 for example. T329 resonance study. By comparing with the output of reproduced resonance in DT329, the analytical model can be verified.

6.6 Verification of the explicit solution

Since circular frequency of damping ω_b is not clearly defined by Fryba, it is necessary to verify the correctness of both explicit solution and deduced ω_b expression.

The verification is done by comparing the result of Eq.6.13 with the result of a explicit solution in a different form obtained by another deducing method.

The result in Abu-Hilal and Mohsen³ is selected to compare. This report is researching vibration of beams with general boundary conditions due to a moving harmonic load. The differential equation is illustrated as follows:

$$EIv'''' + \mu \ddot{v} + r_a \dot{v} + r_i \dot{v}''' = p(x, t) \quad (6.17)$$

The difference between Eq.6.17 and Eq.6.13 is that it offers broader boundary conditions such as changing speed of the load and various kinds of supports. As a result of more general equation, the deduction steps are much more complicated. However, two solutions should yield same results under same boundary conditions that:

1. Load moving at constant speed,
2. Frequency of load equals frequency of the beam,
3. Internal damping is 0,
4. Simple hinge support at both ends of the beam.

One plot from the parametric study of Abu-Hilal and Mohsen³ meets the above requirement and is selected and illustrated in Figure. Parameter used in this plot is $\alpha = 0.25$, $\zeta = 0.05$, $\beta = 1$

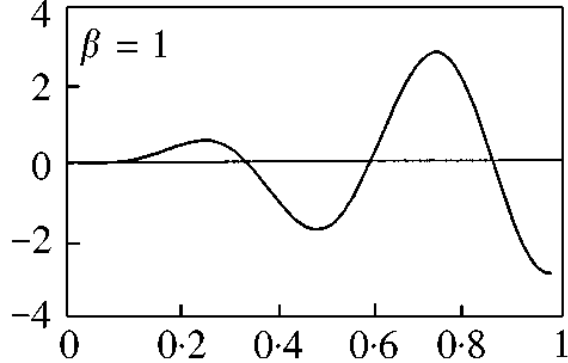


Figure 6.2: Reference plot extracted from Abu-Hilal and Mohsen³. Condition: $\alpha = 0.25$, $\zeta = 0.05$, $\beta = 1$. Y axis for dynamic amplification factor.

Next step is to translate parameters used in above plot to usable parameters in Eq.6.13.

$$c_{cr} = \frac{\omega_1 L}{\pi} = \frac{\pi}{l} \sqrt{\frac{EJ}{\mu}}$$

$$\alpha = \frac{c}{c_{cr}}$$

$$c = \alpha c_{cr} = \frac{\alpha \pi}{l} \sqrt{\frac{EJ}{\mu}}$$

EJ, μ, l needs to be selected to yield value for c , thus following values are randomly selected:

$$EJ = 2.43e10 Nm^2$$

$$l = 54m$$

$$\mu = 6000 kg/m$$

$$c_{cr} = 117.05 m/s$$

$$c = 29.26 m/s$$

A Matlab script is written to automate numerical calculating procedure. By typing
fogtest(2.43e10,54,6000,29.26,0.05)
into the console. Figure.6.3 is obtained.

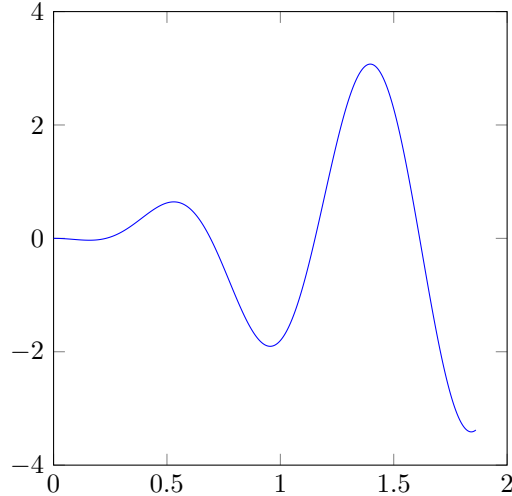


Figure 6.3: Time history of dynamic amplification factor in mid-span of the beam. Parameters: $EJ = 2.43e10 Nm^2$, $L = 54m$, $\mu = 6000 kg/m$, $c = 29.26 m/s$

By observing Figure.6.2 and Figure.6.3 it can be concluded that results are the same on y-axis. The difference of x-axis is because in Figure.6.2 time axis is scaled to 1 but in Figure.6.3 time is not scaled. Then it can be further concluded that Eq.6.13 and expression for ω_b are both correct.

Chapter 7

New practical method for checking lateral resonance response of railway bridges based on VAMPIRE simulation results

7.1 Introduction

This chapter proposes a new method for checking lateral resonance response of railway bridges. This method aims to provide an engineering solution for checking the deflection and acceleration of railway bridges when resonance happens under horizontal dynamic train load. Both creation and verification of the method is based on VAMPIRE simulation results provided in DT329 research.

The method features the combined usage of a simplified analytical structural model and a more refined lateral force model. The analytical structure model simulates a perfect resonance scenario for railway bridge. And the refined load model, which is a concentrated harmonic moving load, represents the lateral dynamic effects that occur because of the passing of the train. The combination of these two analytical elements will generate a resonance response conservative compared to the simulation output in DT329 because various types of disturbance were included in these simulation runs.

The analytical structural model that was introduced in the previous chapter and its explicit solution has already been worked out in the same chapter. Thus the main objective of this chapter is finding a better lateral force load model because current existing ones are too conservative(see Section.7.3). The refined load model shall be able to be adopted universally for all regular train types. Once this load model is obtained and verified, it is then possible to take advantage of the combination of the load model and analytical solution for practical designing purposes.

7.2 Overview of this chapter

To give a clear overview of this chapter, procedure of development of the method as following:

1. *Developing:* Develop a more practical load model to be used in pair with the analytical model introduced in previous chapter based on the VAMPIRE simulation outputs. See Section.7.3
 - 1.1. Overview of both VAMPIRE numerical simulation method and analytical method. See Section.7.3.1

- 1.2. Find the analytical equivalent nosing forces amplitude for freight trains in 3 different cases presented in DT329 resonance research simulation. See Section.7.3.2
- 1.3. Find regular pattern and key parameter for the magnitude of nosing forces amplitude for freight trains. See Section.7.3.3
- 1.4. Develop a conservative load model based on observed pattern of nosing force of freight trains. See Section.7.3.3
2. *Verifying:* Validate the feasibility of combined usage of conservative load model and analytical model
3. *Finalizing:* Illustrate the usage of the method by applying it on a real railway bridge

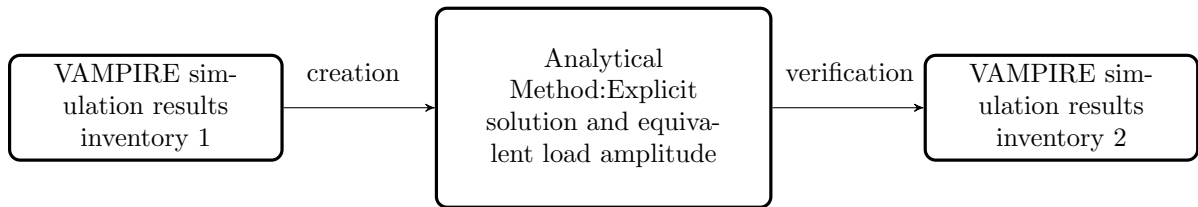


Figure 7.1: Workflow of the creation of analytical method

7.3 Development of refined load model

The load model provided in EN1991-2(nosing force) and D181 RP6(proposed criteria) are too conservative for dynamic analysis. The reason is that these forces are obtained by simulations ran on poorest maintained tracks with 7mm track irregularity standard deviation. In fact tracks are allowed to have lateral irregularities up to 1.8mm according to EN13848(Section.2.3). So existing lateral force models are enormous compared to real-life scenario.

In addition, the existing load models are representative for hunting effects D181 Committee¹⁰, Proposed criteria. However, according to Majka and Hartnett¹⁸, although affected by varies parameters, critical speed for hunting effect is normally at 120km/h for modern railway vehicle and tracks. So at least for trains running slower than 120km/h, it can be conclude that hunting is not occurring. And their lateral force should be much less than the force magnitude mentioned in either EN1991-2 or D181 RP6.

Thus these existing load models are too big and not suitable for the analytical solution. A more precise load model is needed for coupled usage for analytical solution.

7.3.1 Overview of VAMPIRE numerical simulation method and analytical method

The analytical model itself and its explicit expression have already been introduced and described in previous chapter. This section will give a overview on the input parameters of both VAMPIRE simulation and analytical model. This is not only due to the fact that VAMPIRE simulation was proved by D181 committee to be in close prediction with situ measurements, but also because in following sections VAMPIRE simulation results will be used as benchmark data for the development of analytical model's pairing load model.

As demonstrated in Table.7.1, while input parameters for simulation are complicated, analytical model possesses less input parameters.

That table shows that the single moving harmonic load in analytical model shall be capable of providing dynamic effect caused by train speed, track irregularities, wheel profile and wheel-rail interaction to the analytical model. Correct single moving harmonic load input shall yield the same

Table 7.1: Comparison between input parameters of DT329 VAMPIRE simulations and analytical model

	Simulation	Analytical model
Bridge structure	simply supported beam	simply supported beam
Span	Yes	Yes
Stiffness	Yes	Yes
Mass	Yes	Yes
Damping	Yes	Yes
Train	complete train as mass spring system	single moving harmonic load
Train Speed	Yes	Yes
Track irregularities	Yes	No
Wheel profile	Yes	No
Wheel-rail interaction	Yes	No

result as VAMPIRE simulation provided that same span, stiffness, mass and damping value are adopted in both two calculating methods.

Thus finding the correct expression for the harmonic moving force is vital to the analytical model. The harmonic moving force has 3 parameters: speed c , frequency Ω and amplitude Q . Since speed c simply equals to train speed and frequency Ω equals to the first natural bending frequency of the beam ω_1 , the amplitude of the harmonic force remains to be researched. Further development of the amplitude expression will be discussed in following sections.

7.3.2 Finding equivalent lateral force amplitude for specific cases

In this section, equivalent lateral force amplitudes for the analytical solution are obtained. The equivalent lateral force amplitude does not represent real force magnitude in rail/wheel interaction, but a force amplitude that yields same result as VAMPIRE simulations using same input parameters if substituted into analytical solution. So this lateral force amplitude may not be correct if adopted in other structure models. On the other hand, analytical solution may yield imprecise results if not substituted with this exact equivalent force amplitude. They can only be used in pair with each other.

Thus in order to perform the comparison mentioned above, both input and output data of DT 329 VAMPIRE simulations are selected as reference data. The input data will be substituted into analytical model and the output data of VAMPIRE simulation will be compared with output of analytical model.

3 sets of reference data are extracted from DT329 report. They are C1,C3,C9 in Figure.7.2,7.3 and 7.4 respectively. These data are all extracted from resonance study so they are qualified to be used as reference data. Please note that C1,C3,C9 were all done on freight trains on same track sample. Finally 3 equivalent forces are collected from these 3 test samples to see regular pattern and relevant parameters for freight trains.

By observing Eq.6.13, it is concluded that force amplitude is an independent variable and perfectly linear to the analytical output. Thus the equivalent force is obtained by inputting bridge parameters and train speed into the analytical solution Eq.6.13 and manually increasing the force amplitude little by little until the peak response output reaches the same magnitude of peak simulation output. The parameters used and their corresponding results are presented in Table.7.2.

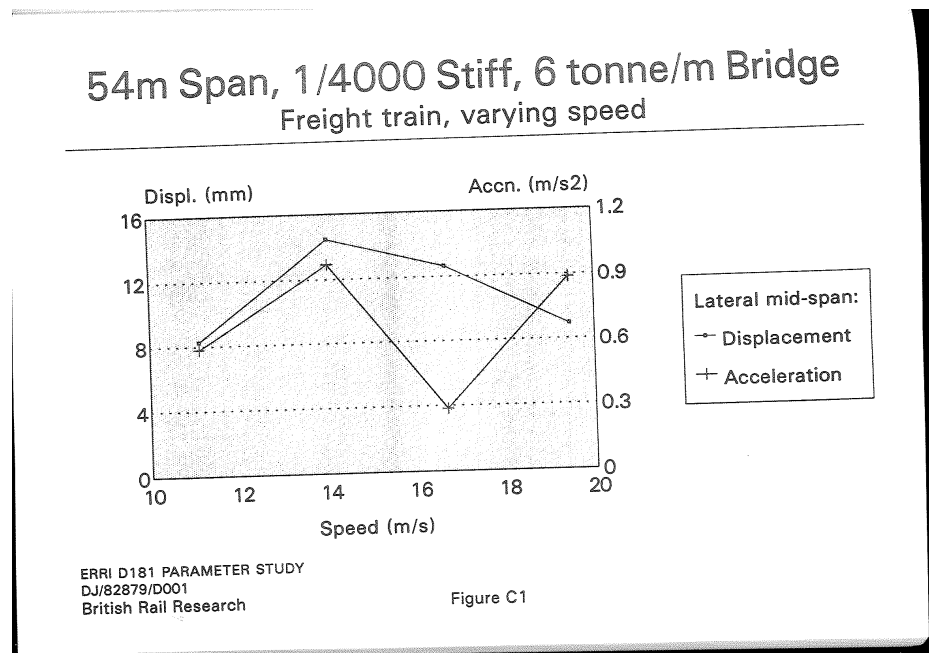


Figure 7.2: Figure C1 extracted from D181Committee¹¹

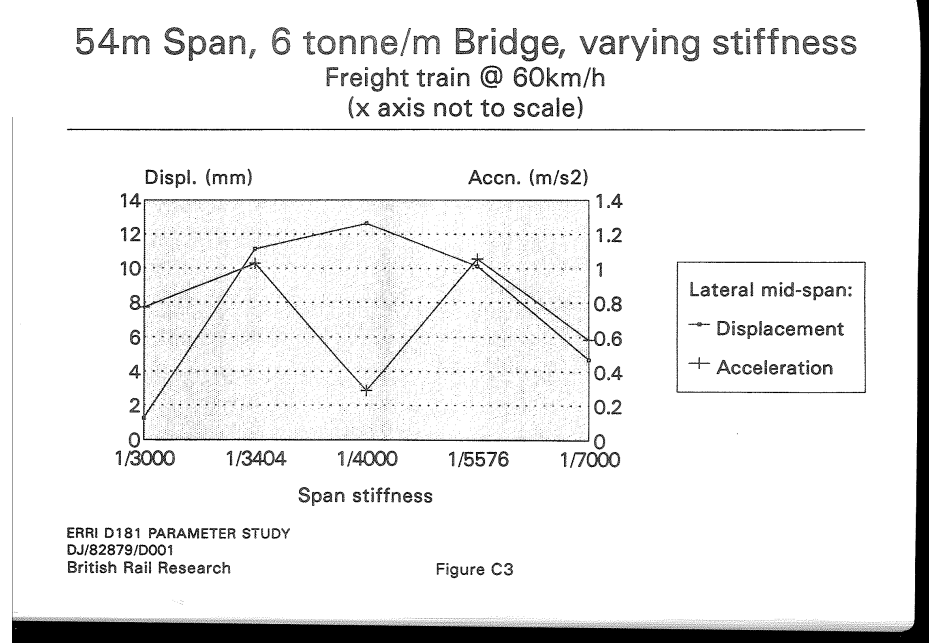


Figure 7.3: Figure C3 extracted from D181Committee¹¹

7.3.3 Key parameter for equivalent force amplitude and hypothesis expression for refined load model

By observing the equivalent load amplitude illustrated in Table.7.2, it is found that the equivalent load amplitude yielded by analytical solution meets the general principle of lateral track force

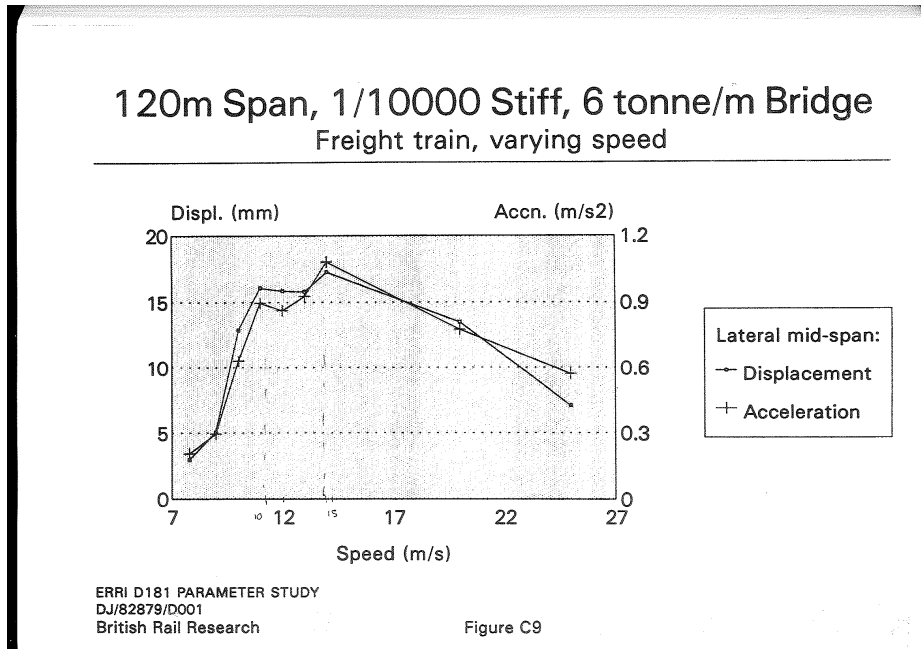


Figure 7.4: Figure C9 extracted from D181Committee¹¹

Table 7.2: Parameter setups and equivalent force amplitude for C1,C3,C9

	C1	C3	C9
Stiffness(δ_0/l)	1/4000	1/4000	1/10000
Span(m)	54m	54	120
Mass per unit length(kg/m)	6000	6000	6000
Speed of train(m/s)	14	16.67(60km/h)	14
Damping ratio	1%	1%	1%
Train type	Freight	Freight	Freight
Track	Coupled freight track	Coupled freight track	Coupled freight track
Equivalent load amplitude(kN)	14	15	14

concluded by DT329 track quality research. The general principle is that the lateral force is only relevant to speed if track quality and wheel conicity are fixed. And lateral force is irrelevant to the bridge parameters.

Because equivalent force amplitude meets the general lateral force principle, it is further expected that the equivalent force amplitude also has a similar form of force-speed relationship of DT329 VAMPIRE simulations. Due to the lack of reference data, it is impossible to make a reliable regression. Only a hypothesis expression can be created by scaling Eq.4.1 to 14kN at 14m/s(reference data set C1). Please note only C1 was used in creating the hypothesis expression so C3 and C9 remains available for the verification.

$$Q = 1928 \times c^{0.7495} \quad (7.1)$$

where:

Q: equivalent force amplitude(N)

c: speed of the train(m/s)

This scaling is reasonable because: according to the conclusion of DT329 track quality re-

search, lateral forces generated on 7mm standard deviation tracks has a certain relationship with speed(Eq.4.1). And it is also concluded that at same speed, lateral forces are linear to the track stand deviation. Thus, since all 3 reference data are run on the same track, force output of analytical model at each speed(14m/s and 16.67m/s) could be scaled from Eq.4.1 's results at these speeds. Furthermore, a scale factor is then applied on Eq.4.1 to reflect the scaling to the whole speed domain and this yields above equation.

As a conclusion, this hypothesis expression is obtained by processing the output of VAMPIRE simulation on freight trains and coupled freight track(poorer than passenger line and high speed line). So it is in closest prediction in the effects generated by freight trains. However, since passenger trains and high speed trains yields lower lateral force compared with freight trains, this hypothesis expression remains conservative for all train types.

7.4 Verification of the method

In this section the combined usage of analytical model and hypothesis expression for equivalent force amplitude is examined and verified. A matlab script is written to function the analytical model with hypothesis expression for equivalent load amplitude implemented. Now that force amplitude Q is a function of speed, it's no longer necessary to input the force amplitude manually. To verify the correctness of combined usage of these two elements, other reference data from resonance research in DT329 are selected and presented in Figure.7.5, 7.6 and 7.7.

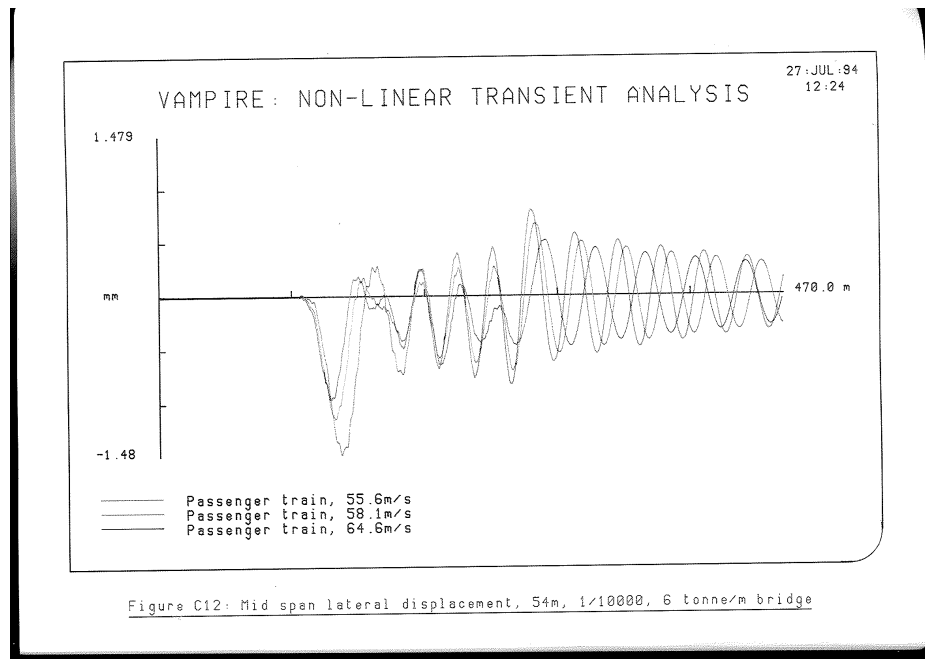


Figure 7.5: Figure C12 extracted from D181Committee¹¹

To assure conservative comparison, only axle repeat pattern resonance results are selected because their output are more pronounced than kinematic resonance effect. Altogether 5 sets of reference data are selected. They include 2 reference data for freight trains(C3,C9), 2 reference data for passenger train(C12,C13) and 1 reference data for high-speed train(C14). Due to the fact that freight trains yield greater force than the other two types of trains, the analytical result should be conservative for the latter 3 cases. Since the output of C3 and C9 are already presented in Table.7.2 so they are not being presented with other 3 sets of data this time. The bridge parameters and

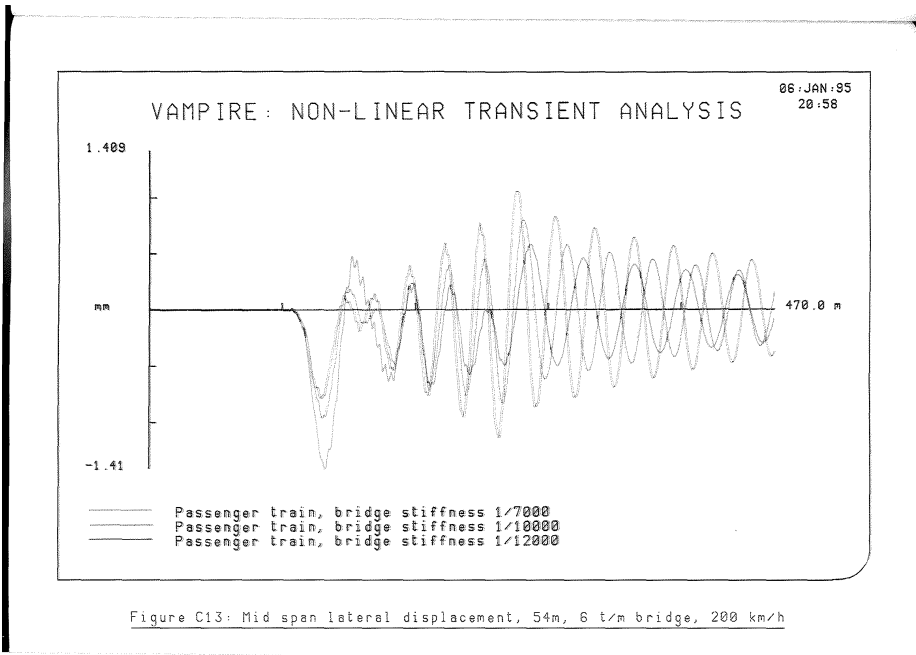


Figure C13: Mid span lateral displacement, 54m, 6 t/m bridge, 200 km/h

Figure 7.6: Figure C13 extracted from D181Committee¹¹

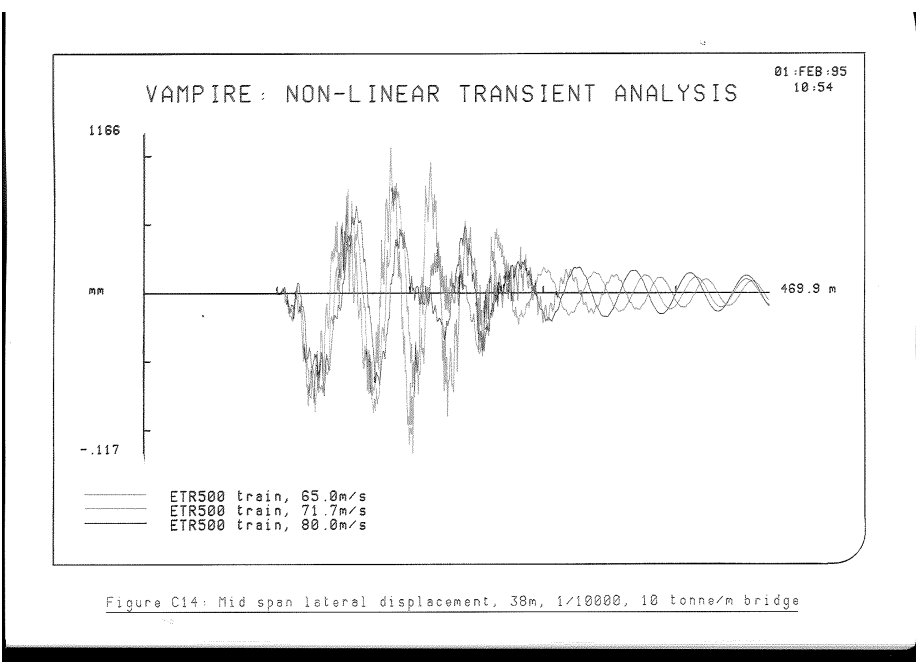


Figure C14: Mid span lateral displacement, 38m, 1/10000, 10 tonne/m bridge

Figure 7.7: Figure C14 extracted from D181Committee¹¹. An minor error is observed in y-axis label. Upper boundary of y-axis should be 0.116

trains speed involved in these 3 cases(C12,C13,C14) are input into the analytical solution to yield analytical results.

In Table.7.3 the parameters involved in these 3 cases and their corresponding peak analytical

Table 7.3: Comparison of results of simulation output and analytical output using refined load model

	C12	C13	C14
Stiffness(δ_0/t)	1/10000	1/12000	1/10000
Span(m)	54	54	38
Mass per unit length(kg/m)	6000	6000	10000
Speed of train(m/s)	55.6	55.6	65
Damping ratio	1%	1%	1%
Train type	Passenger	Passenger	High speed
Track	Passenger Track	Passenger Track	High speed track
Peak Simulation displacement(mm)	1.48	1.41	0.117
Peak Analytical displacement(mm)	6.6	5.8	3.0

results as well as peak simulation results are presented.

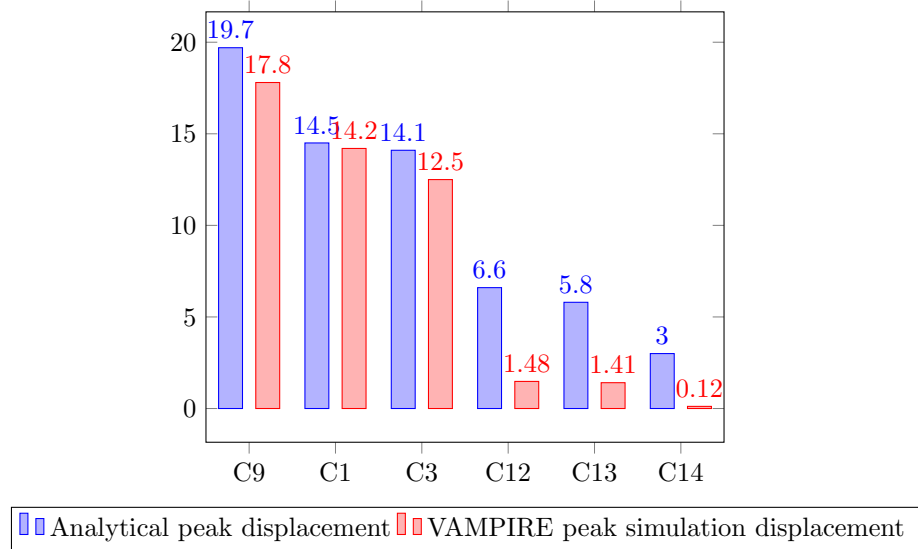


Figure 7.8: Comparison between VAMPIRE peak simulation result and analytical peak result

To clearer illustrate the comparison of both peak results from simulation and analytical, Figure.7.8 is created with rearranged x-axis order to make the descending trend more obvious. Please note all data sets except for C1 are valid for verification(C1 is used in creation of expression).

It can be seen that analytical results always keep a conservative margin above the simulation results. As expected, margins for C12,C13,C14 are bigger compared to C9,C1,C3 proofs that the analytical solution becomes more conservative if adopted to passenger train and high-speed train. What's more, the descending trend of analytical results follows the descending trend of simulation results perfectly regardless of train types. Thus considering these reasons, the analytical solution is sufficient for universal application on all train types.

Chapter 8

Finalizing the method for practical usage using real bridge parameters

In practical usage, the speed that generates the highest peak response is unknown. Thus it is necessary to obtain the peak response for all speeds within the possible speed range. This is done by iterating the existing Matlab script with different speed. The increment in speed iteration is set in a way that ensures at least 1000 runs are done to guarantee precession. An example is illustrated as follows to show the usage on a real bridge project.

For an arch railway bridge located near Amsterdam, first step to is to collect following parameters:

$L = 255m$, $m = 5222e3kg$, $\mu = 2.0478e4kg/m$, $EJ = 6.56e12Nm^2$

where:

L : span of the bridge

μ : uniform mass per unit length of the bridge

EJ : lateral stiffness of the bridge

to test through a speed range of $1m/s - 30m/s$

Before beginning the calculation, make sure you have `fog.m` and `Speedenvelop.m` in your current working directory. By inputting following command in Matlab console,

`Speedenvelop(6.56e12,255,2.0478e4,1,30,0.01)`

the envelop for displacement is generated and illustrated in Figure.8.1

The plot shows that the critical speed appears at approximately $5m/s$ and corresponding peak deflection response is approximately $11mm$.

Since the relationship between end support rotation angle and mid-span deflection is widely known as:

$$\varphi = \frac{3}{L} \cdot \delta_0$$

and rotation is yielded as:

$$\varphi = \frac{3}{255} \times 0.011 = 0.00013$$

This value is much lower than the rotation value regulated in EN1991-2. See Section.3.3.3.1 for criteria details.

Thus the conclusion can be made that this bridge is safe subjected to lateral dynamic load.

However, if encountering unfavourable peak result, a filter can be applied on the train speed to further cut off the peak response. In previous chapter it has been already be concluded that all resonance effects between train and bridge are wavelength phenomenon. In order to couple frequency with bridge's first natural bending frequency, the train needs to operate at a certain speed range.

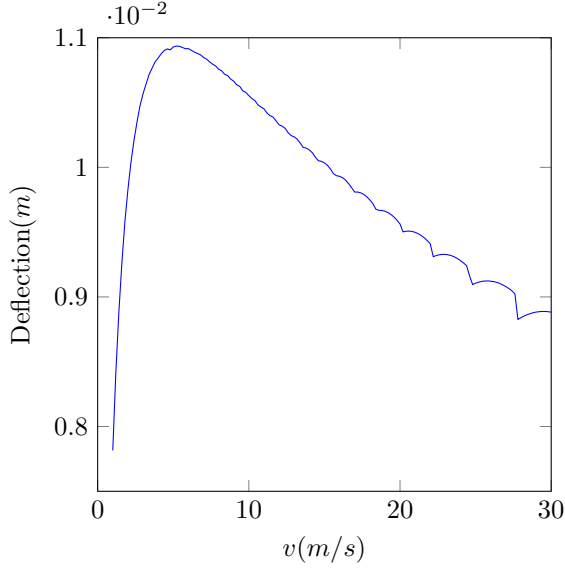


Figure 8.1: Peak deflection at mid-span with regard to changing train speed. Parameters: $EJ = 6.56e12 Nm^2$, $L = 255m$, $\mu = 20478kg/m$, $c_{min} = 1m/s$, $c_{max} = 30m/s$

For example, according to Chapter.5, the possible wavelength range for trains in the Netherlands is approximately 10m-30m, including both axle repeat wavelength and kinematic wavelength.

The natural frequency of the bridge in this example is

$$f_1 = \frac{\pi}{2l^2} \sqrt{\frac{EJ}{\mu}} = \frac{\pi}{2 \times 255^2} \sqrt{\frac{6.56e12}{1.0478e4}} = 0.4Hz$$

so the possible resonance speed is obtained by multiplying wavelength range with natural frequency, yielding: $4m/s$ and $12m/s$

Although this speed filtering range doesn't help to cut off maximum response in this case because critical speed still remains in the speed range, the filter can be more effective for bridges possessing higher first natural frequency simply because both lower and upper boundary for speed filtering range is linear to beam's first natural frequency. While it's not likely for upper boundary to shift to the left side of the critical speed, it's more favourable for lower boundary to shift to the right side of the critical speed.

8.1 Conclusion

The new practical method for checking lateral resonance response of railway bridge is developed in this chapter. This method is capable to simulate a resonance scenario where the bridge was passed by a moving railway vehicle.

The method shows conservative prediction compared to VAMPIRE simulations. However, since lack of data can be used to further verify the practical method, results on longer span bridges can not be verified until new simulations or measurements data are obtained.

A general conclusion in finalizing phase of practical method is, for a certain bridge, faster train speed doesn't necessarily cause higher resonance response of the bridge. As can be seen in Figure.8.1, critical speed appears at approximately $5m/s$, and response start to fall when speed is higher than $5m/s$. This means comparing to higher load amplitude caused by higher train speed, the shorter loading time caused by same reason is more dominating. By considering the fact in Figure.7.8 that

the analytical is even more conservative for higher speed, it can be concluded than high-speed trains cause less dynamic problem for lateral bridge dynamics.

Matlab scripts are already written and attached for the convenience of readers. Since the explicit solution has been given in the chapter, it's completely possible to adopt them in other mathematical software for different preferences.

Chapter 9

Recommendations on improvement on Eurocode

9.1 Recommendations of this thesis

It is advised that Eurocode committee spend more effort in providing background information to structural designers on cross-field topics. For example, railway bridge engineering is related to both fields of structural engineering and railway engineering. The knowledge of railway engineering is seldomly known among structural engineers and they hardly know the key to the problem. So it is vital for the code to provide its users with sufficient background information.

This can be done by adding references of various statements and criteria. Even with good luck, this thesis spent over 3 month of time in trying to find the original research documents for the 1.2Hz criterion. And it can be expected that if no reference is recorded, finding the source would be even more difficult for other researches in the future.

By simply adding reference to the criteria, this amount of wasted time could be saved for a better course. Thus this thesis suggest references to be added for the sake of future researches/designs.

Also, this thesis suggests make deeper evaluation on the criteria being adopted in the code. At least in this report it is found that the 1.2Hz criterion isn't a correct verification strategy.

Last but not least, this thesis suggests Eucocode committee possess a further vision for the future. For example, in EN1991-2 railway bridge dynamics, there's no instruction can be found for bridges with span longer than 150m in the logic diagram. This means during the creation process of EN1991-2, the possibility of longer span bridges in the future is neglected, causing potential problem for future designs.

9.2 Other lateral railway bridge dynamics related criteria extracted from other codes

Following sections provides several orientations for improving criteria for lateral bridge dynamics in terms of safety and serviceability of running stock.

9.2.1 Requirements for traffic safety(horizontal)

Requirements other than bridge first lateral frequency higher than 1.2Hz. Since there's no further requirements mentioned by Eurocode, following requirements are gathered from other European codes, eg. British standards, UIC leaflet, etc.

- Requirements regarding traffic safety for vehicles

- (a) Guiding Force: UIC²², CEN⁷ and Cuadrado Sanguino et al.⁹ propose safety limitations against railway vehicle overturning. From CEN⁷ the maximum guiding force for a vehicle with a load per axle of 170kN(AVE) is 66kN per axle and 48kN per axle for a vehicle with a load per axle of 112kN(ICE2). For the R1 freight wagon(load per axle of 245kN), the maximum guiding force per axle is 78kN.
- (b) Maximum lateral acceleration of the railway vehicle: proposed by UIC²¹
- Requirements regarding safety for bridge
 - CEN⁶ A2.4.4.1(2): Horizontal transverse deflection(to ensure acceptable horizontal track radii) and horizontal rotation of a deck about a vertical axis at ends of a deck(to ensure acceptable acceptable horizontal track geometry and passenger comfort)

9.2.2 Requirements for traffic safety on derailment: Railway vehicle derailment mechanism and safety criteria

Derailment mechanisms

1. vehicle resonant response
2. lateral instability
3. vehicle overturning
4. vertical wheel unloading
5. flange climb
6. rail roll-over
7. track panel shift
8. longitudinal train forces

The four types of derailment: flange climb derailment, derailment caused by gauge widening and rail roll-over, derailment caused by track panel shift, derailment caused by vehicle lateral instability have a common cause of high lateral force at the wheel-rail interface. According to Iwnicki¹⁷, Chapter 8, IV any conditions that lead to high lateral forces or lead to lower the ability of the system to sustain the force should be corrected.

9.2.3 Flange climb derailment

Wheel flange climb derailments are caused by wheels climbing onto the top of the railhead then further running over the rail. Wheel climb derailments generally occur in situations where the wheel experiences a high lateral force combined with circumstances where the vertical force is reduced on the flanging wheel. The high lateral force is usually induced by a large wheelset angle-of-attack. The vertical force on the flanging wheel can be reduced significantly on bogies having poor vertical wheel load equalisations, such as when negotiating rough track, large track twist, or when the car is experiencing roll resonances.

The criterion L/V ratio can be expressed as:

$$\frac{L}{V} = \frac{\tan \delta - \frac{F_2}{F_3}}{1 + \frac{F_2}{F_3} \tan \delta} \quad (9.1)$$

Nadal's famous L/V ratio limiting criterion, given by Equation 9.2, was proposed for the saturated condition $F_2/F_3 = \mu$

$$\frac{L}{V} = \frac{\tan \delta - \mu}{1 + \mu \tan \delta} \quad (9.2)$$

9.2.4 Derailment caused by gauge widening and rail rollover

Derailments caused by gauge widening usually involve a combination of wide gauges and large lateral rail deflections(rail roll), as shown in Figure 9.2. Large lateral forces from the wheels act to spread

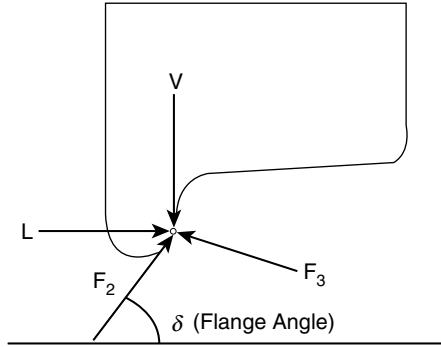


Figure 9.1: Forces at flange contact location. Extracted from Iwnicki¹⁷, Figure8.4

the rails in curves. Both rails may experience significant lateral translation and/or railhead roll, which often cause the nonflanging wheel to drop between rails.

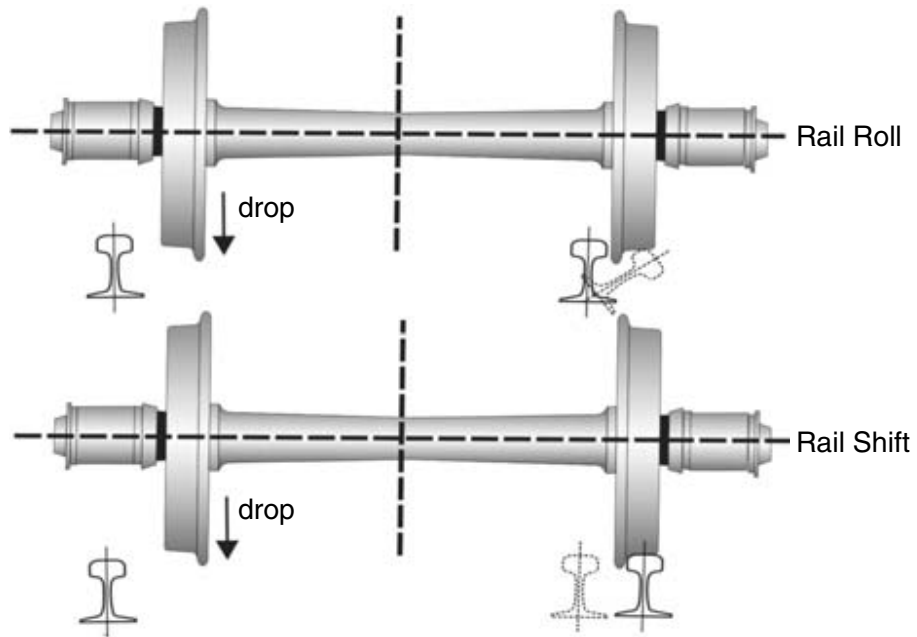


Figure 9.2: Gauge widening derailment. Extracted from Iwnicki¹⁷, Figure8.18

AAR Chapter XI rail roll criterion The AAR Chapter XI rail roll criterion is established by using the L/V ratio. The roll moment about the pivot point is given by,

$$M = Vd - Lh \quad (9.3)$$

under an equilibrium condition, just before the rail starts to roll, M approaches to zero, then,

$$\frac{L}{V} = \frac{d}{h} \quad (9.4)$$

This L/V ratio is considered as the critical value to evaluate the risk of rail roll. When the L/V ratio is larger than the ratio of d/h , the risk of rail roll becomes high. The critical L/V ratio for rail roll can vary from above 0.6 for contact at the gauge side to approximately 0.2 when the contact position is at the far-field side based on the dimension of the rails. This is because the distance d is reduced. Note that this L/V ratio is calculated assuming that neither the rail fasteners nor the torsional stiffness of the rail section provide any restraint.

9.2.5 Derailment caused by track panel shift

Track panel shift is the cumulative lateral displacement of the track panel, including rails, tie plates and ties, over the ballast, as shown in Figure 9.3. A small shift of these components may not immediately cause the loss of guidance to bogies. However, as the situation gradually degrades to a certain level, wheels could lose guidance and drop to the ground at some speed. The derailments caused by track panel usually result in one wheel falling between the rails and the other falling outside of the track.

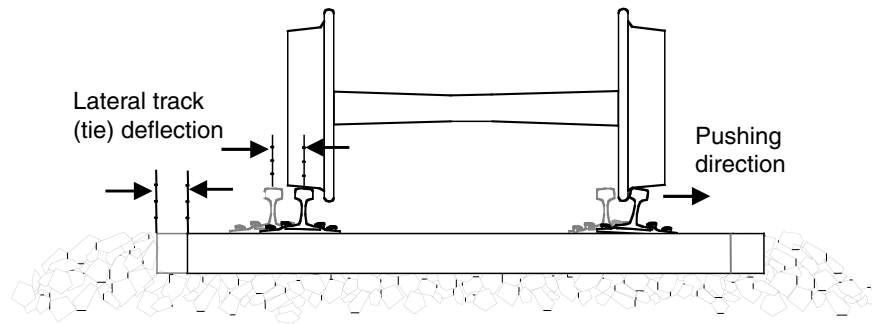


Figure 9.3: Lateral track panel shift. Extracted from Iwnicki¹⁷, Figure 8.27

Panel shift criterion Researched by the French National Railways suggested that the limiting lateral axle load can be defined in a general expression for preventing excessive track panel shift:

$$L_c = aV + b \quad (9.5)$$

where L_c is the critical lateral load and V is the vertical axle load. Iwnicki¹⁷, Table 8.2 lists two groups of suggested values of a and b . It is possible that different values for a and b can be specified in different areas.

9.2.6 Derailment caused by vehicle lateral instability

On tangent track, the wheelset generally oscillates around the track centre due to any vehicle and track irregularities, as shown in Figure 9.4. This movement occurs because vehicle and track are never absolutely smooth and symmetric. This self-centring capability of a wheelset is induced by the coned shape of the wheel tread. However, as speed is increased, if the wheelset conicity is high, the lateral movement of wheelset, as well as the associated bogie and car body motion, can cause oscillations with large amplitude and a well-defined wavelength. The lateral movements are limited only by the contact of the wheel flanges with the rail. This vehicle dynamic response is also termed as vehicle hunting, and can produce high lateral forces to damage track to cause derailments.

Derailment cause by vehicle hunting can have derailment mechanisms of all four types discussed in the previous sections. The high lateral force induced from hunting may cause wheel flange climbing

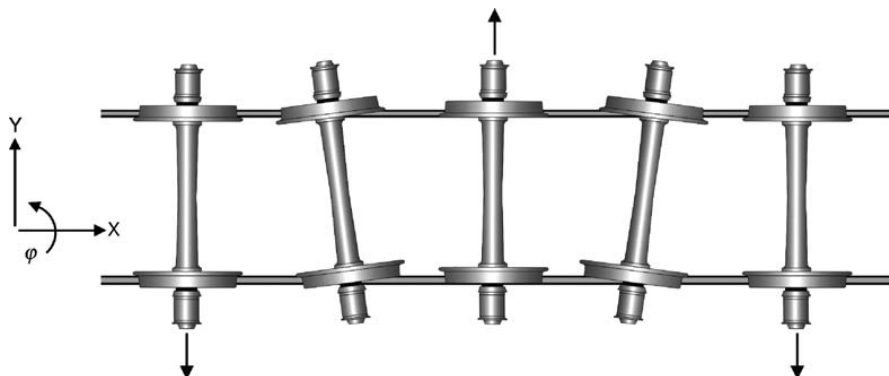


Figure 9.4: Wheelset oscillates around the track centre. Extracted from Iwnicki¹⁷, Figure8.28

on the rail, gauge widening, rail roll-over, track panel shift, or combinations of these. The safety concerns for this type of derailment, usually occurring at higher speeds, make it an important area of study.

Hunting predominantly occurs in empty or lightweight vehicles. The critical hunting speed is highly dependent on the vehicle/track characteristics. Investigation of the critical speed for such a system with nonlinearities is to examine the vehicle response to a disturbance using a numerical solution of the equations of motion.

9.2.7 Requirements for traffic serviceability(horizontal)

The criteria Comfort Indexes for assessing ride comfort in railway vehicles proposed in UIC²⁰. This standard describes a methodology for assessing ride comfort as a function of longitudinal, vertical and transverse accelerations.

Comfort Index indicates the percentage of passengers experiencing discomfort in a specific situation. These indexes can be computed via empiric formula given in the standard, which depend on variables such as lateral acceleration, rate of change of acceleration and rolling velocity. All these values are filtered with a moving average filter that eliminates small wavelength components. Using this methodology for the computed worst-case situations, the comfort indexes have been found excellent, therefore no passenger should feel uncomfortable.

Chapter 10

Conclusion

Two proposed criteria in RP6D181 Committee¹⁰ were adopted in Eurocode 1991-2. One of them is 1.2Hz criterion. It was adopted without amending. The other one is lateral force models. Loading models were adopted in a different name as 'nosing force' in CEN⁵, A6.5.2.

- The 1.2Hz criterion was aiming to avoid the occurrence of resonance between bridge first lateral vibration mode and vehicle sway mode, however, no research can be found among all D181 report series to support this hypothesis. This criterion was proposed without a valid background.
- Nosing force in EN1991-2 has a single characteristic value of 100kN, while RP6 proposes different values for different scenarios. Also, it is proved that nosing force isn't conservative when resonance happens between the vehicle and the bridge.

In addition, D181 did research on other 2 resonance phenomena, including axle repeat pattern resonance and kinematic movement resonance. Resonance was proved to be possible and was successfully reproduced using VAMPIRE software. These two resonance are wavelength phenomenon, meaning resonance can happen on any train/bridge combination.

However, the dynamic effects start to build up at a broader frequency, which means even if the resonance is avoided between bridge and train, the response of the bridge will still be amplified by dynamic loading. The relationship between total peak lateral force of the first two traction units and speed is found by using the simulation output and regression approach. The lateral force is greatly dependant on track quality, train type and speed.

Nosing force model was proposed by investigating the peak lateral force on track with a standard deviation of 7mm. Such track irregularities ensures the occurrence of hunting effects thus this value is conservative. However, for tracks maintained as regulation requires, up to 2mm standard deviation is allowed. Since track force increases as track standard deviation does, it can be concluded that 100kN of characteristic value for nosing force is very conservative.

By using the knowledge above, a practical method for easily calculating real-time mid-span resonance responses of the bridge is also developed. The method features an analytical model and an equivalent amplitude model. The equivalent amplitude model is developed based on both the simulation result of VAMPIRE software and the relationship between lateral force and train speed discovered earlier in the report. The practical method shows reasonable conservative prediction when compared to other reference data in DT329 reports.

However, as VAMPIRE simulation results only have span up to 120m, there's no benchmark can be found to validate the correctness of the formula for longer span inputs. So it is highly advisable that more simulations/measurements to be done to verify the correctness of result for longer span bridges.

Chapter 11

Recommendations on future researches

Future researches to be proposed in this section are mainly related to heavy FEM transient analysis. Although D181 committee conducted a number of simulations in D181 report series, the response of longer span bridges remains unknown. What's more, D181 report series were created in 1990's. The trains and their parameters used in the report are too old for nowadays usage.

The aim of proposed FEM simulations is to verify the practical method described in this thesis. The method is needed to be verified for longer span bridges and modern vehicle design. As a conclusion, simulations with following objectives are needed to be done:

1. Lateral forces on tracks of modern vehicles/tracks
2. Resonance response of bridges with span longer than 150m

These simulations should be done with following extra requirements on the basis of simulations done in resonance study of DT329:

1. More realistic and up-to-date data on modern train vehicles
2. More realistic data on lateral track irregularities
3. Broader range of bridge span to be investigated(greater than 150m)

Transient simulations of this topic is very resource demanding. It is impossible for this thesis to carry out these simulations. Thus above simulations are proposed to whoever possesses the resource and willingness to further investigate the topic. It is further proposed that lateral force data caused by running trains to be evaluated more frequently.

The practical method should be verified by comparing its own result with result of newly conducted simulations. The result of practical method should be conservative according to the comparison.

It is also possible to verify the amplitude in practical method to a less conservative value according to newly conducted simulations. It is expected that newly conducted simulations yield smaller lateral force on tracks because advanced suspension systems implemented in modern vehicle designs and better track quality.

Appendices

Appendix A

Plots and diagrams used in D181 DT 329

Freight train: Principle axle repeat patterns	dist m	Speed	
		60 km/h	100 km/h
wagon n axle 2 - wagon n+1 axle 1	4.00	4.17	6.94
wagon wheelbase	9.00	1.85	3.09
wagon n axle m - wagon n+1 axle m	13.0	1.28	2.14
wagon n axle m - wagon n+2 axle m	26.0	0.64	1.07
Passenger train: Principle axle repeat patterns	dist m	Speed	
		160 km/h	200 km/h
coach n axle 1 - 2, and coach n axle 3 - 4	2.56	17.36	21.70
coach n axle m - coach n+1 axle m	26.4	1.68	2.10
coach n axle m - coach n+2 axle m	52.8	0.84	1.05
ETR 500 train: Principle axle repeat patterns	dist m	Speed	
		300 km/h	350 km/h
coach n axle 1 - 2 and coach n axle 3 - 4	3.0	27.78	32.41
coach n axle m - coach n+1 axle m	26.1	3.19	3.72
coach n axle m - coach n+2 axle m	52.2	1.60	1.86
coach n axle m - coach n+3 axle m	69.3	1.20	1.40

Table A.1: Axle repeat patterns and typical frequencies. Extracted from D181Committee¹¹, Appendix C

Kinematic wavelength, m	Freight train	Passenger train	ETR500 train
Locomotive	39 - 45	32 - 38	39 - 45
Coach/wagon	24 - 39	34 - 38	36 - 40

Table A.2: Kinematic wavelength ranges per vehicle, with BR P1 profiles. Extracted from D181Committee¹¹, Appendix C

VEHICLE MODEL PARAMETER LISTS

VEHICLE TITLE BR CLASS 56 LOCOMOTIVE

MASSES & INERTIAS

Number of bogies	2
Number of axles (per bogie)	3
Body mass	81.2 Mg
Body roll inertia	107.0 Mgm ²
Body pitch inertia	1400.0 Mgm ²
Body yaw inertia	1400.0 Mgm ²
Bogie mass	5.6 Mg
Bogie roll inertia	5.0 Mgm ²
Bogie pitch inertia	21.6 Mgm ²
Bogie yaw inertia	21.6 Mgm ²
Wheelset mass	2.2 Mg
Wheelset roll and yaw inertia	2.7 Mgm ²

DIMENSIONS

Semi pivot spacing	5.19 m
Semi wheelbase	2.09 m
Wheel radius	0.57 m
Body centre of gravity height above rail level	1.85 m
Bogie centre of gravity height above rail level	0.86 m

PRIMARY SUSPENSION

Lateral stiffness (per axle)	0.1 MN/m
Vertical stiffness (per axle)	2.63 MN/m
Yaw stiffness (per axle)	29.0 MNm/r
Lateral damper rate (per axle)	- MNs/m
Vertical damper rate (per axle)	0.05 MNs/m
Vertical friction breakout (per axle)	- KN
Height above rail level of lateral springs	0.67 m
Lateral semi spacing of vertical springs	1.035 m
Height above rail level of lateral dampers	- m
Lateral semi spacing of vertical dampers	1.035 m
Lateral semi spacing of vertical friction	- m

Figure A.1: BR CLASS 56 LOCOMOTIVE. Extract from D181Committee¹¹, Appendix 2

Appendix 2

SECONDARY SUSPENSION

Lateral stiffness (per bogie)	0.77 MN/m
Vertical stiffness (per bogie)	2.72 MN/m
Roll bar stiffness (per bogie)	- MNm/r
Yaw stiffness (per bogie)	1.22 MNm/r
Lateral damper rate (per bogie)	0.084 MNs/m
Vertical damper rate (per bogie)	0.15 MNs/m
Yaw damper rate (per bogie)	0.055 MNms/r
Height above rail level of lateral springs	1.31 m
Lateral semi spacing of vertical springs	1.062 m
Height above rail level of lateral dampers	1.06 m
Lateral semi spacing of vertical dampers	1.062 m

Figure A.2: BR CLASS 56 LOCOMOTIVE. Extract from D181Committee¹¹, Appendix 2

Appendix 2

VEHICLE TITLE UIC FREIGHT WAGON (LADEN)

MASSES & INERTIAS

Number of bogies	-
Number of axles (per wagon)	2
Body mass	41.0 Mg
Body roll inertia	35.0 Mgm ²
Body pitch inertia	500.0 Mgm ²
Body yaw inertia	500.0 Mgm ²
Bogie mass	- Mg
Bogie roll inertia	- Mgm ²
Bogie pitch inertia	- Mgm ²
Bogie yaw inertia	- Mgm ²
Wheelset mass	2.0 Mg
Wheelset roll and yaw inertia	1.7 Mgm ²

DIMENSIONS

Semi pivot spacing	- m
Semi wheelbase	4.5 m
Wheel radius	0.46 m
Body centre of gravity height above rail level	1.5 m
Bogie centre of gravity height above rail level	- m

PRIMARY SUSPENSION

Lateral stiffness (per axle)	1.5 MN/m
Vertical stiffness (per axle)	2.6 MN/m
Yaw stiffness (per axle)	10.0 MNm/r
Lateral damper rate (per axle)	0.034 MNs/m
Vertical damper rate (per axle)	- MNs/m
Vertical friction breakout (per axle)	3.0 KN
Height above rail level of lateral springs	0.46 m
Lateral semi spacing of vertical springs	1.0 m
Height above rail level of lateral dampers	0.46 m
Lateral semi spacing of vertical dampers	- m
Lateral semi spacing of vertical friction	1.0 m

Figure A.3: UIC FREIGHT WAGON (LADEN). Extract from D181Committee¹¹, Appendix 2

SECONDARY SUSPENSION

Lateral stiffness (per bogie)	- MN/m
Vertical stiffness (per bogie)	- MN/m
Roll bar stiffness (per bogie)	- MNm/r
Yaw stiffness (per bogie)	- MNm/r
Lateral damper rate (per bogie)	- MNs/m
Vertical damper rate (per bogie)	- MNs/m
Yaw damper rate (per bogie)	- MNms/r
Height above rail level of lateral springs	- m
Lateral semi spacing of vertical springs	- m
Height above rail level of lateral dampers	- m
Lateral semi spacing of vertical dampers	- m

Figure A.4: UIC FREIGHT WAGON (LADEN). Extract from D181Committee¹¹, Appendix 2

Appendix 2

VEHICLE TITLE FS ETR500 LOCOMOTIVE

MASSES & INERTIAS

Number of bogies	2
Number of axles (per bogie)	2
Body mass	55.98 Mg
Body roll inertia	53.366 Mgm ²
Body pitch inertia	1643.0 Mgm ²
Body yaw inertia	1630.0 Mgm ²
Bogie mass	3.896 Mg
Bogie roll inertia	3.115 Mgm ²
Bogie pitch inertia	5.843 Mgm ²
Bogie yaw inertia	8.107 Mgm ²
Wheelset mass	2.059 Mg
Wheelset roll and yaw inertia	1.164 Mgm ²

DIMENSIONS

Semi pivot spacing	6.0 m
Semi wheelbase	1.5 m
Wheel radius	0.55 m
Body centre of gravity height above rail level	1.65 m
Bogie centre of gravity height above rail level	0.64 m

PRIMARY SUSPENSION

Lateral stiffness (per axle)	12.0 MN/m
Vertical stiffness (per axle)	3.55 MN/m
Yaw stiffness (per axle)	15.4 MNm/r
Lateral damper rate (per axle)	- MNs/m
Vertical damper rate (per axle)	0.3 MNs/m
Vertical friction breakout (per axle)	- KN
Height above rail level of lateral springs	0.55 m
Lateral semi spacing of vertical springs	1.03 m
Height above rail level of lateral dampers	- m
Lateral semi spacing of vertical dampers	1.2 m
Lateral semi spacing of vertical friction	- m

Figure A.5: FS ETR500 LOCOMOTIVE. Extract from D181Committee¹¹, Appendix 2

Appendix 2

SECONDARY SUSPENSION

Lateral stiffness (per bogie)	0.584 MN/m
Vertical stiffness (per bogie)	1.888 MN/m
Roll bar stiffness (per bogie)	1.0 MNm/r
Yaw stiffness (per bogie)	- MNm/r
Lateral damper rate (per bogie)	0.037 MNs/m
Vertical damper rate (per bogie)	0.145 MNs/m
Yaw damper rate (per bogie)	0.938 MNms/r
Height above rail level of lateral springs	0.95 m
Lateral semi spacing of vertical springs	1.03 m
Height above rail level of lateral dampers	0.73 m
Lateral semi spacing of vertical dampers	1.05 m

Figure A.6: FS ETR500 LOCOMOTIVE. Extract from D181Committee¹¹, Appendix 2

Appendix 2

VEHICLE TITLE FS ETR500 COACH

MASSES & INERTIAS

Number of bogies	2
Number of axles (per bogie)	2
Body mass	34.23 Mg
Body roll inertia	54.63 Mgm ²
Body pitch inertia	1821.0 Mgm ²
Body yaw inertia	1760.0 Mgm ²
Bogie mass	2.76 Mg
Bogie roll inertia	2.034 Mgm ²
Bogie pitch inertia	2.504 Mgm ²
Bogie yaw inertia	4.071 Mgm ²
Wheelset mass	1.58 Mg
Wheelset roll and yaw inertia	0.753 Mgm ²

DIMENSIONS

Semi pivot spacing	9.5 m
Semi wheelbase	1.5 m
Wheel radius	0.44 m
Body centre of gravity height above rail level	1.5 m
Bogie centre of gravity height above rail level	0.68 m

PRIMARY SUSPENSION

Lateral stiffness (per axle)	4.35 MN/m
Vertical stiffness (per axle)	1.61 MN/m
Yaw stiffness (per axle)	14.0 MNm/r
Lateral damper rate (per axle)	- MNs/m
Vertical damper rate (per axle)	0.015 MNs/m
Vertical friction breakout (per axle)	- KN
Height above rail level of lateral springs	0.44 m
Lateral semi spacing of vertical springs	0.96 m
Height above rail level of lateral dampers	- m
Lateral semi spacing of vertical dampers	0.96 m
Lateral semi spacing of vertical friction	- m

Figure A.7: FS ETR500 COACH. Extract from D181Committee¹¹, Appendix 2

Appendix 2

SECONDARY SUSPENSION

Lateral stiffness (per bogie)	0.256 MN/m
Vertical stiffness (per bogie)	0.722 MN/m
Roll bar stiffness (per bogie)	1.0 MNm/r
Yaw stiffness (per bogie)	- MNm/r
Lateral damper rate (per bogie)	0.04 MNs/m
Vertical damper rate (per bogie)	0.065 MNs/m
Yaw damper rate (per bogie)	0.70 MNms/r
Height above rail level of lateral springs	0.8 m
Lateral semi spacing of vertical springs	0.96 m
Height above rail level of lateral dampers	0.8 m
Lateral semi spacing of vertical dampers	1.2 m

Figure A.8: FS ETR500 COACH. Extract from D181Committee¹¹, Appendix 2

Appendix 2

VEHICLE TITLE FS E444 LOCOMOTIVE

MASSES & INERTIAS

Number of bogies	2
Number of axles (per bogie)	2
Body mass	64.6 Mg
Body roll inertia	53.366 Mgm ²
Body pitch inertia	1643.0 Mgm ²
Body yaw inertia	1630.0 Mgm ²
Bogie mass	4.0 Mg
Bogie roll inertia	3.115 Mgm ²
Bogie pitch inertia	5.843 Mgm ²
Bogie yaw inertia	8.107 Mgm ²
Wheelset mass	2.1 Mg
Wheelset roll and yaw inertia	1.164 Mgm ²

DIMENSIONS

Semi pivot spacing	4.5 m
Semi wheelbase	1.3 m
Wheel radius	0.55 m
Body centre of gravity height above rail level	1.65 m
Bogie centre of gravity height above rail level	0.64 m

PRIMARY SUSPENSION

Lateral stiffness (per axle)	12.0 MN/m
Vertical stiffness (per axle)	4.0 MN/m
Yaw stiffness (per axle)	15.4 MN/m
Lateral damper rate (per axle)	- MNs/m
Vertical damper rate (per axle)	0.03 MNs/m
Vertical friction breakout (per axle)	- KN
Height above rail level of lateral springs	0.55 m
Lateral semi spacing of vertical springs	1.03 m
Height above rail level of lateral dampers	- m
Lateral semi spacing of vertical dampers	1.2 m
Lateral semi spacing of vertical friction	- m

Figure A.9: FS E444 LOCOMOTIVE. Extract from D181Committee¹¹, Appendix 2

Appendix 2

SECONDARY SUSPENSION

Lateral stiffness (per bogie)	1.0 MN/m
Vertical stiffness (per bogie)	2.1 N/m
Roll bar stiffness (per bogie)	1.0 Nm/r
Yaw stiffness (per bogie)	- Nm/r
Lateral damper rate (per bogie)	0.037 MNs/m
Vertical damper rate (per bogie)	0.145 MNs/m
Yaw damper rate (per bogie)	0.938 MNms/r
Height above rail level of lateral springs	0.95 m
Lateral semi spacing of vertical springs	1.03 m
Height above rail level of lateral dampers	0.73 m
Lateral semi spacing of vertical dampers	1.20 m

Figure A.10: FS E444 LOCOMOTIVE. Extract from D181Committee¹¹, Appendix 2

Appendix 2

VEHICLE TITLE UIC COACH

MASSES & INERTIAS

Number of bogies	2
Number of axles (per bogie)	2
Body mass	32.0 Mg
Body roll inertia	56.8 Mgm ²
Body pitch inertia	1970.0 Mgm ²
Body yaw inertia	1970.0 Mgm ²
Bogie mass	2.615 Mg
Bogie roll inertia	1.722 Mgm ²
Bogie pitch inertia	1.476 Mgm ²
Bogie yaw inertia	3.067 Mgm ²
Wheelset mass	1.70 Mg
Wheelset roll and yaw inertia	1.30 Mgm ²

DIMENSIONS

Semi pivot spacing	9.5 m
Semi wheelbase	1.28 m
Wheel radius	0.445 m
Body centre of gravity height above rail level	1.503 m
Bogie centre of gravity height above rail level	0.68 m

PRIMARY SUSPENSION

Lateral stiffness (per axle)	6.4 MN/m
Vertical stiffness (per axle)	1.46 MN/m
Yaw stiffness (per axle)	60.0 MNm/r
Lateral damper rate (per axle)	- MNs/m
Vertical damper rate (per axle)	0.005 MNs/m
Vertical friction breakout (per axle)	- KN
Height above rail level of lateral springs	0.445 m
Lateral semi spacing of vertical springs	1.0 m
Height above rail level of lateral dampers	- m
Lateral semi spacing of vertical dampers	1.0 m
Lateral semi spacing of vertical friction	- m

Figure A.11: UIC COACH. Extract from D181Committee¹¹, Appendix 2

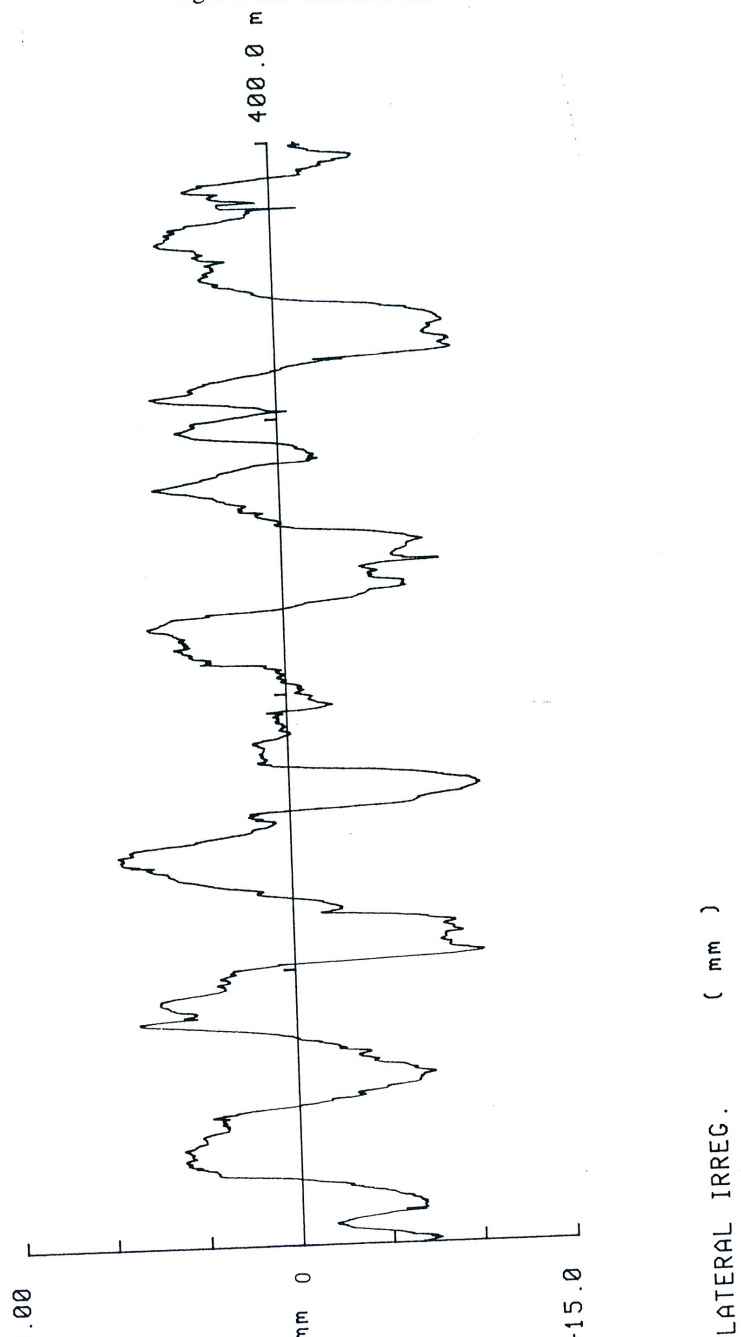
Appendix 2

SECONDARY SUSPENSION

Lateral stiffness (per bogie)	0.32 MN/m
Vertical stiffness (per bogie)	0.86 MN/m
Roll bar stiffness (per bogie)	0.94 MNm/r
Yaw stiffness (per bogie)	- MNm/r
Lateral damper rate (per bogie)	0.059 MNs/m
Vertical damper rate (per bogie)	0.074 MNs/m
Yaw damper rate (per bogie)	0.591 MNms/r
Height above rail level of lateral springs	0.825 m
Lateral semi spacing of vertical springs	1.0 m
Height above rail level of lateral dampers	0.825 m
Lateral semi spacing of vertical dampers	1.3 m

Figure A.12: UIC COACH. Extract from D181Committee¹¹, Appendix 2

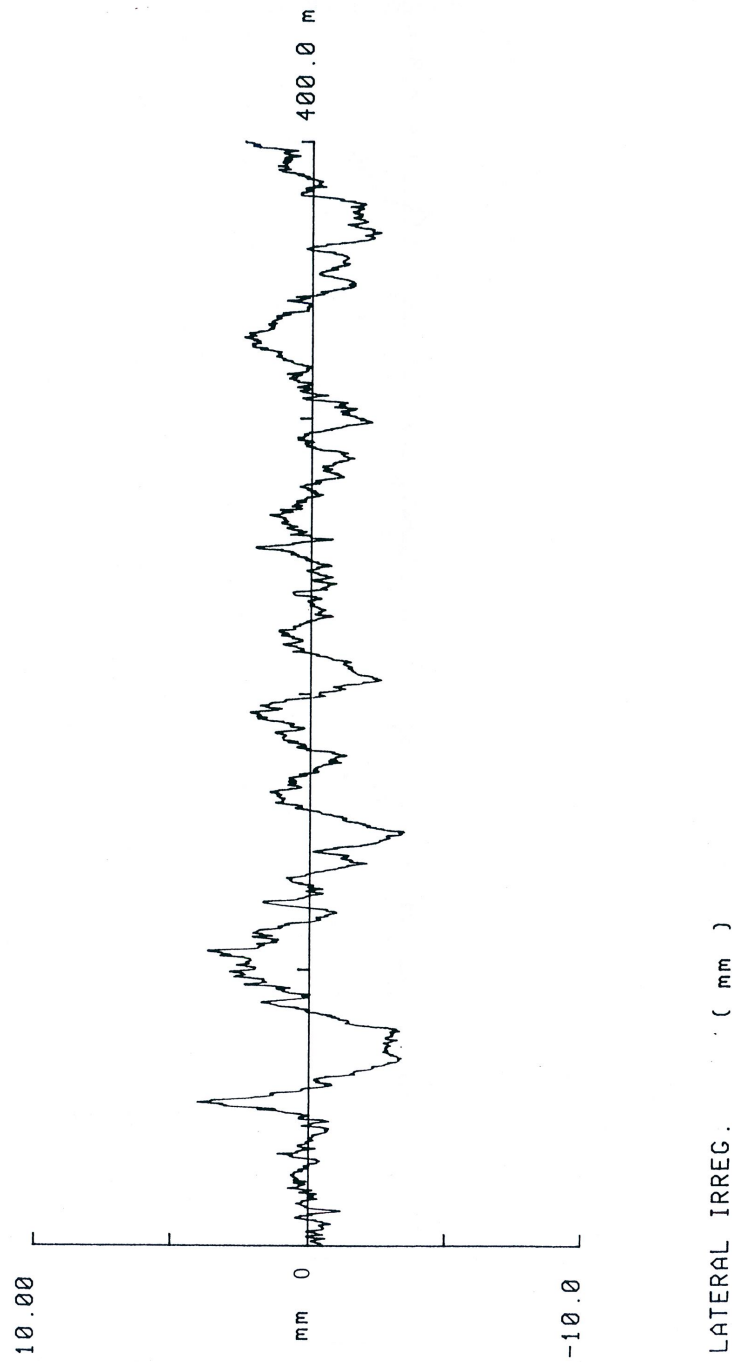
Freight track: Trackfrt. dat



62

Figure A.13: Horizontal track irregularities for freight trains. Extract from D181Committee¹⁰, Figure 2.1

Passenger track: Trackpn. dat



LATERAL IRREG. (mm)

63

Figure A.14: Horizontal track irregularities for standard passenger trains. Extract from D181Committee¹⁰, Figure 2.1

ERRI D 181/RP 6	VAMPIRE HORIZONTAL TRACK IRREGULARITIES (HIGH-SPEED LINE)	Fig. 2.3
-----------------	---	----------

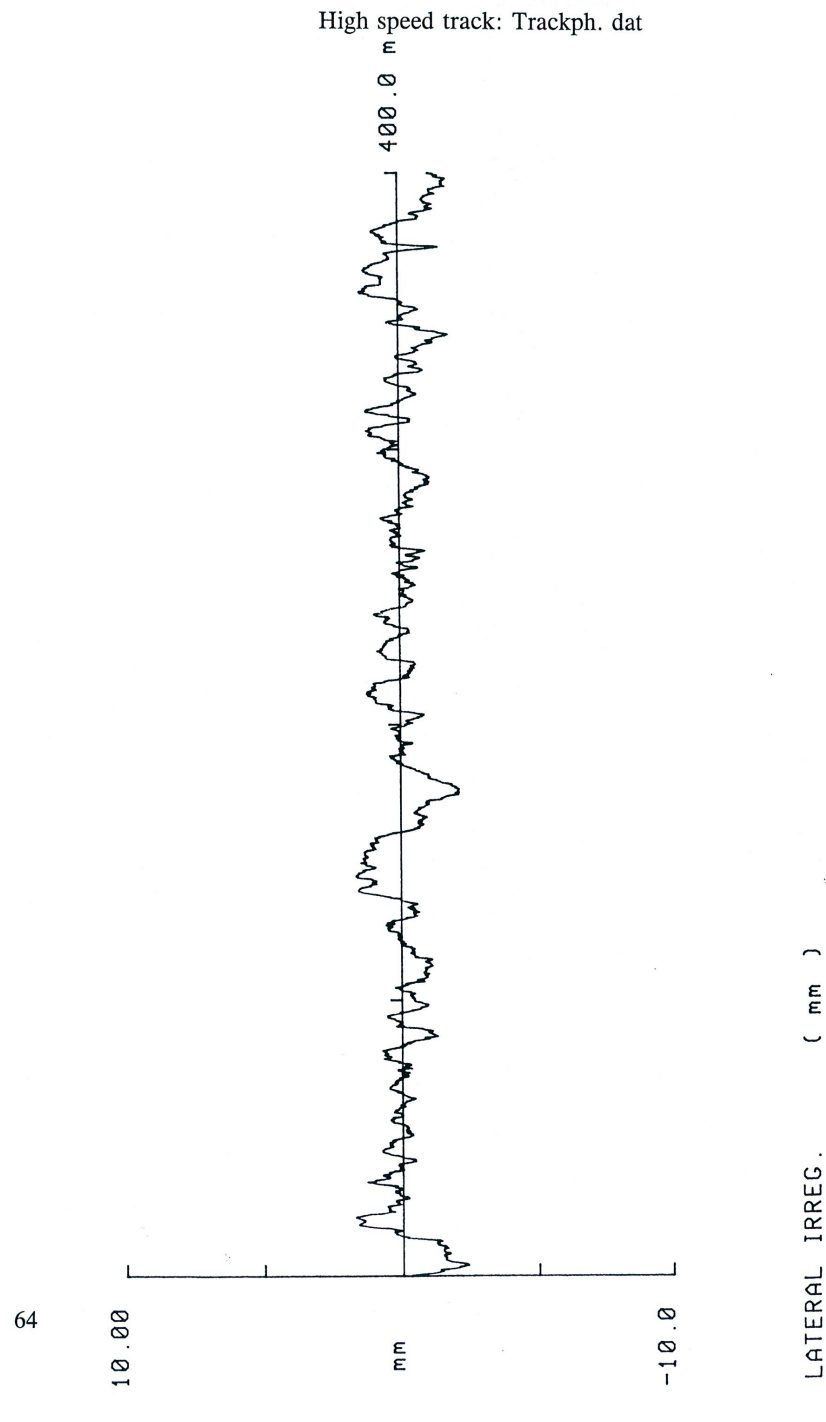


Figure A.15: Horizontal track irregularities for high speed passenger train. Extract from D181Committee¹⁰, Figure 2.1

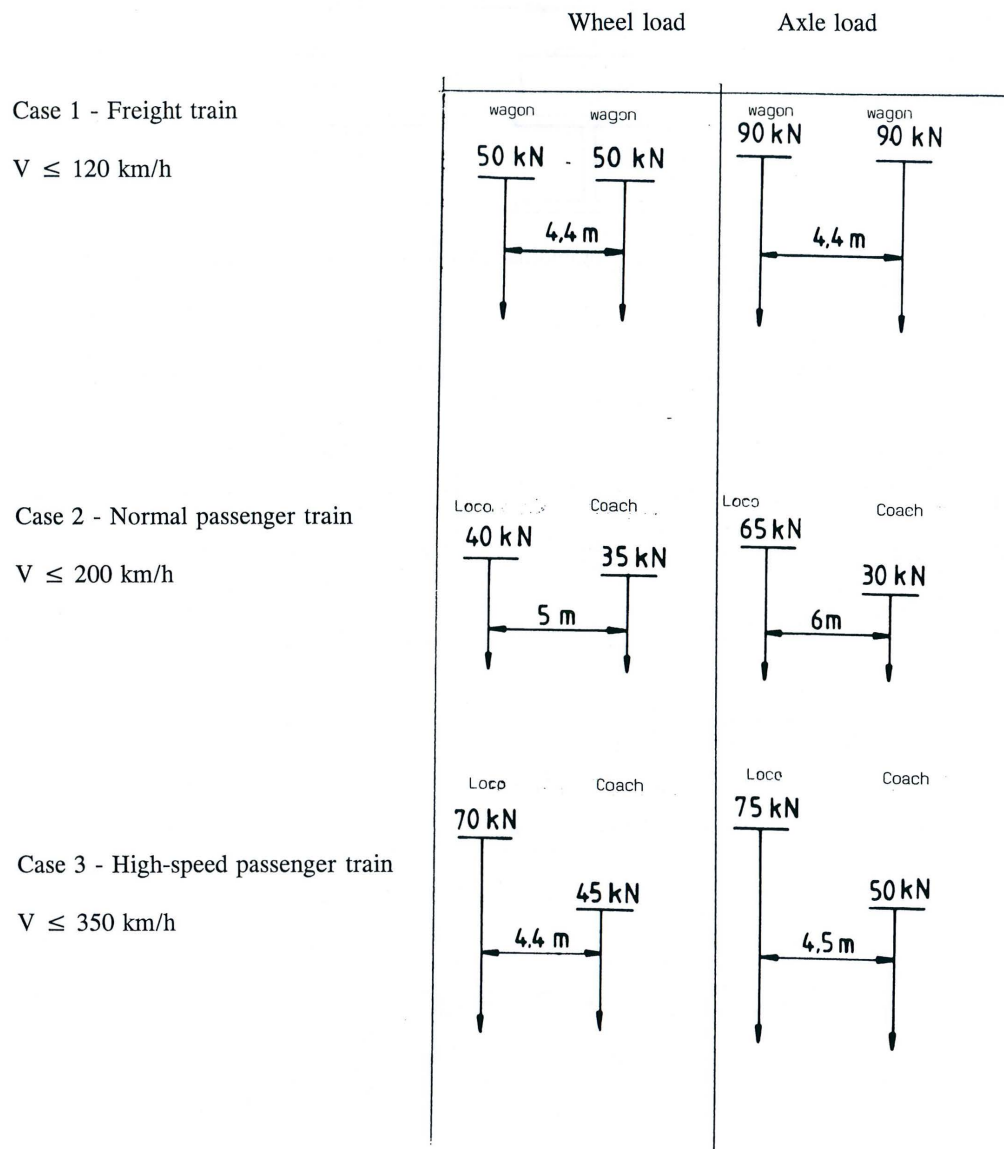
Appendix B

Speeds which do not require dynamic compatibility checks

Line category Locomotive class	Freight wagon	Locomotive	Passenger carriage	Multiple unit	Special vehicle
a10^a	-	-	-	-	-
a12^a	-	-	-	-	-
a14^a	-	-	-	-	-
A	120	120 ^b / 160	160 ^c	160 ^c	120
B1	120	120 ^b / 160	160 ^c	160 ^c	120
B2	120	120 ^b / 160	-	-	120
C2	120	120 ^b / 160	140 ^c	140 ^c	120
C3	120	120	-	-	120
C4	120	120	-	-	120
D2	120	120 ^b / 160	120 ^c	120 ^c	120
D3	120	120	-	-	120
D4	120	120	-	-	120
D4xL	120 ^d	120	-	-	120 ^d
D5	100	-	-	-	100
E4	100	-	-	-	100
E5	100	-	-	-	100
E6	80	-	-	-	80
L4	-	120 ^b / 160	-	-	-
L6	-	120	-	-	-

^a Light railways – normal operating speeds are generally significantly less than speed at which additional dynamic checks would need to be considered.
^b Three or more adjacent couples locomotives.
^c Additional values for max "p" (see Table F.2).
^d Option.

Figure B.1: Speed limit (in km/h) in relationship Line Category/Locomotive Class and vehicle type. Extract from CEN⁸, Appendix F



EXAMPLE RUN FILE

```

Case 7: Passenger train/track, 160kph, 54m span, 1/10000 flex., 6 Mg/m
EUROLONG
*TRANSIENT
    470.  0.0010  0.01
        44.444

trackPN
*CREEP
    0.3000  0.3000  8.0000  0.0000  0.0000
NON-LINEAR
stdp1
*OUTPUT
Lat displacement of bridge @ mid span   mm
    1000*U01
Lat acceleration of bridge @ mid span  m/s2
    U02
LOCO body lat accel @ leading pivot   m/s2
    A01Y + 4.5*A01W
COACH 1 body lat accel @ leading pivot m/s2
    A08Y + 9.5*A08W
LOCO lat accel of leading bogie      m/s2
    A02Y
COACH 1 lat accel of leading bogie   m/s2
    A09Y
Total lat force on LOCO leading bogie kN
    FW01Y + FW02Y
Total lat force on COACH 1 leading bogie kN
    FW05Y + FW06Y
Lat force, COACH 1 wset 1, left wheel  kN
    FL05Y
Lat force, COACH 1 wset 1, right wheel kN
    FR05Y
Lat force, COACH 1 wset 2, left wheel  kN
    FL06Y
Lat force, COACH 1 wset 2, right wheel  kN
    FR06Y
Lat force, LOCO wset 1, left wheel   kN
    FL01Y
Lat force, LOCO wset 1, right wheel  kN
    FR01Y
Lat force, LOCO wset 2, left wheel   kN
    FL02Y
Lat force, LOCO wset 2, right wheel  kN
    FR02Y
Lat force, LOCO wset 3, left wheel   kN
    FL03Y
Lat force, LOCO wset 3, right wheel  kN
    FR03Y
COACH 5 body lat accel @ leading pivot m/s2
    A36Y + 9.5*A36W
COACH 5 lat accel of leading bogie   m/s2
    A37Y
Total lat force on COACH 5 leading bogie kN
    FW21Y + FW22Y
Lat force, COACH 5 wset 1, left wheel  kN
    FL21Y
Lat force, COACH 5 wset 1, right wheel kN
    FR21Y
Lat force, COACH 5 wset 2, left wheel  kN
    FL22Y
Lat force, COACH 5 wset 2, right wheel kN
    FR22Y
*

```

968223/01

Figure B.3: Example run file. Extracted from D181Committee¹¹.

Appendix C

MU-Groups and MU-Classes

C.1 Definition

Multiple units can be grouped according to type of traffic service (high speed - long distance, intercity - regional and commuter/suburban) or to the kind of running gear (conventional bogies, articulated bogies and single axles).

In some cases due to potential excessive dynamic load effects in bridge line category checks are not sufficient to demonstrate compatibility. To minimise the need for undertaking a dynamic check of individual trains, several typical and wide spread MU-designs have been grouped in MU-classes. For these groups of vehicles, load models covering the specified design parameter ranges have been developed to allow the efficient dynamic analysis of bridges. For practical reasons, the number of MU classes was limited and for trains outside the range of parameters covered, the process of checking an individual train existing at the time of publication of this standard as state of the art shall be used.

Each MU-class is defined by:

- ranges of train parameters covered and;
- a corresponding load model for carrying out dynamic checks on bridges.

Each MU-Group comprises of several MU-Classes. Table

MU-Group	MU-Class
conventional bogie(CB)	CB_1 CB_2
articulated bogie(AB)	AB_1 AB_2 AB_3 AB_4
single axle(SA)	SA_1 SA_2

Table C.1: Relationship MU-groups - MU-classes

C.1.1 Train parameters of MU-Class CB_1

C.1.2 Train parameters of MU-Class CB_2

C.1.3 Train parameters of MU-Class AB_1

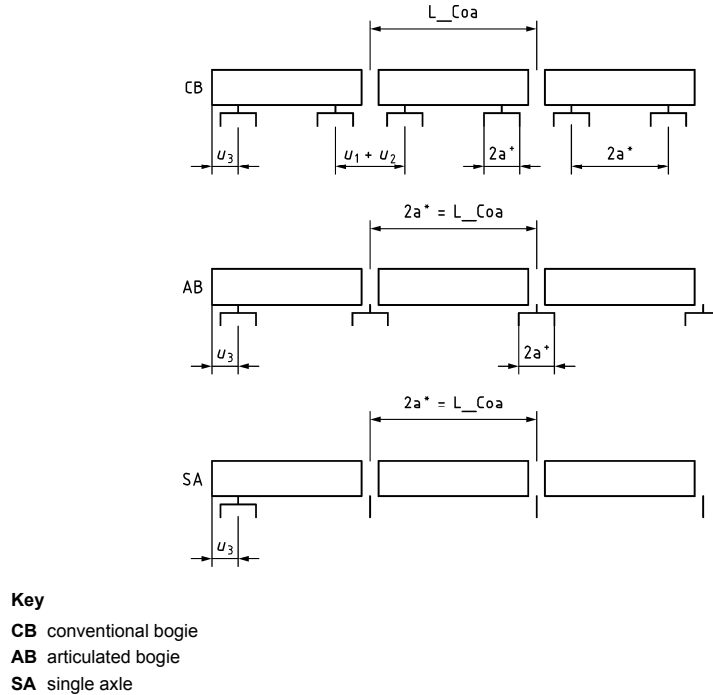


Figure C.1: Train parameters related to MU-Groups. Extracted from CEN⁸, Annex C

Name	Parameter	Unit
$2a^*$	Bogie spacing between pivot centres within a vehicle	m
$2a^+$	Axle spacing in bogie	m
$u_1 + u_2$	Bogie spacing between pivot centres of adjacent vehicles	m
u_3	Overhang of end coaches	m
L_Coa	Coach length	m
No_Coa	Number of coaches within an unit	-
No_Units	Number of units within a train	-

Table C.2: Explanation of train parameters. Extracted from CEN⁸, Annex C

C.1.4 Train parameters of MU-Class AB_2

C.1.5 Train parameters of MU-Class AB_3

C.1.6 Train parameters of MU-Class AB_4

C.1.7 Train parameters of MU-Class SA_1

C.1.8 Train parameters of MU-Class SA_2

max No_Units	2
max No_Coa	8
L_Coa	$23.8m \leq L_Coa \leq 25.3m$
$2a^*$	$16.8m \leq 2a^* \leq 18.0m$
$2a^+$	$2m \leq 2a^+ \leq 3m$
$(u1 + u2)$	$7.0m \leq (u1 + u2) \leq 7.6m$
$u3$	$4m \leq u3 \leq 6m$

Table C.3: Train parameters for conformity with MU-Class CB_1

max No_Units	2
max No_Coa	7
L_Coa	$25.3m \leq L_Coa \leq 27.5m$
$2a^*$	$18.0m \leq 2a^* \leq 19.5m$
$2a^+$	$2m \leq 2a^+ \leq 3m$
$(u1 + u2)$	$7.2m \leq (u1 + u2) \leq 8.0m$
$u3$	$4m \leq u3 \leq 6m$

Table C.4: Train parameters for conformity with MU-Class CB_2

max No_Units	4
max No_Coa	5
$2a^*$	$14.9m \leq 2a^* \leq 16.0m$
$2a^+$	$2m \leq 2a^+ \leq 3m$
$u3$	$3m \leq u3 \leq 5.5m$

Table C.5: Train parameters for conformity with MU-Class AB_1

max No_Units	4
max No_Coa	5
$2a^*$	$18.8m \leq 2a^* \leq 19.5m$
$2a^+$	$2m \leq 2a^+ \leq 3m$
$u3$	$3m \leq u3 \leq 5.5m$

Table C.6: Train parameters for conformity with MU-Class AB_2

max No_Units	2
max No_Coa	11
$2a^*$	$17.0m \leq 2a^* \leq 17.5m$
$2a^+$	$2m \leq 2a^+ \leq 3m$
$u3$	$4.5m \leq u3 \leq 5.7m$

Table C.7: Train parameters for conformity with MU-Class AB_3

max No_Units	2
max No_Coa	10
$2a^*$	$18.7m \leq 2a^* \leq 19.2m$
$2a^+$	$2m \leq 2a^+ \leq 3m$
$u3$	$4.3m \leq u3 \leq 5.3m$

Table C.8: Train parameters for conformity with MU-Class AB_4

max No_Units	3
max No_Coa	10
$2a^*$	$9.2m \leq 2a^* \leq 9.8m$
$u3$	$4.25m \leq u3 \leq 6.25m$

Table C.9: Train parameters for conformity with MU-Class SA_1

max No_Units	2
max No_Coa	14
$2a^*$	$12.8m \leq 2a^* \leq 13.5m$
$u3$	$4.25m \leq u3 \leq 6.25m$

Table C.10: Train parameters for conformity with MU-Class SA_2

Appendix D

Regression commands for R console

```
> F <- c(0,110,170,185)
> v <- c(0,60,100,120)
> f <- function(a,b,v) {a*v^b}
> dat <- data.frame(v,F)
> dat
   v     F
1 0     0
2 60   110
3 100  170
4 120  185

> fm <- nls(F ~ f(a,b,v), data = dat, start = c(a=1, b=1))
> fm
Nonlinear regression model
  model: F ~ f(a, b, v)
  data: dat
      a      b
 5.2064 0.7498
 residual sum of squares: 47.84

Number of iterations to convergence: 6
Achieved convergence tolerance: 2.868e-06
```

Appendix E

Matlab scripts

E.1 fog.m

```
% This script is the main utility to function automated bridge lateral
dynamic response evaluation

function O=fogtest(EJ,l,mu,c,zeta ,linecolor)

if EJ<1
    EJ = 100000*l^2/(48*EJ);
end

omegal = pi^2/l^2*sqrt(EJ/mu);
omega = pi*c/l;
omegab = zeta*sqrt(EJ/mu);
omegab = 0.5*zeta*omegal;
% omegab = omegal*sqrt(1 zeta ^ 2)
omega1a = sqrt(abs(omegal^2 omegab^2));
Omega = 2*pi*c/10;

r1 = Omega + omega;
r2 = Omega - omega;

% if c >= (200/3.6)
%     Q = 3.10*(c*3.6) ^ 0.7495;
% end
%
% if c >= (120/3.6) && c < (200/3.6)
%     Q = 3.58*(c*3.6) ^ 0.7495;
% end
%
% if c < (120/3.6)
%     Q = 5.2064*(c*3.6) ^ 0.7495;
% end
```

```

% Q = Q;
% Q = 10000
Q = 1928*c^0.7495;
f = omega1/(2*pi);
v_0 = Q*l^3/(48*EJ);
%omegab = 0.0001*sqrt(EJ/mu);

beta = omegab/omega1;

v1 = @(t) 1^3*Q*omega1/(pi^4*EJ) * cos(omega1*t)/(omega^2+omegab^2);
v2 = @(t) omega*(cos(omega*t) exp(-omegab*t)) omegab*sin(omega*t);
v = @(t) v1(t) * v2(t);

% v11 = 1/((omega1^2 r2^2)^2+4*omegab^2*r2^2);
% v12 = @(t) (omega1^2 r2^2)*(cos(r2*t) exp(-omegab*t)*cos(omega1a*t));
% v13 = @(t) 2*omegab*r2*sin(r2*t);
% v14 = @(t) omegab/omega1a*(omega1^2+r2^2)*exp(-omegab*t)*sin(omega1a*t);
% v21 = 1/((omega1^2 r1^2)^2+4*omegab^2*r1^2);
% v22 = @(t) (omega1^2 r1^2)*(cos(r1*t) exp(-omegab*t)*cos(omega1a*t));
% v23 = @(t) 2*omegab*r1*sin(r1*t);
% v24 = @(t) omegab/omega1a*(omega1^2+r1^2)*exp(-omegab*t)*sin(omega1a*t);
% v = @(t) Q/(mu*l)*(v11*(v12(t)+v13(t)+v14(t))+v21*(v22(t)+v23(t)+v24(t)));
% v = @(t) Q/(mu*l)*(v11*(v12(t)+v13(t)+v14(t))+v21*(v22(t)+v23(t)+v24(t))));

a11 = @(t) 1^3*Q*omega1^3*cos(omega1*t)/(pi^4*EJ*(omega^2+omegab^2));
a12 = @(t) omega*(cos(omega*t) exp(-omegab*t)) omegab*sin(omega*t);
a21 = @(t) 1^3*Q*omega1*cos(omega1*t)/(pi^4*EJ*(omega^2+omegab^2));
a221 = @(t) omega*(cos(omega*t)*omega^2 exp(-omegab*t)*omegab^2);
a222 = @(t) omegab*sin(omega*t)*omega^2;
a22 = @(t) a221(t)+a222(t);
a31 = @(t) 2*1^3*Q*omega1^2*sin(omega1*t)/(pi^4*EJ*(omega^2+omegab^2));
a32 = @(t) omega*(sin(omega*t)+exp(-omegab*t)*omegab) omegab*cos(omega*t)*omega;
a = @(t) a11(t)*a12(t)+a21(t)*a22(t)+a31(t)*a32(t);

maxt = 1/c;
dt = maxt/1000;
tdomain = [0:dt:maxt]';

for i=1:length(tdomain)
    p(i,1) = v(tdomain(i,1));
    p(i,2) = a(tdomain(i,1));
    p(i,3) = p(i,1)/v_0;
end

```

```

O = [max(abs(p(:,1))),max(abs(p(:,2))),max(abs(p(:,3)))];

namedaf = strcat('EJ', int2str(EJ), 'L', int2str(1), 'mu', int2str(mu), 'c',
    int2str(c), 'daf', '.tikz');

%%%
% figure(1)
% plot(tdomain,p(:,1),linecolor)
% grid on
% title(strcat('Max Deflection:', mat2str(O(1,1))));
% %% matlab2tikz(namedaf, 'height', '\figureheight', 'width', '\
% figurewidth', 'showInfo', false);
%%%
% figure(2)
% plot(tdomain,p(:,2))
% grid on
% title(strcat('Max Acceleration:', mat2str(O(1,2))));
% %% matlab2tikz(nameacc, 'height', '\figureheight', 'width', '\
% figurewidth', 'showInfo', false);
%%%
% figure(3)
% plot(tdomain,p(:,3))
% grid on
% title(strcat('Max Deflection:', mat2str(O(1,1)), ',Max Acceleration:',
% mat2str(O(1,2))));

matlab2tikz(namedaf, 'height', '\figureheight', 'width', '\figurewidth',
    'showInfo', false);

```

E.2 Speedenvelop.m

```

function O=Speedenvelop(EJ,l,mu,min,max,zeta)

dv = 0.2;
v = [min:dv:max]';

for i=1:length(v)
    maxres(:,i) = fog(EJ,l,mu,v(i,1),zeta,'b');
    speed = v(i,1);
end

%% figure('name','speed_envelop');
%% plot(v,maxres);

namedef = strcat('speedef', 'EJ', int2str(EJ), 'L', int2str(1), 'min', int2str(
    min), 'max', int2str(max), 'mu', int2str(mu), '.tikz')
nameacc = strcat('speacc', 'EJ', int2str(EJ), 'L', int2str(1), 'min', int2str(
    min), 'max', int2str(max), 'mu', int2str(mu), '.tikz')
nameaco = strcat('speaco', 'EJ', int2str(EJ), 'L', int2str(1), 'min', int2str(
    min), 'max', int2str(max), 'mu', int2str(mu), '.tikz')

figure(1)

```

```

plot(v,maxres(1,:))
title(strcat('SpeedEnvelop def from',int2str(min),' to ', int2str(max)))
;
matlab2tikz(namedef, 'height', '\figureheight', 'width', '\figurewidth
', 'showInfo', false);

figure(2)
plot(v,maxres(2,:))
title(strcat('SpeedEnvelop acc from',int2str(min),' to ', int2str(max)))
;
%matlab2tikz(nameacc, 'height', '\figureheight', 'width', '\figurewidth
', 'showInfo', false);

figure(3)
plot(v,maxres(3,:))
title(strcat('SpeedEnvelop dc from',int2str(min),' to ', int2str(max)));
%matlab2tikz(nameaco, 'height', '\figureheight', 'width', '\figurewidth
', 'showInfo', false);

```

Appendix F

Train vehicles

F.1 Locomotives

F.1.1 4-axle locomotives

Generally, the relevant parameters for categorisation of 4-axle locomotives are axle load P (18 t to 22,5 t) and the bogie axle spacing (2,2 m to 3,4 m).

Typically the mass per unit length is less than 6,4 t/m and the distance from the end axle to the end of the nearest coupling plane is greater than 1,9 m

F.1.2 6-axle locomotives

Generally, the relevant parameters for categorisation of 6-axle locomotives are:

- the maximum axle load P (18 t to 22 t) in combination with;
- the distance between axles within a bogie (1,80 m to 2,25 m).

Typically, the mass per unit length (p) is less than 6,4 t/m and the distance from end axle to the end of the nearest coupling plane (a) is greater than 2,1 m.

F.2 Trains in Netherlands

Passenger trains now in service include following models:

1. The DD-AR (Dubbeldeksaggloregiomaterieel)

EMUs were delivered as DDM-2/3 resembling the bilevel rail cars series DDM-1 from 1985 and operates in fixed formations of 3 or 4 coaches. 4 car trains use a class 1700 locomotive for traction, 3 car trains use an mDDM motorcar, which resembles a DD-AR driving trailer but has electric motors and a single passenger deck on top; the level of this deck is higher than that of a regular single deck rail car, but lower than the upper deck of the other coaches. Three types of coaches are available: Bv (second class), ABv (first and second class) and Bvk (second class driving trailer). The DDM-2/3 series are being modernised from 2010/2013 and after modernisation the series was renamed as NID (Nieuwe Intercity Dubbeldekker).

2. The VIRM (Verlengd Interregiomaterieel)

also called Regiorunner was partially rebuilt from trainsets DD-IRM (Dubbeldeks Interregiomaterieel). DD-IRM was delivered in 3- and 4-car trainsets. 3-car trainsets got one extra coach, 4-car trainsets got two extra coaches. Also, new 4- and 6-car trainsets were built. Thus, a train consists of one or more combinations of 4 or 6 double deck coaches; each combination (multiple unit) has electric motors. More than three hundred coaches are currently operative in the Netherlands.

3. The Koploper (ICM) (Intercitymaterieel)

is a 3- or 4-car multiple unit that when coupled with another one, allows passengers to walk through (the name Koploper being a play on words literally "head walker", but in actual use meaning "front runner"). The Dutch Railway Company decided to close the heads permanently on 31 October 2005 because the mechanism broke down too often. A scheduled modernisation of around 7 million euro will see the ICM fleet updated. The renovated ICM trains provide 13% more seats (reducing the leg room to uncomfortable small for the long haul journeys they serve in 2nd class, which is further aggravated by a waste bin that is placed on the backsides of the seats in front), have a new interior, a bathroom accessible by wheelchairs, airconditioning as well as upgrades to the engine and connection systems. The head doors are removed. Also, these (renovated) trains are the first trains in the NS fleet equipped with OBIS. OBIS provides a (free) WiFi-connection on board, along with in-train journey information provided through screens and (automated) vocal announcements through the trains speakers. This journey information provides the actual status, and thus is always up-to-date to the actual situation this trip, and the stations is passes.

4. The Sprinter (SGM, Stads Gewestelijk Materieel)

is a two or three car electric, used on small distances. They are named Sprinter because they're able to accelerate and brake quite fast, making them very suitable for 'stoptrein' services. They were also specifically designed for urban environments where they run commuter services. As a result, they are most commonly found in the Randstad area. The initial idea was that the Sprinter would provide somewhat of a subway/metro service but this plan failed as the cities of Amsterdam and Rotterdam continued to construct their own rapid transit systems. Nevertheless, in the densely populated Randstad, the Sprinters remain popular. Two car versions were revised and renamed to Citypendel. All Sprinters are now refurbished into the new white/yellow/dark blue livery.

Bibliography

- [1] EN 1990 AMD 2 : 2005(E) Annex A2 to EN 1990.
- [2] Gegevens trein materieel tbv dynamica analyses.
- [3] M Abu-Hilal and M Mohsen. Vibration of beams with general boundary conditions due to a moving harmonic load. *Journal of Sound and Vibration*, 232(4):703–717, 2000.
- [4] CEN. EN 13848-5:2008+A1 Railway applications - Track - Track geometry quality - Part 5: Geometric quality levels - Plain line.
- [5] CEN. 1: Actions on structures, part 2: Traffic loads on bridges. Brussels: European Standard EN, 2:2003, 1991.
- [6] CEN. Eurocode: Basis of structural design. BSI, 2002.
- [7] CEN. 14363: 2005. Railway applications-Testing for the acceptance of running characteristics of railway vehicles-Testing of running behavior and stationary tests, pages 6–36, 2007.
- [8] CEN. pren 15528:2013, railway applications line categories for managing the interface between load limits of vehicles and infrastructure. Brussels: European Standard EN, 2013.
- [9] Manuel Cuadrado Sanguino, Pedro González Requejo, Jose María Goicolea Ruigomez, Jorge Nasarre, and Rui Dias. Analysis of lateral displacements in large railway viaducts under traffic loads. impact on ride safety and passenger comfort. 2008.
- [10] D181Committee. RP6: Final report, D181 LATERAL FORCES ON RAILWAY BRIDGES. UIC, .
- [11] D181Committee. ERRI D 181/DT 329 E: LATERAL FORCES ON RAILWAY BRIDGES, PARAMETRIC STUDY PART1,PART 2. UIC, .
- [12] D181Committee. RP2: Submitted programs and example of application. UIC, .
- [13] Rui Filipe da Silva Dias. Dynamic behaviour of high speed railway bridges. vehicles lateral dynamic behaviour. 2007.
- [14] Coenraad Esveld. Modern railway track. 2001.
- [15] L. Fryba. Dynamics of railway bridges. T. Telford, 1996. ISBN 9780727720443.
- [16] Ladislav Fryba. Vibration of solids and structures under moving loads. Thomas Telford, 1999.
- [17] Simon Iwnicki. Handbook of railway vehicle dynamics. CRC Press, 2006.
- [18] Michal Majka and Michael Hartnett. Effects of speed, load and damping on the dynamic response of railway bridges and vehicles. *Computers & Structures*, 86(6):556–572, 2008.

- [19] A.V. Metrikine. *Dynamics, Slender Structures and an Introduction to Continuum Mechanics: CT 4145*. Delft University of Technology.
- [20] UIC. *UNE-ENV 12299: Aplicaciones ferroviarias. Comodidad de viaje para los viajeros. Medición y evaluación.* .
- [21] UIC. *UNE-ENV 13803-1 EX: Aplicaciones ferroviarias. Parámetros de proyecto de trazado de la vía. Ancho de vía de 1 435mm y mayores. Parte 1: Plena vía.* .
- [22] UIC. 518: Testing and approval of railway vehicles from the point of view of their dynamic behaviour–safety–track fatigue–ride quality. *International Union of Railways, 3rd ed., Paris*, 2005.
- [23] UIC. *UIC Leaflet 776-2:Design requirements for rail-bridges based on interaction phenomena between train, track and bridge*. UIC, June 2009.